Using Dynamic Covalent Chemistry in Crosslinked Glassy Polymers to Achieve Stress Relaxation and Improve Material Performance

by

Nancy Sowan

B.S., University of Jordan, 2011

A thesis submitted to the

Faculty of the Graduate School of the

University of Colorado in partial fulfillment

of the requirement for the degree of

Doctor of Philosophy

Materials Science and Engineering

2019

This thesis entitled:

Using Dynamic Covalent Chemistry in Crosslinked Glassy Polymers to Achieve Stress Relaxation and Improve Material Performance

written by Nancy Sowan

has been approved for the Materials Science and Engineering

_____

Christopher N. Bowman, Committee Chair

_____

Jeffrey W. Stansbury, Committee Member

Date _____

The final copy of this thesis has been examined by the signatories, and we Find that both the content and the form meet acceptable presentation standards Of scholarly work in the above mentioned discipline.

Sowan, Nancy (PhD, Materials Science and Engineering)

Using Dynamic Covalent Chemistry in Crosslinked Glassy Polymers to Achieve Stress Relaxation and Improve Material Performance

Thesis directed by Professor Christopher N. Bowman

Covalent adaptable network (CAN) has attracted significant interest in the soft matter community, as it enables stress relaxation in a crosslinked polymer network. However, all CAN systems have developed thus far are in the rubbery state. This thesis is focused on the development of mechanically strong, high glass transition temperature (T_g) polymer networks that are capable of dynamic bond exchange at ambient temperature while maintaining superior mechanical properties. This goal was achieved by introducing moieties capable of dynamic covalent chemistry (DCC) in the resin matrix and at the resin-filler interface of thermosetting polymers to relax internal and applied stresses at the glassy state. The first part of this thesis covers the implementation of reversible addition fragmentation transfer (RAFT) into the resin phase of glassy copper(I)-catalyzed azide-alkyne cycloaddition (CuAAC) polymer networks. Correspondingly, various azide and alkyne monomers containing structurally variable allyl sulfide (AS) or trithiocarbonate (TTC) moieties were designed and synthesized following a scalable synthetic strategy. While CuAAC reactions as a highly efficient and orthogonal “click” chemistry yields glassy polymers composed of rigid triazole linkages with enhanced stiffness and toughness, the RAFT moieties independently undergo bond exchange leading to glassy state stress relaxation upon light exposure. This capability of glassy state stress relaxation enables significant enhancement in toughness and ductility, light-activated shape reconfiguration and photoreversal of physical aging.

The second part of this thesis covers the development of adaptive interface (AI) platform by introducing moieties capable of RAFT and thiol-thioester exchange (TTE) at the resin-filler interface of a highly crosslinked, glassy thiol-ene polymer network to promote interfacial stress relaxation in the glassy state and explore the resulting evolution of composite performance. Employing this active, bond-exchanging interface overcomes the limitation of interfacial stress concentration in polymer composites that incorporate filler materials of different modulus relative to the resin phase and imparts significant benefits to the composite performance including improvements in toughness and polymerization shrinkage stress. This improvement in mechanical performance that results from the successful relaxation of interfacial stresses is a platform technology that will broadly impact the field of polymeric composites.

To my parents…

Acknowledgments

I would like to thank my advisor Dr. Christopher Bowman for giving me the opportunity to be a graduate student in his respective group and for his amazing mentorships and guidance during my entire years of Ph.D. program. Working in such professional group is a great honor. He has supported me and encouraged me in both professional and personal life aspects in every step of this journey. I could never fully express how thankful I am for working and knowing him. I also would like to thank my committees, Prof. Yifu Ding, Prof. Jeffrey W. Stansbury, Prof. Robert McLeod, and Prof. Rong Long, for their advises, ideas, time and mentorships.

I would also like to acknowledge all the current and former Bowman/ Stansbury lab members for their discussions and input throughout this work. Especially, I am gratefully thankful to Han Byul Song for being there for me whenever I need help. I also want to thank Matthew McBride, Lewis Cox, Maciej Podgorski, Brady Worell, Parag Shah, Abeer Alrazhani, Benjamin Fairbanks, Marvin Alim, Kimberly Childress, Chen Wang, Nicholas Bongiardana, Adam Dobson, Caroline Szczepanski and Devatha Nair, whom I worked closely, and spent great time with them. Working and interacting with such amazing people in both Bowman and Stansbury group was fruitful experience and I surely learned a lot from them. Multiple undergraduate students have contributed to this work including Mohamad Eid, James Ryan Patton, and Kevin Kolb. Further, I thank our collaborator, Yinan Lu, Shane Fraizer, Xiaoming Mu, Prof. Jerry Qi and Prof. John Torkelson.

Most of all, I would like to thank my family for their endless love and support. My parents, brothers and sisters who have sacrificed enormously for me to be in this position and I would never be a doctorate without their love and support. I want also to specially thank my husband Ayman

Alawneh and my adorable kids Yousef and Yahya, for their love, without their existence, I would have never been courageous to start and continue the journey.

Lastly, I would like to acknowledge my funding. This work was supported by NSF and NIH grants, and Industry University Collaborative Research Center (IUCRC).

Table of Contents

List of Figures

List of Tables

List of Schemes

Chapter 1

Introduction

1.1. Polymeric Materials and Current Challenges

Thermosetting polymers have sustained industrial and academic interests in the history of synthetic polymers due to their thermal/chemical resistance and mechanical strength, resulting from permanent crosslinking. Contrarily, thermoplastics due to the lack of permanent crosslinking allow material flow upon heating, yielding recyclability and reprocessability of polymers. Despite of unique characteristics associated with thermosets and thermoplastics, several industrial applications including self-healing and dental restorative materials demand unique properties of both thermosets and thermoplastics to yield reprocessable and recyclable polymers while exhibiting outstanding mechanical and physical properties. Unfortunately, the permanent cross-linked nature (the key behind the desirable attributes of thermosets) is unfavorable for designing materials with dynamic properties.[1–3]

In contrast to traditional thermosets, covalent adaptable networks (CANs) are dynamically cross-linked polymers that can relax internal/external stresses via bond reconfiguration within the networks in response to the application of a triggering stimulus such as light or heat.[4,5] Recently, there has been a significant interest focusing on achieving adaptive properties in thermosets such as malleability, and self-healing while maintaining their strength and stability, by introducing dynamic covalent linkages into their backbone.[6] However, most chemistries developed so far are often relatively soft materials or require either catalyst or change of environmental conditions such as heating to high temperature to activate dynamic behaviors, limiting their uses in the practical industrial applications. In an attempt to address the existing shortcomings of both the thermosets

and CANs, a few studies designing thermosets capable of catalyst-free, low-temperature dynamic property have been reported.[7–11] However, it is still ongoing challenges to develop readily photopolymerizable and mechanically strong, high T_g polymer networks that are capable of dynamic bond exchange at ambient temperature with spatial and temporal controls.

1.2. Covalent Adaptable Networks (CANs)

Covalent adaptable networks (CANs) are smart, crosslinked polymers, based on dynamic covalent chemistry (DCC) that enables bond rearrangement within the networks in response to the application of a specific stimulus. This on demand dynamic behavior gives CANs the ability to act as a bridge between thermosets and thermoplastics with unique characteristics such as adaptability, malleability, and self-healing after forming a network, while maintaining properties of thermosets such as mechanical strength and thermal and chemical stability.[4–6] Broadly, two types of reactions have been implemented for designing CANs; reversible exchange reactions and reversible addition reactions. Reversible exchange reactions, such as addition fragmentation chain transfer (RAFT),[12–15] cinnamates,[16] thiuram disulfides,[17] and metal-catalyzed transesterification,[18] preserve the crosslink density during bond rearrangement, as bond breaking and reforming of a crosslink occur at the same time. Unlike the exchange CANs, reversible addition-based CANs, such as the Diels–Alder reaction, often shift the reaction equilibrium towards the reactant during the DCC, and alter the crosslink density.[5,19] The two dynamic covalent reactions that are used in this thesis are discussed below.

1.2.1. Reversible Addition Fragmentation Chain Transfer (RAFT) Reactions

Reversible addition-fragmentation chain transfer (RAFT) polymerization process is a controlled radical polymerization in which a chain transfer agent such as tri-thiocarbonate or allyl

sulfide is used to produce polymers with controlled molecular weight and polymer architecture.[20,21] Recently, RAFT moieties have been incorporated into multi-functional monomer backbones, followed by the photo-chemically initiating RAFT mechanism, leading to rearrangement of the network connectivity and allowing re-equilibration of the polymer network in a spatial and temporal controlled manner, without altering the total number of crosslinks. RAFT exchange reaction occurs when light is applied to the network in the presence of photoinititors, to generate a radical species which reacts with the RAFT functional group, forming a tri-centered radical that then fragments to regenerate a radical species and the RAFT unit (**Scheme 1.1**).[12,22] Utilizing Light for triggering bond exchange offers spatial and temporal control to alter the bond connectivity and mechanical properties, because photons are delivered remotely enabling stress relaxation for multiple application including mechanophotopatterning,[14,23,24] self-healing,[25] polymerization shrinkage stress reduction[26,27], and photo-induced shape shifting[28].

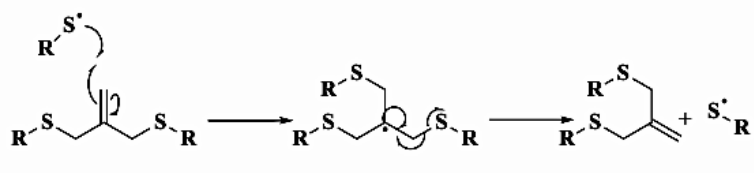

Scheme 1.1. RAFT radical mediated allyl sulfide bond rearrangement mechanism.

1.2.2. The Anion-Mediated Thiol-Thioester Exchange (TTE) Reaction

Exchange reactions involving thioesters have been effectively utilized f to develop native chemical ligation (NCL),[29] degradable hydrogel networks,[30] and synthetic sequence-controlled polymers.[31] In addition, due to the high molar refraction value of sulfur atoms, thioester moieties have been incorporated in bulk polymers as a means to increase refractive indices.[32] Recently, Worrell et.al introduced thiol-thioester exchange reaction (TTE) as a new class of CANs that that enable rapid, continuous ambient temperature stress relaxation. This exchange reaction only

proceeds under the condition that free thiol, thioester, and base/nucleophile as a catalyst are all present in the network. The exchange reaction happens when the unreacted thiol groups are deprotonated by basic catalysts, which generates thiolate anions that then attack the carbonyl functional groups to form a short-lived symmetrical intermediate, followed by the regeneration of the thioester and thiolate anion (**Scheme 1.2.**). If any of these three elements are missing, the polymer behaves as a typical crosslinked elastomer.[33] Furthermore, utilizing light to release basic or acidic catalysts, to turn "on" or "off" the exchange reactions, allows for spatiotemporal control over the dynamic behavior and introduce this type of CANs as a great candidate for applications including nanoscale surface patterning and optical materials.[33,34]

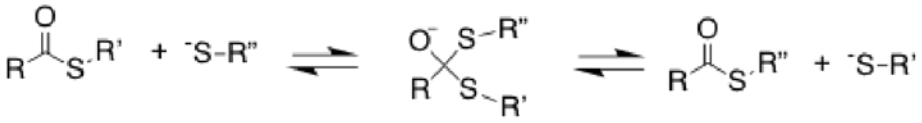

Scheme 1.2. Thiol-thioester exchange mechanism.

1.3. Step Growth Polymerization Reactions and "Click" Chemistry

Crosslinked polymers formed by step growth polymerization reactions have significant differences associated with the gel-point conversion, vitrification, and material properties than the networks formed by chain growth polymerization reactions. In step-growth polymerizations, a stepwise reaction between the reactive functional groups on multifunctional monomers, leads to slow molecular weight development, forming more homogenous network structure with narrow glass transition temperature and considerably delayed gelation. In contrast, chain-growth polymerizations occur between the active centers propagating through reactive functional groups on multifunctional monomers, forming more heterogeneous networks with early gelation. The properties of polymers such as resin viscosity, backbone rigidity, and thermo-mechanical

behaviors as well as gel point conversion can be readily altered in step growth polymerization via alterations in the chemical structures and the numbers of reactive functional groups in monomers.[35,36]

"Click" reactions have been utilized as an efficient polymerization reactions with little to no byproducts, to form homogeneous step growth networks in selective, orthogonal manner, under mild reaction conditions. "Click" chemistry was first introduced by Sharpless and coworkers in 2001, [36,37] which along with other attributes introduced "Click" chemistry as a successful polymerization technique to form homogeneous step growth networks. The two click reactions that are used in this thesis, the copper catalyzed azide alkyne cycloaddition (CuAAC) and thiol-ene reaction are discussed below.

1.3.1. The Photo-Initiated Copper-Catalyzed Azide-Alkyne Cycloaddition (CuAAC) Polymerization Reaction

Thermally activated 1,3-dipolar cycloaddition of organic azides and terminal alkynes in the absence of a catalyst was first discovered in 1964.[38] Later in 2001, copper(I)-catalyzed azide-alkyne cycloaddition (CuAAC) reaction was introduced by Meldal and Sharpless independently, as highly efficient "Click" reaction, that proceeds under relatively facile reaction conditions in an orthogonal manner.[39,40] Later on, bulk photo-initiated CuAAC polymerization was enabled by utilizing a photoinitiator to reduce Cu(II) to Cu(I) upon light irradiation, which affords a spatio-temporal control over the polymerization process.[41–43] As such, copper (I) coordinates to a terminal alkyne to form a copper-acetylide intermediate followed by the deprotonation of the terminal hydrogen and the formation of a transition state with two copper atoms. Later on, the weakly coordinated ligand is displaced by the azide to generate a copper-azide-acetylide complex, followed by cyclization then protonation, to release triazole molecule as a product, and regenerate

the copper ligand complex.[44–46] The general reaction mechanism of the photo-initiated CuAAC reaction is shown in **Scheme 1.3**. The formation of rigid, thermally and chemically stable 1,2,3-triazoles moieties as a product throughout the network enables the formation of polymer networks with enhanced mechanical properties.[37,39] Additionally, the step-growth polymerization mechanism of CuAAC reaction affords beneficial properties including delayed gelation, reduced polymerization shrinkage stress, and inherently uniform network structures when compared to conventional chain growth polymerization.[47–50]

Due to its unique advantages, CuAAC reaction has been utilized for several applications including synthesis of linear polymers, dendrimers, and other polymeric architectures, polymer coupling reactions, surface modification, bioconjugation, adhesive polymers and shape memory materials.[37,39,48,51–55] Although CuAAC polymerization has shown unique properties, the following equation must be considered during the design and the synthesis procedure of organic azides, and safety precautions be made when handling azides for bulk polymerization:

$$(N_C+N_O)/N_N \geq 3$$

where N_C presents the number of carbon atoms, N_O presents the number of oxygen atoms, and N_N presents the number of nitrogen atoms in azide monomers.[37]

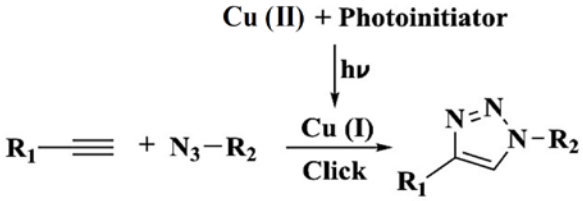

Scheme 1.3. Photo-initiated CuAAC polymerization reaction diagram: photoinitiation upon light irradiation, copper reduction to form Cu(I), and 'click' Cu(I)-catalyzed cycloaddition of azides and alkynes to form 1,2,3-triazoles adducts.

1.3.2. The Radical Thiol-ene Polymerization Reaction

The radical mediated thiol-ene reaction is an efficient, clean "Click" reaction occurs between a thiol and a double bond when a thiyl radical attacks the double bond forming a carbon-centered radical intermediate which then abstracts a proton from a thiol and reinitiate the process (**Scheme 1.4)**. This reaction proceeds in stoichiometric proportions when the alkene has a minimum tendency for homopolymerization such as vinyl ethers and allyl ethers.[36,56] In contrast to acrylate polymerization, the rate of thiol-ene reaction is non-sensitive to the presence or absence of oxygen, as the peroxide radical formed in the presence of oxygen undergoes chain transfer reaction to thiols to regenerate the thiyl radical. The unique characteristics of thiol-ene reactions including rapid polymerization kinetics, "Click" reactions, and step growth nature have made it useful for several applications including coatings, adhesives, and polymer functionalization.[57,58]

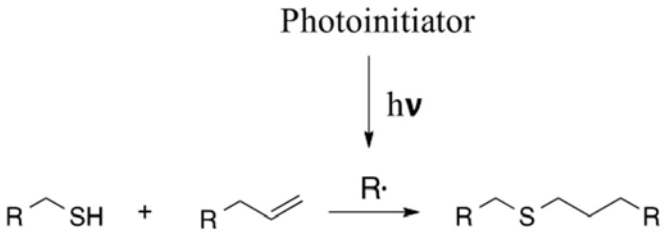

Scheme 1.4. Reaction scheme for radical thiol-ene polymerization reaction.

1.4. Polymer Composites

Polymers reinforced by inorganic fillers (such as glass beads, silica and alumina particles) are widely used in many engineering fields due to the flexibility they provide in targeting desired physical and mechanical properties. Clay reinforced composites emerged in the early 1900's, but interest within the scientific community surged in 1993 when Toyota researchers reported the incredible increases in yield and tensile strengths exhibited by nylon 6 when combined with

montmorillonite.[59] Since that time enormous effort has been invested into enhancing the performance of polymer nanocomposites, due in part to the enormous surface area associated with nanofillers, which cause the particle-polymer interfaces to play a crucial role in a great number of physical and chemical phenomena responsible for targeted desirable material properties for several applications.[60–63] However, it is also known that these inorganic particles, with their significantly higher modulus and generally lower thermal expansion, act as stress concentrators,[62,64] and this behavior leads to particle-matrix debonding and void formation, which significantly influences the failure of composite materials.[65,66] Generally, the mechanical properties of particulate-filled polymer nanocomposites are affected by particle size, particle content and particle/matrix interfacial adhesion, which is the most important factor for effective stress transfer between the particles and the matrix.[62] Accordingly, several decades of work have been directed towards reducing the interfacial stress, improving stress transfer between the filler and the matrix, and examining impacts of filler size, content, and the adhesive strength.[62] Despite these efforts, alleviating the concentration of interfacial stresses in order to prevent premature composite failure and improve crack-growth resistance is an ongoing challenge. Inspired by this limitation, recent developments in dynamic polymer composites have showcased the incorporation of dynamic covalent chemistries (DCC). The presence of DCC-capable moieties in the resin formulation leads to chemical bond reshuffling and promotes stress relaxation while maintaining connectivity of the polymer network. These dynamic networks exhibit static thermoset properties under ordinary circumstances but reversibly rearrange covalent bonds, often in response to an externally applied stimulus.[4,5] Recently, mechanoresponsive DCC-based composites, such as addition fragmentation chain transfer (AFT) based dental composites,[27,67] transesterification-based epoxy composites,[68,69] and disulfide-based vitrimer composites,[70] have been developed.

1.4.1. Dental Composites

Particularly, dental restorative composites are mechanically stiff, highly-crosslinked networks formulated from inorganic fillers dispersed in photocured dimethacrylate resins. Though there are problems associated with incomplete methacrylate conversion and insufficient fracture toughness, the primary failure modes for these materials are largely attributed to the considerable shrinkage stress of several mega pascals that develops during the polymerization, due to early gelation and vitrification of methacrylate network along with considerable volumetric shrinkage in a restricted environment.[71–74] Typically, inorganic fillers are used in dental composite to enhance composites mechanical performance including hardness, strength, wear resistance, thermal expansion coefficient and polymerization-induced volumetric shrinkage. However, high filler loadings in dental composites significantly affect their viscosity and hinder photopolymerization kinetic. Additionally, the inorganic filler is also a source for large stress gradients due to the modulus and thermal expansion mismatch between the filler and the resin matrix.[71,73,75–78] Even though dental restorative materials have been greatly improved over the past few decades, shrinkage stress induced microcracking that cause serious clinical issues, such as microleakage, secondary cavities and thermal sensitization, remain problematic.[79,80] As a result, several approaches have been directed to reduce shrinkage stress of dental restoratives while maintaining all other desirable material properties. Several researchers examined the effect of the type, size distribution, loading content and surface modification of the filler on composites properties.[73,76,78] Other efforts have been directed to facilitate improvements in dental composite by reducing the reactive group concentration,[81–83], modifying the dimethacrylate monomer formulations,[84,85] and exploring alternative polymerization techniques, such as thiol-ene reaction,[26,77] ring-opening polymerizations,[74] copper(I)-catalyzed azide-alkyne cycloaddition (CuAAC) reaction.[47,72]

Recently, the implementation of CANs, into dental restoratives has been explored as a successful transformative technology to eliminate stresses that arise from polymerization shrinkage and external loading, while conserve the overall covalently bonded structure. Particularly, since the radical-mediated addition-fragmentation chain transfer (AFT) demonstrated its capability to reduce polymerization stress in thiol-ene photopolymerization,[22] great interest has been directed to implement monomers containing functional groups capable of undergoing AFT process into the conventional dental restoratives. Allyl sulfide addition fragmentation monomer was incorporated in ternary thiol-yne-methacrylate system, containing a methacrylate monomer with rigid core, to formulate high T_g dental resin while maintaining the reduced shrinkage stress.[27] Furthermore, several allyl sulfide-core monomers having a multitude of polymerizable functional groups such as norbornene allyl sulfide were incorporated into the methacrylate resin to achieve a network with T_g, glassy modulus, and crosslink density comparable to the conventional BisGMA/TEGDMA dental resins, while exhibiting shrinkage stress reduction.[22,67] Later on, allyl sulfide was replaced with trithiocarbonate functional group to increase the AFT network rearrangement rate, which significantly minimize the polymerization stress and maintain identical mechanical properties to the typical BisGMA/TEGDMA composites.[86,87] In recent studies, other AFT agent such as β-allyl sulfone[88] and AFT-based dimethacrylate [89] have been successfully implemented into dental restoratives, enabled the network to rearrange while polymerizing, and reduced shrinkage stress.

1.5 References

(1) Ligon-Auer, S. C.; Schwentenwein, M.; Gorsche, C.; Stampfl, J.; Liska, R. Toughening of Photo-Curable Polymer Networks: A Review. *Polym. Chem.* **2016**, *7* (2), 257–286.

(2) Crivello, J. V.; Reichmanis, E. Photopolymer Materials and Processes for Advanced Technologies. *Chem. Mater.* **2014**, *26* (1), 533–548.

(3) Jeffrey, G.; Bruce, P. R. *Thermosets*; Major Reference Works; 2017.

(4) Kloxin, C. J.; Bowman, C. N. Covalent Adaptable Networks: Smart, Reconfigurable and Responsive Network Systems. *Chem. Soc. Rev.* **2013**, *42* (17), 7161–7173.

(5) Kloxin, C. J.; Scott, T. F.; Adzima, B. J.; Bowman, C. N. Covalent Adaptable Networks (CANs): A Unique Paradigm in Cross-Linked Polymers. *Macromolecules* **2010**, *43* (6), 2643–2653.

(6) Mcbride, M. K.; Worrell, B. T.; Brown, T.; Cox, L. M.; Sowan, N.; Wang, C.; Podgorski, M.; Martinez, A. M.; Bowman, C. N. Enabling Applications of Covalent Adaptable Networks. **2019**, *10*, 175.

(7) Fortman, D. J.; Brutman, J. P.; Cramer, C. J.; Hillmyer, M. A.; Dichtel, W. R. Mechanically Activated, Catalyst-Free Polyhydroxyurethane Vitrimers. *J. Am. Chem. Soc.* **2015**, *137* (44), 14019–14022.

(8) Ying, H.; Zhang, Y.; Cheng, J. Dynamic Urea Bond for the Design of Reversible and Self-Healing Polymers. *Nat. Commun.* **2014**, *5*, 1–9.

(9) Cash, J. J.; Kubo, T.; Bapat, A. P.; Sumerlin, B. S. Room-Temperature Self-Healing Polymers Based on Dynamic-Covalent Boronic Esters. *Macromolecules* **2015**, *48* (7), 2098–2106.

(10) Oehlenschlaeger, K. K.; Guimard, N. K.; Brandt, J.; Mueller, J. O.; Lin, C. Y.; Hilf, S.; Lederer, A.; Coote, M. L.; Schmidt, F. G.; Barner-Kowollik, C. Fast and Catalyst-Free Hetero-Diels-Alder Chemistry for on Demand Cyclable Bonding/Debonding Materials. *Polym. Chem.* **2013**, *4* (16), 4348–4355.

(11) Röttger, M.; Domenech, T.; Van Der Weegen, R.; Breuillac, A.; Nicolaÿ, R.; Leibler, L. High-Performance Vitrimers from Commodity Thermoplastics through Dioxaborolane Metathesis. *Science* **2017**, *356* (6333), 62–65.

(12) Scott, T. F.; Schneider, A. D.; Cook, W. D.; Bowman, C. N. Photoinduced Plasticity in Cross-Linked Polymers. *Science* **2005**, *308* (5728), 1615–1617.

(13) Kloxin, C. J.; Scott, T. F.; Bowman, C. N. Stress Relaxation via Addition−Fragmentation Chain Transfer in a Thiol-Ene Photopolymerization. *Macromolecules* **2009**, *42* (7), 2551–2556.

(14) Cox, L. M.; Li, Z.; Sowan, N.; Nair, D.; Xiao, J.; Bowman, C. N.; Ding, Y. Reconfigurable Surface Patterns on Covalent Adaptive Network Polymers Using Nanoimprint Lithography. *Polymer* **2014**, *55* (23), 5933–5937.

(15) Sowan, N.; Cox, L. M.; Shah, P. K.; Song, H. B.; Stansbury, J. W.; Bowman, C. N. Dynamic Covalent Chemistry at Interfaces: Development of Tougher, Healable Composites through Stress Relaxation at the Resin-Silica Nanoparticles Interface. *Adv. Mater. Interfaces* **2018**, 1800511.

(16) Chung, C. M.; Roh, Y. S.; Cho, S. Y.; Kim, J. G. Crack Healing in Polymeric Materials via Photochemical [2+2] Cycloaddition. *Chem. Mater.* **2004**, *16* (21), 3982–3984.

(17) Amamoto, Y.; Otsuka, H.; Takahara, A.; Matyjaszewski, K. Self-Healing of Covalently Cross-Linked Polymers by Reshuffling Thiuram Disulfide Moieties in Air under Visible Light. *Adv. Mater.* **2012**, *24* (29), 3975–3980.

(18) Capelot, M.; Montarnal, D.; Tournilhac, F.; Leibler, L. Metal-Catalyzed Transesterification for Healing and Assembling of Thermosets. *J. Am. Chem. Soc.* **2012**, *134* (18), 7664–7667.

(19) Kloxin, C. J.; Bowman, C. N. Covalent Adaptable Networks: Smart, Reconfigurable and Responsive Network Systems. *Chem. Soc. Rev.* **2013**, *42* (17), 7161–7173.

(20) Coote, M. L.; Henry, D. J. Effect of Substituents on Radical Stability in Reversible Addition Fragmentation Chain Transfer Polymerization: An Ab Initio Study. *Macromolecules* **2005**, *38* (4), 1415–1433.

(21) Nicolaÿ, R.; Kamada, J.; Van Wassen, A.; Matyjaszewski, K. Responsive Gels Based on a Dynamic Covalent Trithiocarbonate Cross-Linker. *Macromolecules* **2010**, *43* (9), 4355–4361.

(22) Kloxin, C. J.; Scott, T. F.; Bowman, C. N. Stress Relaxation via Addition−Fragmentation Chain Transfer in a Thiol-Ene Photopolymerization. *Macromolecules* **2009**, *42* (7), 2551–2556.

(23) Kloxin, C. J.; Scott, T. F.; Park, H. Y.; Bowman, C. N. Mechanophotopatterning on a Photoresponsive Elastomer. *Adv. Mater.* **2011**, *23* (17), 1977–1981.

(24) Cox, L. M.; Sun, X.; Wang, C.; Sowan, N.; Killgore, J. P.; Long, R.; Wu, H. A.; Bowman, C. N.; Ding, Y. Light-Stimulated Permanent Shape Reconfiguration in Cross-Linked Polymer Microparticles. *ACS Appl. Mater. Interfaces* **2017**, *9* (16), 14422–14428.

(25) Amamoto, Y.; Kamada, J. pd.; Otsuka, H.; Takahara, A.; Matyjaszewski, K. Photoinduced Self-Healing of Covalently Cross-Linked Polymers through Reshuffling of Trithiocarbonate Units. *Angew. Chemie - Int. Ed.* **2011**, *50* (7), 1660–1663.

(26) Park, H. Y.; Kloxin, C. J.; Abuelyaman, A. S.; Oxman, J. D.; Bowman, C. N. Stress Relaxation via Addition–Fragmentation Chain Transfer in High T g , High Conversion Methacrylate-Based Systems. *Macromolecules 45* (14), 5640-5646.

(27) Park, H. Y.; Kloxin, C. J.; Fordney, M. F.; Bowman, C. N. Stress Reduction and T g Enhancement in Ternary Thiol-Yne-Methacrylate Systems via Addition-Fragmentation Chain Transfer. *Macromolecules* **2012**, *45* (14), 5647–5652.

(28) Mu, X.; Sowan, N.; Tumbic, J. a.; Bowman, C. N.; Mather, P. T.; Qi, H. J. Photo-Induced Bending in a Light-Activated Polymer Laminated Composite. *Soft Matter* **2015**, *11* (13), 2673–2682.

(29) Nilsson, B. L.; Soellner, M. B.; Raines, R. T. Ynthesis Of. **2005**, 91–118.

(30) Ghobril, C.; Charoen, K.; Rodriguez, E. K.; Nazarian, A.; Grinstaff, M. W. Angewandte A Dendritic Thioester Hydrogel Based on Thiol – Thioester Exchange as a Dissolvable Sealant System for Wound Closure. **2013**, 14070–14074.

(31) Price, J. L.; Hadley, E. B.; Steinkruger, J. D.; Gellman, S. H. NIH Public Access. **2011**, *49* (2), 368–371.

(32) Liu, J.; Ueda, M. High Refractive Index Polymers: Fundamental Research and Practical Applications. *J. Mater. Chem.* **2009**, *19* (47), 8907.

(33) Worrell, B. T.; McBride, M. K.; Lyon, G. B.; Cox, L. M.; Wang, C.; Mavila, S.; Lim, C.-H.; Coley, H. M.; Musgrave, C. B.; Ding, Y.; et al. Bistable and Photoswitchable States of Matter. *Nat. Commun.* **2018**, *9* (1), 2804.

(34) Wang, C.; Mavila, S.; Worrell, B. T.; Xi, W.; Goldman, T. M.; Bowman, C. N. Productive Exchange of Thiols and Thioesters to Form Dynamic Polythioester-Based Polymers. **2018**.

(35) Odian, G. *Principles of Polymerization*; John Wiley & Sons, 2004.

(36) Hoyle, C. E.; Lowe, A. B.; Bowman, C. N. Thiol-Click Chemistry: A Multifaceted Toolbox for Small Molecule and Polymer Synthesis. *Chem. Soc. Rev.* **2010**, *39* (4), 1355.

(37) Kolb, H. C.; Finn, M. G.; Sharpless, K. B. Click Chemistry: Diverse Chemical Function from a Few Good Reactions. *Angew. Chemie - Int. Ed.* **2001**, *40* (11), 2004–2021.

(38) Finn, P. M. G.; Fokin, V.; Hein, J. E.; Fokin, V. V. Copper-Catalyzed Azide–Alkyne Cycloaddition (CuAAC) and beyond: New Reactivity of Copper(I) Acetylides. *Chem. Soc. Rev.* **2010**, *39* (4), 1302–1315.

(39) Rostovtsev, V. V.; Green, L. G.; Fokin, V. V.; Sharpless, K. B. A Stepwise Huisgen Cycloaddition Process: Copper(I)-Catalyzed Regioselective "Ligation" of Azides and Terminal Alkynes. *Angew. Chemie - Int. Ed.* **2002**, *41*, 2596–2599.

(40) Tornøe, C. W.; Christensen, C.; Meldal, M. Peptidotriazoles on Solid Phase: [1,2,3]-Triazoles by Regiospecific Copper(I)-Catalyzed 1,3-Dipolar Cycloadditions of Terminal Alkynes to Azides. *J. Org. Chem.* **2002**, *67* (9), 3057–3064.

(41) Gong, T.; Adzima, B. J.; Baker, N. H.; Bowman, C. N. Photopolymerization Reactions Using the Photoinitiated Copper (I)-Catalyzed Azide-Alkyne Cycloaddition (CuAAC) Reaction. *Adv. Mater.* **2013**, *25*, 2024–2028.

(42) Adzima, B. J.; Tao, Y.; Kloxin, C. J.; DeForest, C. a; Anseth, K. S.; Bowman, C. N. Spatial and Temporal Control of the Alkyne-Azide Cycloaddition by Photoinitiated Cu(II) Reduction. *Nat. Chem.* **2011**, *3* (3), 256–259.

(43) Song, H. B.; Baranek, A.; Worrell, B. T.; Cook, W. D.; Bowman, C. N. Photopolymerized Triazole-Based Glassy Polymer Networks with Superior Tensile Toughness. *Adv. Funct. Mater.* **2018**, *28* (22), 1–9.

(44) Gong, T.; Adzima, B. J.; Bowman, C. N. A Novel Copper Containing Photoinitiator, *Chem. Commun.* **2013**, *49* (72), 7950–7952.

(45) Sun, S.; Wu, P. Mechanistic Insights into Cu (I) -Catalyzed Azide - Alkyne " Click " Cycloaddition Monitored by Real Time Infrared Spectroscopy. **2010**, No. I, 8331–8336.

(46) Worrell, B. T.; Malik, J. A.; Fokin, V. V. Direct Evidence of a Dinuclear Copper Intermediate in Cu(I)-Catalyzed Azide-Alkyne Cycloadditions. *Science* **2013**, *340*, 457–461.

(47) Song, H. B.; Sowan, N.; Shah, P. K.; Baranek, A.; Flores, A.; Stansbury, J. W.; Bowman, C. N. Reduced Shrinkage Stress via Photo-Initiated Copper(I)-Catalyzed Cycloaddition Polymerizations of Azide-Alkyne Resins. *Dental Materials*. Elsevier Inc. June 25, 2016.

(48) Alzahrani, A. A.; Saed, M.; Yakacki, C. M.; Song, H. B.; Sowan, N.; Walston, J. J.; Shah, P. K.; McBride, M. K.; Stansbury, J. W.; Bowman, C. N. Fully Recoverable Rigid Shape Memory Foam Based on Copper-Catalyzed Azide-Alkyne Cycloaddition (CuAAC) Using a Salt Leaching Technique. *Polym. Chem.* **2018**, *9* (1), 121–130.

(49) Song, H. B.; Baranek, A.; Bowman, C. N. Kinetics of Bulk Photo-Initiated Copper(I)-Catalyzed Azide-Alkyne Cycloaddition (CuAAC) Polymerizations. *Polym. Chem.* **2016**, *7*, 603–612.

(50) Baranek, A.; Song, H. B.; Mcbride, M.; Finnegan, P.; Bowman, C. N. Thermomechanical Formation − Structure − Property Relationships in Photopolymerized Copper-Catalyzed Azide − Alkyne (CuAAC) Networks. **2016**.

(51) McBride, M. K.; Gong, T.; Nair, D. P.; Bowman, C. N. Photo-Mediated Copper(I)-Catalyzed Azide-Alkyne Cycloaddition (CuAAC) "Click" Reactions for Forming Polymer Networks as Shape Memory Materials. *Polym.* **2014**, *55* (23), 5880–5884.

(52) Johnson, J. A.; Finn, M. G.; Koberstein, J. T.; Turro, N. J. Construction of Linear Polymers , Dendrimers , Networks , and Other Polymeric Architectures by Copper-Catalyzed Azide-Alkyne Cycloaddition '" Click "' Chemistry. **2008**, 1052–1072.

(53) Di, D. D.; Fokin, V. V; Finn, M. G. Click Chemistry in Materials Synthesis . 1 . Adhesive Polymers from Copper-Catalyzed Azide-Alkyne. **2004**, 4392–4403.

(54) Zajdowicz, S.; Byul, H.; Baranek, A.; Bowman, C. N. Evaluation of Biofilm Formation on Novel Copper-Catalyzed Azide-Alkyne Cycloaddition (CuAAC) -Based Resins for Dental Restoratives. *Dent. Mater.* **2018**, *34* (4), 657–666.

(55) Han Byul, S.; Wang, X.; Patton, J. R.; Stansbury, J. W.; Bowman, C. N. Kinetics and Mechanics of Photo-Polymerized Triazole-Containing Thermosetting Composites via the Copper (I) -Catalyzed Azide-Alkyne Cycloaddition. *Dent. Mater.* **2017**, *33* (6), 621–629.

(56) Cramer, N. B.; Bowman, C. N. Kinetics of Thiol – Ene and Thiol – Acrylate Photopolymerizations with Real-Time Fourier Transform Infrared. **2001**, 3311–3319.

(57) Desroches, M.; Caillol, S.; Lapinte, V.; Boutevin, B.; Charles, I.; Montpellier, G.; Cnrs-um-enscm-um, U. M. R.; Om, E. I. A. M. S.; De, R.; Normale, E.; et al. Synthesis of Biobased Polyols by Thiol À Ene Coupling from Vegetable Oils. **2011**, 2489–2500.

(58) Nair, D. P.; Cramer, N. B.; Scott, T. F.; Bowman, C. N.; Shandas, R. NIH Public Access. **2011**, *51* (19), 4383–4389.

(59) Kojima Yoshitsugu; Usuki Arimitsu; Kawasumi Masaya; Okada Akane; Fukushima Yoshiaki; Kurauchi Toshio; Kamigaito Osami. Mechanical Properties of Nylon 6-Clay Hybrid. *J. Mater. Res.* **1993**, *8* (5), 1185–1189.

(60) Zheng, Y.; Zheng, Y.; Ning, R. Effects of Nanoparticles SiO2 on the Performance of Nanocomposites. *Mater. Lett.* **2003**, *57* (19), 2940–2944.

(61) Chen, Q.; Chasiotis, I.; Chen, C.; Roy, A. Nanoscale and Effective Mechanical Behavior and Fracture of Silica Nanocomposites. *Compos. Sci. Technol.* **2008**, *68* (15–16), 3137–3144.

(62) Fu, S. Y.; Feng, X. Q.; Lauke, B.; Mai, Y. W. Effects of Particle Size, Particle/Matrix Interface Adhesion and Particle Loading on Mechanical Properties of Particulate-Polymer Composites. *Compos. Part B Eng.* **2008**, *39* (6), 933–961.

(63) Qiu, M.; Wu, S.; Tang, Z.; Guo, B. Exchangeable Interfacial Crosslinks towards Mechanically Robust Elastomer/Carbon Nanotubes Vitrimers. *Compos. Sci. Technol.* **2018**, *165*, 24–30.

(64) Üstündag, E.; Dragoi, D.; Clausen, B.; Brown, D.; Bourke, M. A. M.; Balch, D. K.; Dunand, D. C. Internal Stresses in Bulk Metallic Glass Matrix Composites. **2001**, *644* (4), 1–6.

(65) Eiras, D.; Pessan, L. A. Mechanical Properties of Polypropylene/Calcium Carbonate Nanocomposites. *Mater. Res.* **2009**, *12* (4), 517–522.

(66) Sun, S.; Li, C.; Zhang, L.; Du, H. L.; Burnell-Gray, J. S. Effects of Surface Modification of Fumed Silica on Interfacial Structures and Mechanical Properties of Poly(Vinyl Chloride) Composites. *Eur. Polym. J.* **2006**, *42* (7), 1643–1652.

(67) Park, H. Y.; Kloxin, C. J.; Abuelyaman, A. S.; Oxman, J. D.; Bowman, C. N. Stress Relaxation via Addition–Fragmentation Chain Transfer in High T g , High Conversion Methacrylate-Based Systems. *Macromolecules 45* (14), 5640-5646.

(68) Yang, Z.; Wang, Q.; Wang, T. Dual-Triggered and Thermally Reconfigurable Shape Memory Graphene-Vitrimer Composites. *ACS Appl. Mater. Interfaces* **2016**, *8* (33), 21691–21699.

(69) Legrand, A.; Souli-Ziakovic, C. Silica-Epoxy Vitrimer Nanocomposites. *Macromolecules* **2016**, *49* (16), 5893–5902.

(70) Ruiz de Luzuriaga, A.; Martin, R.; Markaide, N.; Rekondo, A.; Cabañ ero, G.; Rodrí guez, J.; Odriozola, I. Epoxy Resin with Exchangeable Disulfide Crosslinks to Obtain Reprocessable, Repairable and Recyclable Fiber-Reinforced Thermoset Composites. *Mater. Horizons* **2016**, 241–247.

(71) Schneider, L. F. J.; Cavalcante, L. M.; Silikas, N. Shrinkage Stresses Generated during Resin-Composite Applications: A Review. *J. Dent. Biomech.* **2010**, *1* (1), 131630–131630.

(72) Moszner, N.; Salz, U. Recent Developments of New Components for Dental Adhesives and Composites. *Macromol. Mater. Eng. 2007*, **2007**, *292*, 245–271.

(73) Cramer, N. B.; Stansbury, J. W.; Bowman, C. N. Recent Advances and Developments in Composite Dental Restorative Materials. *J. Dent. Res.* **2011**, *90* (4), 402–416.

(74) Ms, S.; Auj, Y.; Physicomechanical, S. A. Physicomechanical Evaluation of Low-Shrinkage Dental Nanocomposites Based on Silsesquioxane Cores. **2007**, 230–238.

(75) Drummond, J. L. Materials. **2009**, *87* (8), 710–719.

(76) Shah, P. K.; Stansbury, J. W. Role of Filler and Functional Group Conversion in the Evolution of Properties in Polymeric Dental Restoratives. *Dent. Mater.* **2014**, *30* (5), 586–593.

(77) Podgórski, M.; Becka, E.; Claudino, M.; Shah, P. K.; Stansbury, J. W.; Bowman, C. N. Ester-Free Thiol – Ene Dental Restoratives — Part A : *Dent. Mater.* **2015**, *31* (11), 1255–1262.

(78) Gonalves, F.; Azevedo, C. L. N.; Ferracane, J. L.; Braga, R. R. BisGMA/TEGDMA Ratio and Filler Content Effects on Shrinkage Stress. *Dent. Mater.* **2011**, *27* (6), 520–526.

(79) Durner, J.; Spahl, W.; Zaspel, J.; Schweikl, H.; Hickel, R.; Reichl, F. Eluted Substances from Unpolymerized and Polymerized Dental Restorative Materials and Their Nernst Partition Coefficient. **2009**, *6*, 91–99.

(80) Ferracane, J. L. Resin-Based Composite Performance : Are There Some Things We Can ' t Predict ? *Dent. Mater.* **2012**, *29* (1), 51–58.

(81) Liu, J.; Howard, G. D.; Lewis, S. H.; Barros, M. D.; Stansbury, J. W. A Study of Shrinkage Stress Reduction and Mechanical Properties of Nanogel-Modified Resin Systems. *Eur. Polym. J.* **2012**, *48* (11), 1819–1828.

(82) Moraes, R. R.; Garcia, J. W.; Barros, M. D.; Lewis, S. H.; Pfeifer, C. S.; Liu, J.; Stansbury, J. W. Control of Polymerization Shrinkage and Stress in Nanogel-Modified Monomer and Composite Materials. *Dent. Mater.* **2011**, *27* (6), 509–519.

(83) Carioscia, J. A.; Lu, H.; Stanbury, J. W.; Bowman, C. N. Thiol-Ene Oligomers as Dental Restorative Materials. **2005**, 1137–1143.

(84) Klee, J. E.; Schneider, C.; Ho, D.; Burgath, A.; Frey, H.; Mu, R. Hyperbranched Polyesters and Their Application in Dental Composites : Monomers for Low Shrinking Composites. **2001**, *354* (June 2000), 346–354.

(85) Chung, C.; Kim, J.; Kim, M.; Kim, K.; Kim, K. Development of a New Photocurable Composite Resin with Reduced Curing Shrinkage. **2002**, *18*, 174–178.

(86) Leung, D.; Bowman, C. N. Reducing Shrinkage Stress of Dimethacrylate Networks by Reversible Addition – Fragmentation Chain Transfer. **2012**, 198–204.

(87) Park, H. Y.; Kloxin, C. J.; Fordney, M. F.; Christopher, N. NIH Public Access. **2013**, *28* (8), 888–893.

(88) Gauss, P.; Ligon-auer, S. C.; Griesser, M.; Gorsche, C.; Svajdlenkova, H.; Koch, T.; Moszner, N.; Liska, R. The Influence of Vinyl Activating Groups on b -Allyl Sulfone-Based Chain Transfer Agents for Tough Methacrylate Networks. **2016**, 1417–1427.

(89) Shah, P. K.; Stansbury, J. W.; Bowman, C. N. Application of an Addition-Fragmentation-Chain Transfer Monomer in Di(Meth)Acrylate Network Formation to Reduce Polymerization Shrinkage Stress. *Polym. Chem.* **2017**, *8* (30), 4339–4351.

Chapter 2

Objectives

The scope of this thesis aims to design novel smart materials with high glass transition temperature (T_g), superior mechanical properties, and spatio-temporally controlled dynamic behavior in order to expand the range of practical applications. To achieve this goal, two types of "click" reactions, copper-catalyzed azide-alkyne cycloaddition (CuAAC) and thiol-ene photopolymerizations, are used to form glassy polymer networks, and dynamic moieties capable of reversible addition fragmentation transfer (RAFT) and thiol-thioester exchange (TTE) are incorporated either in the monomer backbones or at the interface of inorganic silica nanoparticles. Herein, I hypothesize that the incorporation of dynamic covalent chemistry (DCC) such as RAFT and TTE in glassy thermosetting resins and composites solve current limitations of thermosets by relaxing internal and applied stresses in their glassy states, both in the resin matrix and at the resin-filler interface, while maintaining superior mechanical properties. In order to test this hypothesis, the following specific aims have guided my research:

Specific Aim 1: Investigate the capability of a highly crosslinked glassy polymer containing moieties capable of dynamic bond exchange to efficiently mediate resin phase stress relaxation in the glassy state.

The development of mechanically strong, high T_g polymer networks that are capable of dynamic bond exchange at ambient temperature while maintaining enhanced mechanical properties has been an ongoing challenge. In the present study, various azide and alkyne monomers containing structurally variable RAFT moieties were designed and synthesized in order to form highly crosslinked, glassy CuAAC photopolymer networks with DCC containing backbones. The *in situ* formation of triazole moieties by CuAAC polymerizations enables a high T_g network with enhanced mechanical properties. The stress relaxation capacity of RAFT-based CuAAC polymers upon light activation in the glassy state was explored. The mechanical properties of RAFT-CuAAC networks such as modulus, toughness, and ductility were determined and compared with structurally analogous control networks without RAFT moieties. In addition, the effect of RAFT

bond exchange on the physical aging behavior of CuAAC polymers, specifically changes in mechanical properties, were elucidated. Lastly, the formation of a 3D-shaped complex object and a surface mechano-patterning are highlighted as potential applications of the RAFT-based CuAAC polymer.

Specific Aim 2: Develop an adaptive interface (AI) platform by introducing moieties capable of dynamic bond exchange at the resin-filler interface of glassy polymer-based composites to promote interfacial stress relaxation in the glassy state and explore the resulting evolution of composite performance.

While stress relaxation by DCC has largely been focused on the resin or continuous phase, little attention has been paid to the interfacial stress relaxation. The interfacial region of composites between resins and fillers of dramatically different modulus results in a highly-stressed region and serves as a primary locus for composite failure. Here, we demonstrate that interfacial stress relaxation is achieved by functionalizing silica nanoparticles (SNP) with a DCC containing silane, and copolymerizing with highly crosslinked, glassy thiol-ene resins. This aim includes implementing two types of dynamic covalent chemistry at the resin-filler interface:

a. Photo-induced RAFT.
b. Anion-mediated thiol-thioester exchange (TTE).

In the present study, the capacity of the aforementioned adaptive interfaces (AI) to relax both the polymerization-induced shrinkage stress and an externally applied stress in the glassy state is demonstrated. The improvement in AI-composite performance; including toughness, tensile strength and fatigue behavior as compared with the control composite is determined. Additionally, the effects of *in situ* interfacial bond exchange during fracture on the crack propagation and the failure mechanisms were explored.

Specific Aim 3: Apply the AI platform to conventional di-methacrylate based dental restorative composites to improve material properties that are critical for long-term durability of dental composites such as polymerization-induced shrinkage stress, fracture toughness, and fatigue behaviors.

Photopolymerizable di-methacrylate composites have been predominantly utilized in dental restorations due to the rapid formation of a highly-crosslinked network with desirable mechanical properties. However, significantly high shrinkage stress is developed during the polymerization, primarily due to early gel-point conversion along with considerable volumetric shrinkage in a restricted environment. This large stress along with the interfacial stress induces microcracking and reduces fracture toughness, resulting in a premature failure of dental composites. In the present study, we aimed to resolve the current limitation of conventional dental composites, by functionalizing SNP with DCC moieties capable of undergoing either radical-mediated RAFT or anionic TTE bond rearrangements and copolymerizing with the conventional di-methacrylate dental resins. The changes in composites performance; including toughness and fatigue behavior enabled by enhanced shrinkage stress, along with the *in situ* stress relaxation when composites under the mechanical loading are explored and compared to control dental composites without DCC moieties at the resin-filler interface.

Specific Aim 4: Incorporate two types of DCC moieties, RAFT and TTE, in the resin matrix and resin-filler interface to further enhance the performance of composites.

The primary focus of this aim is to combine two types of DCC, radical-triggered RAFT and anion-mediated TTE, in both the resin matrix and at the resin-filler interfaces. In specific, RAFT moieties are incorporated in thiol-ene matrix, while SNP are functionalized with TTE moieties to trigger an interfacial exchange reaction. This approach enables the stress relaxation in both locations: (1) within the composite resin matrix when the RAFT-based exchange is activated during polymerization, or during the light exposure. (2) at the resin-filler interface which provides continuous stress relaxation throughout the entire life of the composite. In this study, 4 different composite formulations were examined to determine the effect of the AFT/thioester combination on the composite performance, in which no stress relaxation is enabled through elimination of the AFT functional groups and/or the TTE catalyst. The capacity of all four composites to relax both polymerization stress, and applied stress, along with the resulting improvement in composites mechanical properties are explored. In addition, mechanical testing on polymerization-induced shrinkage stress, fracture toughness and post-polymerization stress relaxation characteristic will be conducted at varying concentration of RAFT monomer, particles loading, and base/nucleophile catalyst to estimate the optimal conditions necessary for efficient stress relaxation.

Chapter 3

Light-Activated Stress Relaxation, Toughness Improvement, and Photoreversible Physical Aging in Glassy Polymer Networks*

A covalent adaptable network (CAN) with high glass transition temperature (T_g), superior mechanical properties including toughness and ductility, and unprecedented spatio-temporally controlled dynamic behavior is prepared by introducing dynamic moieties capable of reversible addition fragmentation chain transfer (RAFT) into photo-initiated copper(I)-catalyzed azide-alkyne cycloaddition (CuAAC)-based networks. While the CuAAC polymerization yields glassy polymers composed of rigid triazole linkages with enhanced toughness, the RAFT moieties in the CuAAC networks undergo bond exchange leading to stress relaxation upon light exposure. This behavior leads to numerous desirable attributes including glassy state photo-induced plasticity, toughness improvement during large deformation, and even photoinduced reversal of the effects of physical aging resulting in the rejuvenation of mechanical and thermodynamic properties in physically-aged RAFT-CuAAC networks that undergo bond exchange in the glassy state. Surprisingly, when an allyl sulfide containing azide monomer (AS-N_3) was used to form the network, the fully cured RAFT-based network exhibited up to 80% stress relaxation in the glassy state (T_g - 45 $^{\circ}$C) under fixed displacement. *In situ* activation of RAFT during mechanical loading resulted in a 50% improvement in elongation to break and 40% improvement in the toughness when compared to the same network without light-activation of RAFT during the tensile testing.

*Manuscript in preparation.

3.1. Introduction

Thermosetting polymers are important industrial materials that possess mechanical robustness, as well as thermal and chemical resistance. These desired properties are attributed to the permanent chemical crosslinking that unfortunately sacrifices the recyclability, malleability, and processability commonly associated with thermoplastic polymers.[1–3] This tradeoff has inspired recent development of covalent adaptive networks (CANs) that dynamically reconfigure the chemical bonds within the network and therefore allow stress relaxation and plastic deformation while maintaining the network connectivity.[4,5] One highly efficient CAN chemistry is the reversible addition fragmentation chain transfer (RAFT) process[6,7] that has enabled applications including surface patterning,[8–10] self-healing,[11] photo-induced shape shifting[12] and toughening of thermosetting composites.[13] Despite its significant industrial potential,[14] the incorporation of CAN chemistry into conventional thermosets has been largely limited to relaxation above the glass transition temperature (T_g).[15] Recently, progress has been made in designing thermosets that possess catalyst-free, low-temperature dynamic properties.[16–20] However, no networks have been reported that have high T_g, and are mechanically robust with the capability of dynamic bond exchange in the glassy state.

Here, we report the designing of polymer networks that possess all these desired attributes: T_g well above ambient temperature, superior ductility, and unprecedented light-activated network reconfiguration in the glassy state. All of these behaviors are achieved by incorporating RAFT agents within networks formed via the photo-initiated copper(I)-catalyzed azide-alkyne cycloaddition (CuAAC) reaction. CuAAC is a highly efficient, orthogonal, “click” reaction that occurs readily under mild conditions[21–24] and which yields homogeneous network structures with low polymerization-induced shrinkage stress.[25–27] Recent work shows that glassy networks with

high T_g are obtained due to the formation of rigid, thermally and chemically stable triazole moieties present at high concentrations within the network(**Scheme 3.1A**).[28–30] By also incorporating the RAFT moiety into the CuAAC networks, we demonstrate light-activated bond-exchange capabilities (**Scheme 3.1B**) within glassy polymer networks, as manifested in enhanced stress relaxation, extended plastic deformation post yielding, and intriguing rejuvenation of mechanical properties in physically aged samples.

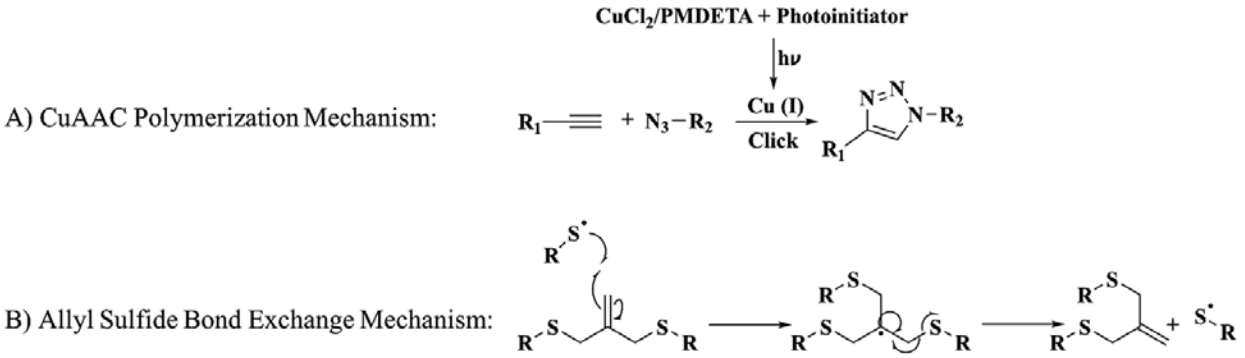

Scheme 3.1. A) Photo-initiated CuAAC polymerization reaction diagram: photoinitiation upon light irradiation, copper reduction to form Cu(I), and 'click' Cu(I)-catalyzed cycloaddition of azides and alkynes to form 1,2,3-triazole adducts. B) RAFT radical mediated allyl sulfide bond rearrangement mechanism.

3.2. Materials and Methods

Detailed synthetic procedures of monomers along with nuclear magnetic resonance (NMR) results are presented in the Supporting Information.

Sample Preparation

CuAAC networks were prepared from stoichiometric mixtures (1:1 azide: alkyne functional group ratio) of di-functional azide (BZ-N_3), tri-functional alkyne (Tri-AK), and 20 mol % of either the

RAFT based di-functional monomers or the analogous control di-functional monomers. $CuCl_2$/PMDETA was utilized as a copper catalyst, while 1 wt% I819 was used as a photoinitiator for CuAAC photopolymerization, and 2 wt% DMPA was used as a latent photoinitiator to induce the bond exchange in the network after polymerization. Since these monomer mixtures are not completely miscible, methanol was used to homogenize the mixture, and this was later removed in vacuo. Samples were photocured with 400-500 nm visible light at 10 mW/cm^2 for 10 min and then post-cured in an oven at 70 °C for 24 h.

Fourier Transform Infrared Spectroscopy

The functional group conversion (presented in the Supporting Information) was monitored via Fourier transform near infrared spectra (Nicolet 6700, Fisher Scientific) in transmission mode, to ensure near-complete conversion. Irradiation of samples placed between NaCl plates was performed using a light guide connected to a mercury lamp (Acticure 4000, EXFO) with a 400-500 nm bandgap filter and an irradiance of 10 mW cm^{-2}. The conversions of the alkyne functional group were determined by monitoring the infrared absorption peaks centered at 6538–6455 cm^{-1} (C≡C-H stretching, overtone).

DMTA Measurements

These measurements were performed with a TA Instruments Q800 DMA in tension mode at a frequency of 1 Hz, using a heating rate of 3 °C min^{-1} to a maximum temperature of 120 °C, to yield the storage (E″) and the tan δ. The glass transition temperature (T_g), was taken to be the temperature at the peak of the tan δ curve. The DMTA specimens were ≈0.1 mm in thickness, 5 mm in width, and 7 mm in length between grips.

Density measurement

A multipycnometer (Quantachrome instruments) was used to measure the density of polymer samples. Each sample with known mass was placed in a 4.5 cm^3 cell and pressurized with helium gas. The release of pressure resulted in the volume expansion of helium gas, which was converted to density of the sample.

Tensile Testing

It was performed using an MTS Exceed E42 universal testing machine with a 500N load cell to give the engineering stress–strain curve, the Young's modulus (determined from the initial linear elastic region of the stress–strain curve), the yield stress (the stress at the maximum), the elongation to break, and the toughness (as measured from the area under the stress–strain curve). Dogbone samples were cut or molded (for brittle specimens) similar to the ASTM dogbone die D638-V,[31] with a 3.15 mm width and 0.1 mm thickness, however the gage length was ≈15 mm rather than the 7.62 mm specified by ASTM D638-V. The specimens were clamped in the grip areas and tested under uniaxial tensile loading at a crosshead speed of 1 mm min^{-1}.

Differential scanning calorimetry

Thermal data were collected using a TA Instruments Q2000 Differential Scanning Calorimeter (DSC) in a N_2 environment using a purge rate of 50 mL/min. 5 mg samples of CuAAC were placed in hermetically sealed aluminum pans. The samples were first equilibrated to 0 °C for 5 minutes followed by heating at a rate of 10 °C/min to 100 °C. The samples were then cooled at a rate of 50 °C/min to 20 °C. Enthalpy calculations were analyzed using Universal Analysis software (TA Instruments).

3.3. Results and Discussion

All RAFT-CuAAC systems reported here consist of (**Figure 3.1A**): a di-functional azide (BZ-N_3), a tri-functional alkyne (Tri-AK), and RAFT-based di-functional monomers (20% molar fraction of all the monomers). The azide:alkyne functional group ratio is 1:1 for all formulations. Each system also contains $CuCl_2$/PMDETA as a copper catalyst, 1 wt% I819 as a visible light sensitive photoinitiator for initiating the CuAAC photopolymerization, and 2 wt% DMPA as a latent ultraviolet sensitive photoinitiator to induce the bond exchange in the network after polymerization. Four different RAFT monomers were synthesized by incorporating allyl sulfide (AS) or trithiocarbonate (TTC), i.e. the RAFT-moieties, into one difunctional azide and three difunctional alkynes. The four monomers were designed to examine both the generality of the network reconfiguration in the RAFT-CuAAC systems and the potential impact of secondary functional groups on the effectiveness of the bond exchange. In comparison, we also prepared control CuAAC systems that are incapable of bond-exchange, by replacing the RAFT-monomers with structurally analogous difunctional monomers that do not contain RAFT moieties (**Figure 3.1A**). Details of the monomer synthesis are provided in the experimental section. After curing, all the CuAAC networks show over 96% conversion (**Table S3.1**).

The RAFT- CuAAC networks based on the above formulations have T_g values ranging from 40 °C to 75 °C, as indicated by the tan δ maximum (**Figure 3.1B**) of the samples from dynamic mechanical analysis (DMA) measurements. Specifically, the T_g value of the four RAFT-CuAAC systems follow the order of, AS-AK_1 < AS-AK_2 < AS-N_3 < TTC-AK_3, which correlates well with the conformational rigidity of the secondary groups in the RAFT monomers: higher T_g for benzene-containing monomers and lower T_g for ester-containing monomers. Consequently, all RAFT-CuAAC polymers display a typical glassy modulus at ambient temperature, ranging from

1.2 to 2.6 GPa (**Figure 3.1C**). In comparison with the RAFT-CuAAC networks, the control CuAAC networks exhibit similar T_g values and storage modulus at ambient conditions (**Figure 3.1B and 1C**), which decouples the effects caused by the bond-exchange process from the other aspects of the polymer network structure. The T_g values, glassy moduli, and rubbery moduli of all CuAAC systems are presented in **Table S3.1**.

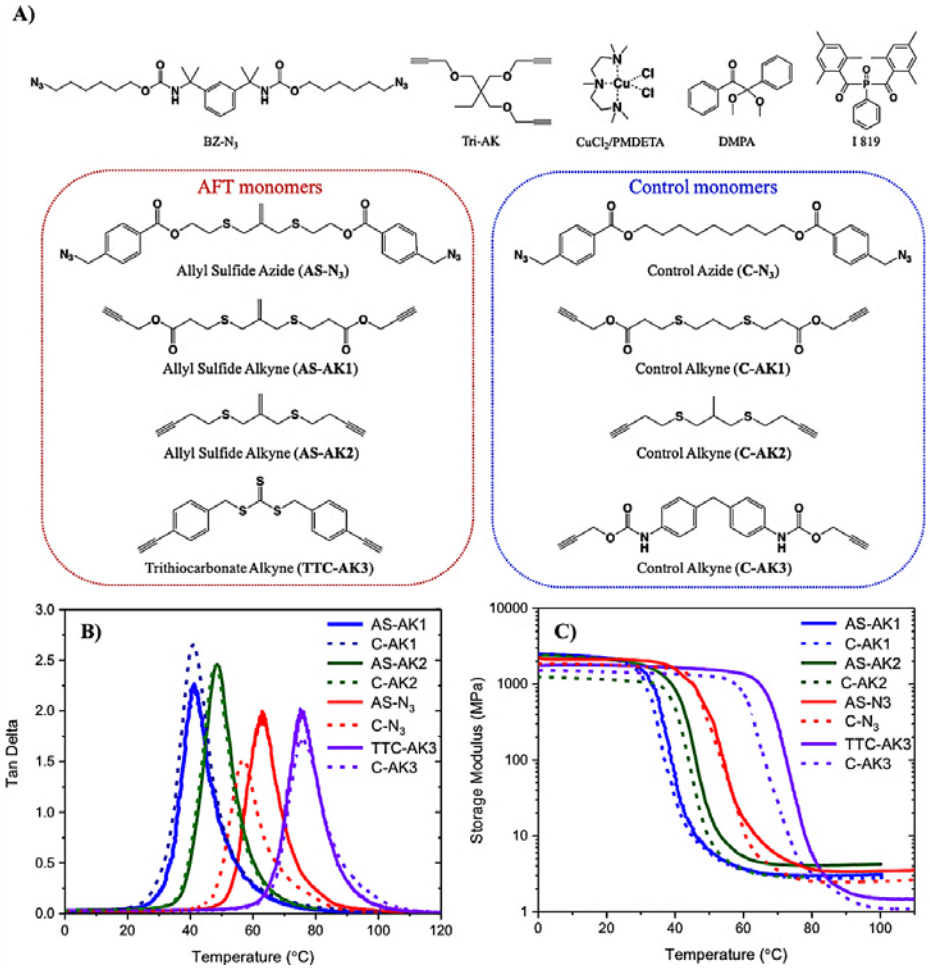

Figure 3.1. A) Monomer structures used in the formulation of CuAAC resin: di-functional azide ($BZ\text{-}N_3$), tri-functional alkyne (Tri-AK), $CuCl_2$/PMDETA, I 819 photoinitiator, and DMPA. Four different RAFT monomers and the corresponding control monomers are presented. Samples were photocured with 400-500 nm visible light at 10 mW/cm^2 for 10 min and then post-cured in an oven at 70 °C for 24 h. B and C) The tan δ curves and storage modulus curves of RAFT-based (solid lines) and corresponding control (dotted lines) CuAAC polymers, obtained from DMTA measurements at 1 Hz.

The stress-relaxation behavior of all the CuAAC systems was examined by observing the time-evolution of stress under constant 5% strain tensile loading, with 5 min UV exposure. Unless specified, all UV exposures to induce bond exchange used 365 nm with a light intensity of 8 mW/cm^2. At high temperatures (T_g + 45 °C) in the rubbery state, AS-AK1, AS-AK2, AS-N_3 and TTC-AK3 networks relax 93%, 80%, 96% and 97% of the total stress, respectively, while the corresponding control-CuAAC networks relax only 5%, 6%, 10%, and 8% of the total stress, respectively (**Figure 3.2A)**. Evidently, the RAFT-moieties enable highly effective network reconfiguration in all four CuAAC systems in the rubbery state, while the control systems yield negligible stress relaxation.

In contrast, in the glassy state, at T_g - 45 °C, all four RAFT-CuAAC systems under 1% strain loading still show significant stress relaxation upon UV exposure: 45%, 60%, 80%, and 90% for AS-AK1, AS-AK2, AS-N3 and TTC-AK3 systems, respectively **(Figure 3.2B)**. Systems with higher T_g values have higher degree of stress relaxation when assessed at the same level below their respective T_g. This level of stress relaxation in the glassy state is unprecedented for similar thermosets. Without the bond-exchange process, typical glassy polymers normally relax 10-20% stress in their glassy state,[6,13,32] as evidenced in the control CuAAC systems where only 20%-25% stress relaxation is observed. The presence of the RAFT moieties enhanced the stress relaxation by 2-4 times when compared with the corresponding control CuAAC system. We further measured the stress relaxation in AS-N_3 sample under identical loading but without UV exposure. Only 20% of the initial stress was relaxed, further validating that the photo-induced RAFT process is the cause of stress relaxation in the glassy RAFT-CuAAC systems. Furthermore, we verified the effectiveness of photo-induced stress relaxation in glassy AS-AK2 sample (T_g – 45 °C) at three different strain levels within the elastic deformation regime (**Figure S3.1**). In situ temperature

measurements made during tensile testing and light exposure with a microthermocouple indicated that only minimal temperature changes of less than 5°C occurred upon light exposure.

Bond-exchange in the CuAAC systems facilitates tuning of the amount of plastic deformation at small strain levels (below the yield point of the polymers). We demonstrate this capability using an AS-N_3 sample as an example because of its relatively high T_g (65 °C). Under a constant loading of 4 N at ambient conditions, 2% total strain is generated in the sample over 2 min. Upon load release, 90% of the total strain is recovered, which is typical for CuAAC networks.[26,30] In stark contrast, under identical creep condition, only 20% of the total strain is recovered if UV exposure is applied (**Figure 3.2C**). In other words, the bond-exchange process raises the plastic strain during creep of AS-N_3 sample by 8 times (from 10% to 80%). In comparison, the control (C-N_3) CuAAC sample recovers 86% of the total strain (or 14% plastic strain) under identical UV exposure, eliminating the potential for the deformation to be explained by a UV-induced temperature rise. To assess further this capability, successful mechano-patterning of glassy AS-N_3 CuAAC films is achieved at ambient condition (T_g - 45 ^{o}C) under low mechanical loading and UV exposure (**Figure 3.2D**) for 15 min. Micro-scale patterns on the contacting mold are faithfully and irreversibly replicated on the glassy AS-N_3 CuAAC films.

The effect of the bond-exchange process on the large deformation behavior of glassy RAFT-CuAAC systems under ambient conditions was investigated. Under uniaxial tensile loading with a strain rate of 0.0011 s^{-1}, except TTC-AK3, all three other RAFT-CuAAC systems tested display highly ductile behavior with extended plastic deformation after yielding **(Figure 3.2E)**. For AS-AK1, AS-AK2, and AS-N_3 systems, the average yield stress values are 11 MPa, 21 MPa, and 30 MPa, respectively, and the average stains-to-break are 560%, 200%, and 120%. Accordingly, the tensile toughness of AS-AK1, AS-AK2, and AS-N_3 are 82, 34, and 26 MJ/m^3.

Such high values of the toughness in CuAAC systems have been attributed to the presence of the triazoles and their capacity for secondary bonding.[30] Comparing the AS-AK1, AS-AK2, and AS-N_3 systems, the increase in tensile strength and decrease in strain-to-failure is associated with the measurements being conducted at ambient temperature which is 20 °C, 30 °C, and 40 °C below the corresponding T_g values of the polymers, respectively.

After reaching 33% tensile strain (post-yielding), all three samples were subjected to 5 min UV exposure to activate the bond exchange process. As a result, the AS-AK1, AS-AK2, and AS-N_3 samples show approximately 15%, 40%, and 50% increase in strain-to-failure, and correspondingly the overall sample toughness (**Figure 3.2E**). In contrast, no enhancement of ductility and toughness is observed in a control sample (C-AK2 CuAAC) under identical loading conditions with UV exposure (**Table S3.2**). Collectively, the above results suggest that the bond-exchange process is highly efficient in glassy RAFT-CuAAC systems both for small deformation and post-yielding large deformation, and RAFT monomers with higher degrees of stress relaxation also show larger enhancements in ductility. Harnessing these unique capabilities, an object with complex 3D shape is illusrtated in **Figure S3.2**, by spatially controlling the photoplasticity of the glassy polymer networks generated both laterally and vertically (gradient along thickness). Such photo-programable complex shape control is of significant interest in a range of applications in aerospace and biomedical devices, which require materials that remotely change shape while preserving other important properties such as mechanical robustness.[12,33]

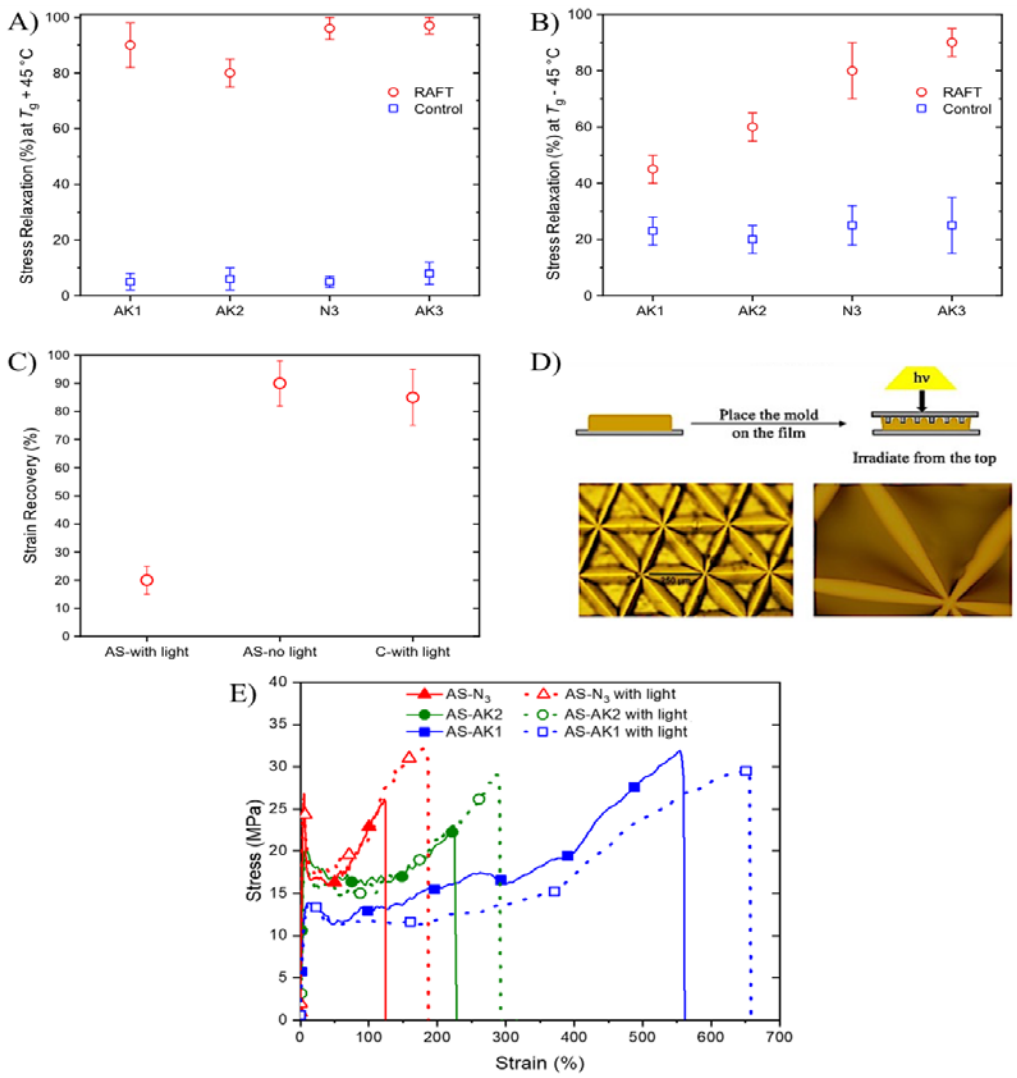

Figure 3.2. A) Photo-induced stress relaxation achieved on fully-cured, 0.1 mm thick sample of both RAFT and control based CuAAC networks at constant 5% strain at T_g + 45 °C. B) Photo-induced stress relaxation achieved on fully-cured, 0.1 mm thick sample of both RAFT and control based CuAAC networks at constant 1% strain at T_g - 45 °C. Each sample was irradiated at the start of the test with 8 mW/cm^2 of 365 nm light for 5 min. C) Strain recovery as quantified using DMTA by applying 4 N constant force on both AS-N_3 and C-N_3 polymer films, with 8 mW/cm^2 of 365 nm light for 2 minutes, while the pre-stretch force still imposed. D) Surface topographies resulting from the surface patterning on RAFT AS-N_3 film using the reflective tape mold to generate micro scale surface patterns. E) Representative runs of tensile testing of three different RAFT-CuAAC polymer systems including AS-N_3 (triangle), AS-AK1 (square), and AS-AK2 (circle). Dotted lines represent the same systems that were radically triggered with 8 mW/cm^2 of 365 nm light during the tensile test at 33% tensile strain for 5 minutes. All specimens were fully-cured, dog bone shaped (15mm in gage length) and tested at a strain rate of 0.0011 s^{-1}.

Recent work shows that triazole-based, glassy CuAAC networks display significant

physical aging phenomenon.[30] Specifically, networks formed by BZ-N_3 and Tri-AK (**Figure 3.1A**) lose most of the ductility after being stored at ambient conditions for as little as 32 h. To examine the aging behavior in the RAFT-CuAAC systems, the AS-AK2 based system was used as an example since it has the intermediate ductility. After being aged at ambient conditions for 72 h, the sample displays significant embrittlement: the strain-to-failure decreases from 200% to 10% (**Figure 3.3A and 3B, Table S3.3**), and accordingly the toughness is reduced from 33 MJ m^{-3} to 3 MJ m^{-3}. At the same time, both the Young's modulus and yield strength increase by 2 fold. Similar aging-induced embrittlement is observed in the control sample (C-AK2 CuAAC, **Figure 3.3B**). Most surprisingly and significantly, the effect of aging-induced embrittlement in the AS-AK2 based CuAAC sample is nearly entirely erased by UV exposure when the exposure occurs after the same 32 h period. As shown in **Figure 3.3A**, 2 min of UV exposure (365 nm, 5 mW/cm^2) on both sides of the samples results in nearly complete recovery of strain-to-failure and even preserves the increased Young's modulus and yield strength (**Table S3.3**). Such a "rejuvenation" is not observed in the aged control sample upon identical UV exposure (**Figure 3.3B and Table S3.3**), indicating that the RAFT-based bond exchange reaction is the underlying cause. This outcome is indicative of an increase in the free volume of the polymer when the RAFT is activated in the glassy state.

The aging and UV-induced "rejuvenation" in the AS-AK2 CuAAC network are also evident in several thermodynamic properties including both relaxation enthalpy **(Figure 3.3C)**. From differential scanning calorimetry (DSC) measurements (**Figure S3.3**), both AS-AK2 and control CuAAC samples display characteristic excess enthalpy (compared with the unaged samples) after 72 h of physical aging, ~ 16 J/g (**Figure 3.3C**). With 2 min of UV exposure on both sides of the aged samples, the excess enthalpy of the AS-AK3 sample decreases to 8 J/g, while no

changes in excess enthalpy were observed for the control sample (**Figure 3.3C and Figure S3.3**). Clearly, the degree of rejuvenation in thermodynamic properties of the AS-AK3 sample is less than that of the ductility (**Figure 3.3A and 3B**). Note that the impact of physical aging in polymers is also erased for samples with and without the capacity for AFT by thermal cycling above the T_g of the polymer. However, photo-induced physical aging reversal and the corresponding erasure of the thermal history has never before been reported in the absence of high temperatures above the T_g.

All of the above results show that the RAFT enabled bond exchange process in CuAAC networks dramatically enhances the stress relaxation in elastically deformed samples both above and below T_g (**Figure 3.2A and 2B**), increases ductility after yielding (**Figure 3.2E**), and (partially) erases the physical aging-induced changes in mechanical and thermodynamic properties (**Figure 3.3**). The UV induced bond-exchange in the glassy state is unique to the combination of the RAFT and CuAAC system elements. For example, a RAFT-containing thiol-ene network was synthesized with a similar degree of crosslinking, monomer structure, and RAFT monomer concentration (**Figure S3.4**) as the RAFT-based AS-AK1 CuAAC system. Despite highly efficient stress relaxation in the rubbery state,[7] the RAFT-thiol-ene network shows no enhanced photo-induced stress relaxation in the glassy state (T_g - 45 ^{o}C) (**Figure S3.4**). Combining all these observations, due to the presence of the triazole structures in molar concentrations, we hypothesize that the glassy state of the CuAAC networks contain higher degrees of free volume as evidenced by the significant aging effect, which enables local segment mobility that is sufficient for the bond-exchange process to occur.[34] Once activated, the geometric changes and ratcheting like behavior of the addition-fragmentation reaction leads to a further increase in the free volume that reverses the effects of physical aging.

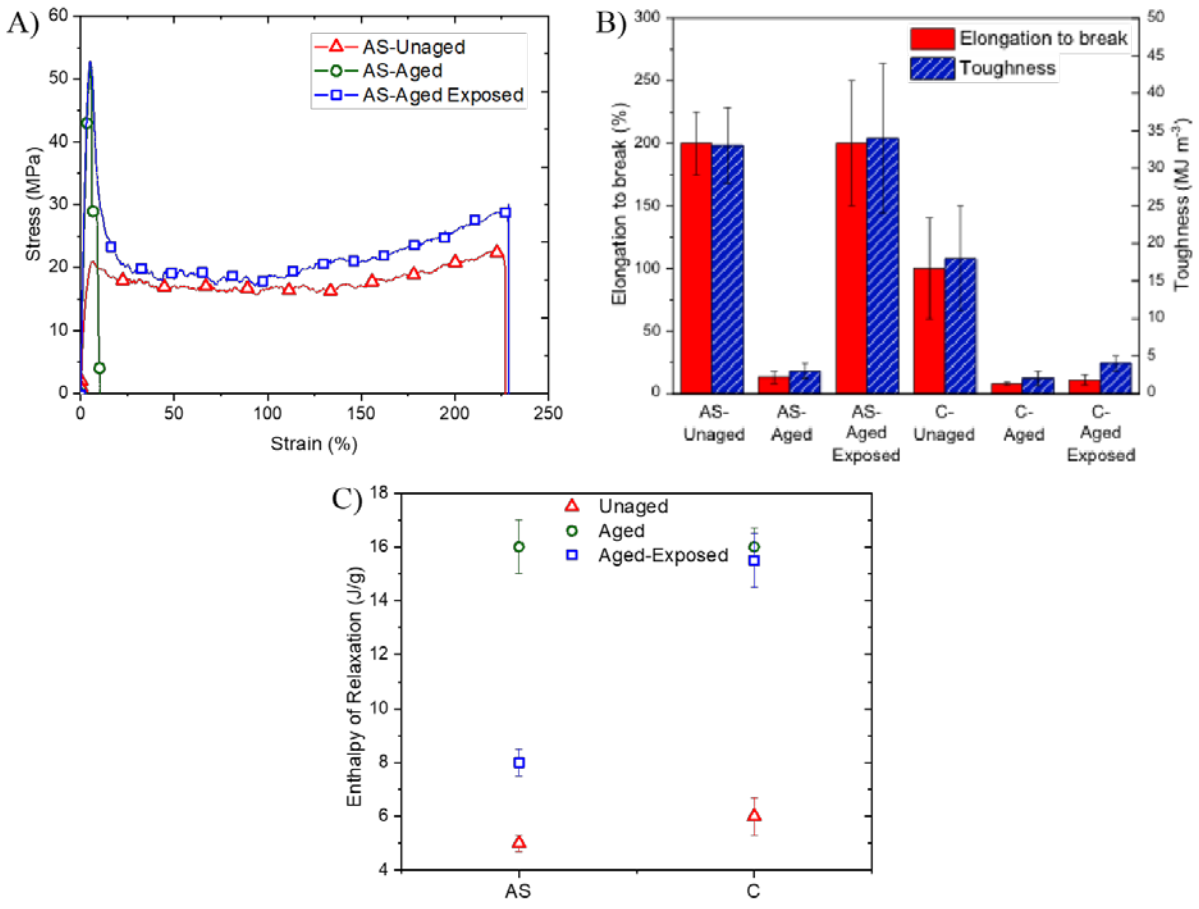

Figure 3.3 A) Tensile testing of three different RAFT AS-AK2 polymer systems: Unaged by heating the film to 100 °C (>T_g) before tensile testing (triangle), aged for 72 hr (circle), and aged for 72 hr following exposure to UV-light for 2 min on each side before mechanical testing (square). B) Elongation to break and toughness of unaged, aged, and aged then exposed to 5 mW/cm^2 of UV-light for 2 min on each side after ageing and before tensile testing for both RAFT based AS-AK2 and control C-AK2 polymer films. All specimens were fully-cured, dog bone shaped (15 mm in gage length), and tested at strain rate of 0.0011 s^{-1}. C) Enthalpy of relaxation (J/g) for AS-AK2 and C-AK2 samples before ageing, after 3 days of ageing, and after 3 days of ageing but subsequent exposure to 5 mW/cm^2 UV-light before the density measurement.

3.4. Conclusions

In conclusion, a series of polymer networks was prepared by incorporating reversible addition fragmentation transfer (RAFT) reactions into photo-initiated copper(I)-catalyzed azide-alkyne cycloaddition (CuAAC)-based polymer networks. These crosslinked polymers are capable of network reconfiguration not only in the rubbery state but also within the glassy state. Upon light

activation, the RAFT process enables the CuAAC networks to significantly increase the degree of stress relaxation during elastic deformation, improve the tensile toughness during large deformation, and reverse the effects of physical aging resulting in the rejuvenation of the mechanical and thermodynamic characteristics. Such a unique system will inspire a broad range of applications of active materials from complex shape programming to stimuli-responsive actuation.

3.5. Acknowledgments

The authors acknowledge financial support from the National Science Foundation (NSF DMR 1310528) and the National Institutes of Health (NIH 1U01DE023777).

3.5. Supporting information

Mechanical properties for all RAFT and control CuAAC samples:

Table S3.1: DMTA mechanical properties for various RAFT-CuAAC systems .

	Conversion (%)	T_g (°C) from tan δ max	Storage modulus at ambient (GPa)	Rubbery modulus at T_g + 30 °C (MPa)
AS-AK1	98 ± 1	40	2.6	3
C-AK1	98 ± 2	40	2.5	2.8
AS-AK2	97 ± 1	50	2.1	4.4
C-AK2	98 ± 1	48	1.2	2.8
AS-N_3	96 ± 1	63	2.4	4.5
C-N_3	98 ± 2	58	1.9	3.2
TTC-AK3	99 ± 1	75	1.8	1.5
C-AK3	98 ± 1	70	1.5	1.1

Photo-induced stress relaxation in glassy AS-AK2 sample (T_g – 45 °C) at three different strain level within the elastic deformation regime:

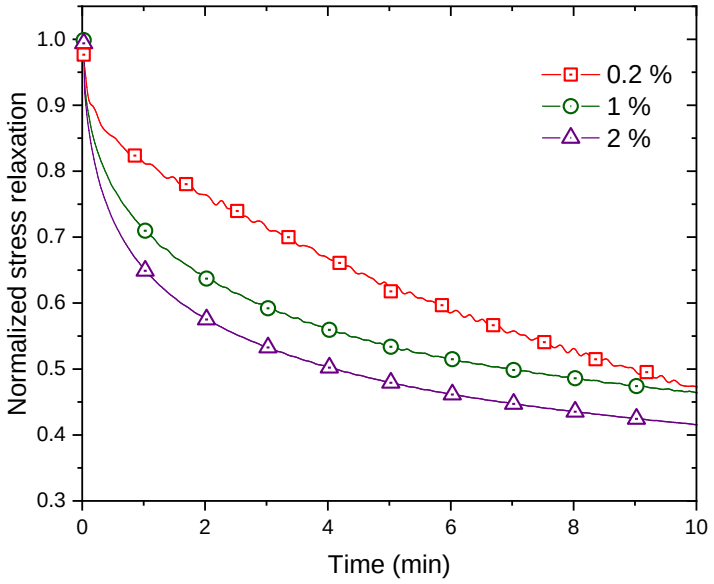

Figure S3.1. Photo-induced stress relaxation achieved on fully-cured (conversion of ~99%) 0.1 mm thick sample of AS-AK2 CuAAC network at different strain (0.2%, 1% and 2%). Each sample was irradiated at the start of the test with 8 mW/cm2 of 365 nm light for 5 min at T_g - 45 °C.

Mechanical properties of AS-N_3, AS-AK1, AS-AK2 and C-AK2 CuAAC polymer systems, either with or without light exposure:

Table S3.2. Mechanical properties of three different RAFT-CuAAC polymer systems, AS-N_3, AS-AK1, AS-AK2, and control system, C-AK2, either with or without light exposure. Each sample was fully cured, dog bone shaped, and tested at a displacement rate of 0.0011 s^{-1}. The sample which requires light exposure was radically irradiated with 8 mW/cm^2 of 365 nm light during the tensile test from 33% strain for 5 minutes.

	Tensile yield stress (MPa)	Tensile Young's modulus (MPa)	Tensile toughness (MJ m^{-3})	Tensile elongation at break (%)
AS-AK1	11 ± 3	390 ± 60	82 ± 23	560 ± 40
AS-AK1 with light	10 ± 3	370 ± 20	92 ± 17	640 ± 20
AS-AK2	21 ± 4	800 ± 80	34 ± 3	200 ± 10
AS-AK2 with light	24 ± 5	870 ± 120	50 ± 7	280 ± 20
C-AK2	25 ± 4	800 ± 80	20 ± 10	100 ± 60
C-AK2 with light	23 ± 7	750 ± 100	17 ± 8	110 ± 50
AS-N_3	30 ± 7	950 ± 110	26 ± 8	120 ± 10
AS-N_3 with light	27 ± 3	1010 ± 90	37 ± 1	180 ± 10

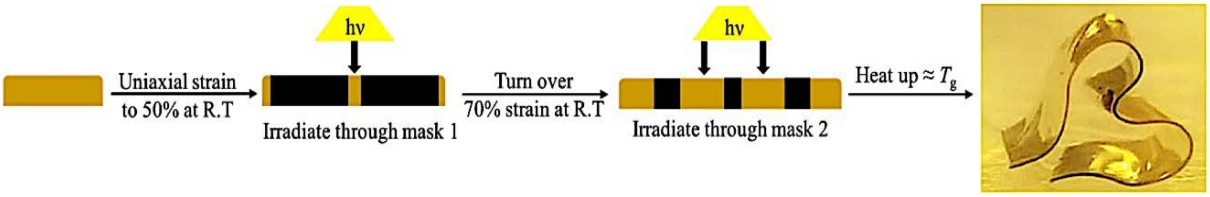

Figure S3.2. Fabrication process of origami structure, following a modified procedure from literature.[33] Step 1: An AS-AK2 strip containing a UV photo-absorber (1 wt% Tinuvin 5060) was stretched up to 50% of its original length, maintained at a fixed strain. Step 2: the sample was released from clamps and irradiated with 20 mW/cm^2 of 365 nm light through photomask 1. Step 3: the sample was flipped over to the other side and stretched further to 70% strain. Step 4: the sample was released and irradiated through photo mask 2. Step 5: the sample was heated in water bath to 50 °C. The light intensity became gradually reduced through the thickness of the optically thick film, which generated a gradient in stress relaxation and subsequent bending after annealing the sample to achieve mechanical equilibrium, leading to the formation of the heart shape as shown above.

Ageing and photo-induced rejuvenation of aged RAFT-CuAAC glassy polymer:

Table S3.3. Mechanical properties for AS-AK2 and C-AK2 samples before aging, after 3 days of aging, and after 3 days of aging following exposure to 5 mW/cm^2 of UV-light before mechanical testing.

Sample	Tensile yield stress (MPa)	Tensile elongation at break (%)	Tensile toughness (MJ m^{-3})	Tensile Young's modulus (MPa)
AS-AK2 (Unaged)	22 ± 4	200 ± 30	33 ± 5	800 ± 75
AS-AK2 (Aged)	50 ±15	10 ± 5	3 ±1	1500 ±150
AS-AK2 (Aged then exposed)	45 ± 5	200 ± 50	34 ± 3	1600 ± 130
C-AK2 (Unaged)	25 ± 4	100 ± 60	20 ± 10	800 ± 80
C-AK2 (Aged)	50 ± 10	8 ± 1	2 ± 1	1400 ± 200
C-AK2 (Aged then exposed)	54 ± 4	10 ± 4	4 ± 1	1400 ± 300

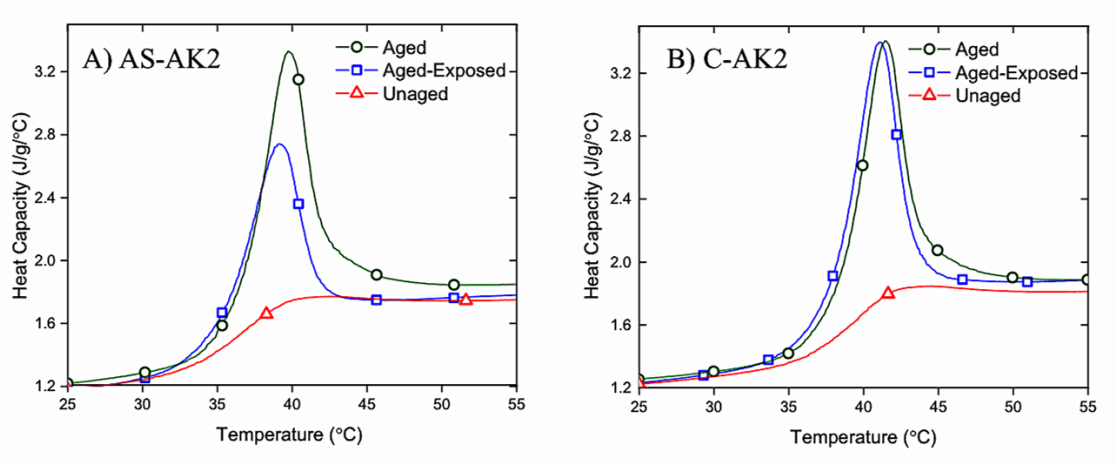

Figure S3.3. Heat capacity as a function of temperature of both AS-AK2 (A) and C-AK2 (B) systems at various conditions including unaged by heating above the T_g, aged for 3 days at ambient temperature, and exposed to UV-light after ageing for 3 days without heating.

Photo-induced stress relaxation of RAFT-thiol-ene polymer network in glassy state:

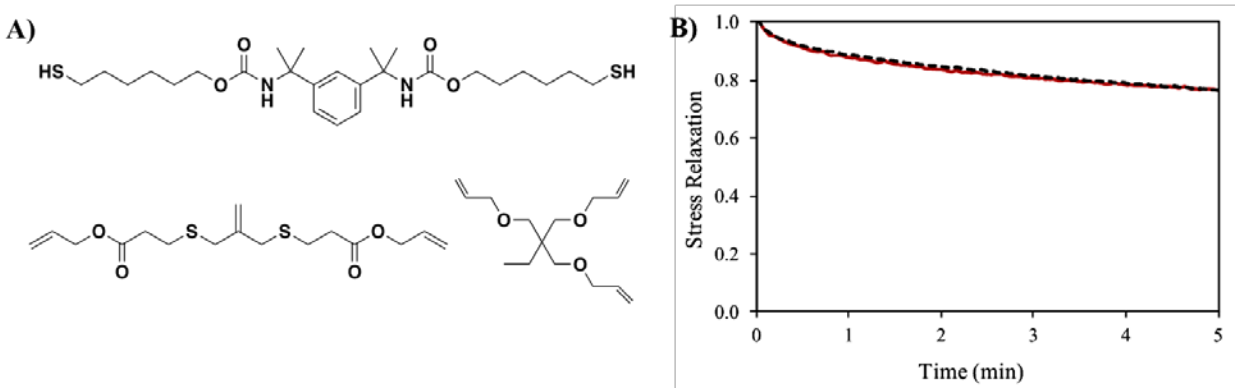

Figure S3.4. A) Monomer structures used in the formulation of RAFT-based Thiol-ene network. B) Post polymerization stress relaxation was measured on a fully cured, thermally cycled sample (0.1 mm in thickness) of RAFT-based thiol-ene network. Red solid line represents RAFT-based thiol-ene sample without light exposure. Dotted black lines represent the same system that was irradiated with 8 mW/cm^2 of 365 nm light for 5 minutes in its glassy state at -50 °C (T_g - 45 °C). The RAFT-based thiol-ene resin was composed of a molar ratio per functional group of 1: 1 (thiol: ene) with 1 wt% of I819 and 2 wt% of DMPA. Samples were photocured with 400-500 nm visible light at 10 mW/cm^2 for 10 min and then post-cured in an oven at 70 °C for 24h.

3.6. References

(1) Ligon-Auer, S. C.; Schwentenwein, M.; Gorsche, C.; Stampfl, J.; Liska, R. Toughening of Photo-Curable Polymer Networks: A Review. *Polym. Chem.* **2016**, *7* (2), 257–286.

(2) Crivello, J. V.; Reichmanis, E. Photopolymer Materials and Processes for Advanced Technologies. *Chem. Mater.* **2014**, *26* (1), 533–548.

(3) Jeffrey, G.; Bruce, P. R. *Thermosets*; Major Reference Works; 2017.

(4) Kloxin, C. J.; Bowman, C. N. Covalent Adaptable Networks: Smart, Reconfigurable and Responsive Network Systems. *Chem. Soc. Rev.* **2013**, *42* (17), 7161–7173.

(5) Kloxin, C. J.; Scott, T. F.; Adzima, B. J.; Bowman, C. N. Covalent Adaptable Networks (CANs): A Unique Paradigm in Cross-Linked Polymers. *Macromolecules* **2010**, *43* (6), 2643–2653.

(6) Scott, T. F.; Schneider, A. D.; Cook, W. D.; Bowman, C. N. Photoinduced Plasticity in Cross-Linked Polymers. *Science* **2005**, *308* (5728), 1615–1617.

(7) Kloxin, C. J.; Scott, T. F.; Bowman, C. N. Stress Relaxation via Addition−Fragmentation Chain Transfer in a Thiol-Ene Photopolymerization. *Macromolecules* **2009**, *42* (7), 2551–2556.

(8) Cox, L. M.; Li, Z.; Sowan, N.; Nair, D.; Xiao, J.; Bowman, C. N.; Ding, Y. Reconfigurable Surface Patterns on Covalent Adaptive Network Polymers Using Nanoimprint Lithography. *Polymer* **2014**, *55* (23), 5933–5937.

(9) Kloxin, C. J.; Scott, T. F.; Park, H. Y.; Bowman, C. N. Mechanophotopatterning on a Photoresponsive Elastomer. *Adv. Mater.* **2011**, *23* (17), 1977–1981.

(10) Cox, L. M.; Sun, X.; Wang, C.; Sowan, N.; Killgore, J. P.; Long, R.; Wu, H. A.; Bowman, C. N.; Ding, Y. Light-Stimulated Permanent Shape Reconfiguration in Cross-Linked Polymer Microparticles. *ACS Appl. Mater. Interfaces* **2017**, *9* (16), 14422–14428.

(11) Amamoto, Y.; Kamada, J. pd.; Otsuka, H.; Takahara, A.; Matyjaszewski, K. Photoinduced Self-Healing of Covalently Cross-Linked Polymers through Reshuffling of Trithiocarbonate Units. *Angew. Chemie - Int. Ed.* **2011**, *50* (7), 1660–1663.

(12) Mu, X.; Sowan, N.; Tumbic, J. a.; Bowman, C. N.; Mather, P. T.; Qi, H. J. Photo-Induced Bending in a Light-Activated Polymer Laminated Composite. *Soft Matter* **2015**, *11* (13), 2673–2682.

(13) Sowan, N.; Cox, L. M.; Shah, P. K.; Song, H. B.; Stansbury, J. W.; Bowman, C. N. Dynamic Covalent Chemistry at Interfaces: Development of Tougher, Healable Composites through Stress Relaxation at the Resin-Silica Nanoparticles Interface. *Adv. Mater. Interfaces* **2018**, 1800511.

(14) Kloxin, C. J.; Bowman, C. N. Covalent Adaptable Networks: Smart, Reconfigurable and Responsive Network Systems. *Chem. Soc. Rev.* **2013**, *42* (17), 7161–7173.

(15) Denissen, W.; Rivero, G.; Nicolaÿ, R.; Leibler, L.; Winne, J. M.; Du Prez, F. E. Vinylogous Urethane Vitrimers. *Adv. Funct. Mater.* **2015**, *25* (16), 2451–2457.

(16) Fortman, D. J.; Brutman, J. P.; Cramer, C. J.; Hillmyer, M. A.; Dichtel, W. R. Mechanically Activated, Catalyst-Free Polyhydroxyurethane Vitrimers. *J. Am. Chem. Soc.* **2015**, *137* (44), 14019–14022.

(17) Ying, H.; Zhang, Y.; Cheng, J. Dynamic Urea Bond for the Design of Reversible and Self-Healing Polymers. *Nat. Commun.* **2014**, *5*, 1–9.

(18) Cash, J. J.; Kubo, T.; Bapat, A. P.; Sumerlin, B. S. Room-Temperature Self-Healing Polymers Based on Dynamic-Covalent Boronic Esters. *Macromolecules* **2015**, *48* (7), 2098–2106.

(19) Oehlenschlaeger, K. K.; Guimard, N. K.; Brandt, J.; Mueller, J. O.; Lin, C. Y.; Hilf, S.; Lederer, A.; Coote, M. L.; Schmidt, F. G.; Barner-Kowollik, C. Fast and Catalyst-Free Hetero-Diels-Alder Chemistry for on Demand Cyclable Bonding/Debonding Materials. *Polym. Chem.* **2013**, *4* (16), 4348–4355.

(20) Röttger, M.; Domenech, T.; Van Der Weegen, R.; Breuillac, A.; Nicolaÿ, R.; Leibler, L. High-Performance Vitrimers from Commodity Thermoplastics through Dioxaborolane Metathesis. *Science* **2017**, *356* (6333), 62–65.

(21) Kolb, H. C.; Finn, M. G.; Sharpless, K. B. Click Chemistry: Diverse Chemical Function from a Few Good Reactions. *Angew. Chemie - Int. Ed.* **2001**, *40* (11), 2004–2021.

(22) Tasdelen, M. A.; Yagci, Y. Light-Induced Copper(I)-Catalyzed Click Chemistry. *Tetrahedron Lett.* **2010**, *51* (52), 6945–6947.

(23) Rostovtsev, V. V.; Green, L. G.; Fokin, V. V.; Sharpless, K. B. A Stepwise Huisgen Cycloaddition Process: Copper(I)-Catalyzed Regioselective "Ligation" of Azides and Terminal Alkynes. *Angew. Chemie - Int. Ed.* **2002**, *41*, 2596–2599.

(24) Tornøe, C. W.; Christensen, C.; Meldal, M. Peptidotriazoles on Solid Phase: [1,2,3]-Triazoles by Regiospecific Copper(I)-Catalyzed 1,3-Dipolar Cycloadditions of Terminal Alkynes to Azides. *J. Org. Chem.* **2002**, *67* (9), 3057–3064.

(25) Song, H. B.; Sowan, N.; Shah, P. K.; Baranek, A.; Flores, A.; Stansbury, J. W.; Bowman, C. N. Reduced Shrinkage Stress via Photo-Initiated Copper(I)-Catalyzed Cycloaddition Polymerizations of Azide-Alkyne Resins. *Dental Materials*. **2016**, *32*,11.

(26) Alzahrani, A. A.; Saed, M.; Yakacki, C. M.; Song, H. B.; Sowan, N.; Walston, J. J.; Shah, P. K.; McBride, M. K.; Stansbury, J. W.; Bowman, C. N. Fully Recoverable Rigid Shape Memory Foam Based on Copper-Catalyzed Azide-Alkyne Cycloaddition (CuAAC) Using a Salt Leaching Technique. *Polym. Chem.* **2018**, *9* (1), 121–130.

(27) Song, H. B.; Baranek, A.; Bowman, C. N. Kinetics of Bulk Photo-Initiated Copper(I)-Catalyzed Azide-Alkyne Cycloaddition (CuAAC) Polymerizations. *Polym. Chem.* **2016**, *7*, 603–612.

(28) Gong, T.; Adzima, B. J.; Baker, N. H.; Bowman, C. N. Photopolymerization Reactions Using the Photoinitiated Copper (I)-Catalyzed Azide-Alkyne Cycloaddition (CuAAC) Reaction. *Adv. Mater.* **2013**, *25*, 2024–2028.

(29) Adzima, B. J.; Tao, Y.; Kloxin, C. J.; DeForest, C. a; Anseth, K. S.; Bowman, C. N. Spatial and Temporal Control of the Alkyne-Azide Cycloaddition by Photoinitiated Cu(II) Reduction. *Nat. Chem.* **2011**, *3* (3), 256–259.

(30) Song, H. B.; Baranek, A.; Worrell, B. T.; Cook, W. D.; Bowman, C. N. Photopolymerized Triazole-Based Glassy Polymer Networks with Superior Tensile Toughness. *Adv. Funct. Mater.* **2018**, *28* (22), 1–9.

(31) ASTM D638-02a, Standard Test Method for Tensile Properties of Plastics, ASTM International, West Conshohocken, 2002.

(32) Capaldi, F. M.; Boyce, M. C.; Rutledge, G. C. Molecular Response of a Glassy Polymer to Active Deformation. **2004**, *45*, 1391–1399.

(33) Ryu, J.; D'Amato, M.; Cui, X.; Long, K. N.; Jerry Qi, H.; Dunn, M. L. Photo-Origami-Bending and Folding Polymers with Light. *Appl. Phys. Lett.* **2012**, *100*, 161908.

(34) K. Ganesh, R. Nagarajan, J. L. D. Rate of Gas Transport in Glassy Polymers: A Free Volume Based Predictive Model. *Ind. Eng. Chem. Res.* **1992**, *31*, 746–755.

Chapter 4

Dynamic Covalent Chemistry at Interfaces: Development of Tougher, Healable Composites through Stress Relaxation at the Resin-Silica Nanoparticles Interface*

The interfacial region in composites that incorporate filler materials of dramatically different modulus relative to the resin phase acts as a stress concentrator and becomes a primary locus for composite failure. We introduce a novel adaptive interface (AI) platform formed by coupling moieties capable of dynamic covalent chemistry (DCC) to the resin-filler interface to promote stress relaxation. Specifically, silica nanoparticles (SNP) are functionalized with a silane capable of addition fragmentation chain transfer (AFT), a process by which DCC-active bonds are reversibly exchanged upon light exposure and concomitant radical generation, and copolymerized with a thiol-ene resin. At a fixed SNP loading of 25 wt%, the toughness (2.3 $MJ.m^{-3}$) is more than doubled and polymerization shrinkage stress (0.4 MPa) is cut in half in the AI composite relative to otherwise identical composites that possess a passive interface (PI) with similar silane structure, but without the AFT moiety. In situ activation of the AI during mechanical loading results in 70 % stress relaxation and three times higher fracture toughness than the PI control. When interfacial DCC was combined with resin-based DCC, the toughness was improved by 10 times relative to the composite without DCC in either the resin or at the resin-filler interface.

*Manuscript appears under the same tittle in *Adv. Mater. Interfaces* 2018, 5, 1800511.

4.1. Introduction

For decades, nanoparticles have been introduced into polymerizable resins to form composites with mechanical properties that combine desired physical and mechanical properties of the constituent phases.[1] Clay reinforced resins emerged in the early 1900's, but interest within the scientific community surged in 1993 when Toyota researchers reported the incredible increases in yield and tensile strengths exhibited by nylon 6 when combined with montmorillonite.[2] Since that time enormous effort has been invested into enhancing the performance of polymer nanocomposites, due in part to the enormous surface area associated with nanofillers, which cause the particle-polymer interfaces to play a crucial role in a great number of physical and chemical phenomena responsible for targeting desired properties for several applications.[1] However, it is also known that these inorganic particles, with their significantly higher modulus and generally lower thermal expansion, act as stress concentrators,[3,4] and this behavior leads to particle-matrix debonding and void formation, which significantly influences the failure of composite materials.[5,6] Generally, the mechanical properties of particulate-filled polymer nanocomposites are affected by particle size, particle content and particle/matrix interfacial adhesion, which is the most important factor for effective stress transfer between the particles and the matrix.[3] Since the adhesive strength at the filler interface determines the stress transfer between the components, several techniques have been developed to improve the interactions between the fillers and the surrounding polymer such as bonding the filler to the resin using SAMs[7] and surface modification of nanoparticles.[3,6,8] However, these techniques improve the efficiency of stress transfer at the interface but do not eliminate the issue of stress concentration or enable stress relaxation. Obviously, enabling stress reduction at this interface would dramatically impact the broad field of polymer composites, especially since numerous applications such as coatings, structural materials, dental materials, and

others would benefit from enhanced mechanical performance associated with low polymerization stress, resistance to crack propagation and extremely high toughness that would result from a reduction in interfacial stress.[9,10]

With these potential benefits in mind, here, a new set of adaptive interfaces is introduced which overcome the limitations of polymer nanocomposites using dynamic covalent chemistry (DCC) to induce triggerable interfacial bond exchange resulting in stress relaxation (significantly and on-demand) while retaining a strong, covalent chemical attachment between the matrix and filler phases.

Covalent adaptable networks (CANs) are crosslinked polymers, capable of relaxing internal stress *via* bond rearrangement within the networks in response to the application of a triggering stimulus such as light or heat. This phenomenon is achieved by implementing one of several DCC motifs[11] such as reversible exchange reactions including addition fragmentation chain transfer moieties (either allyl sulfide[12,13]or trithiocarbonates[14,15]), cinnamates,[16] thiuram disulfides,[17] metal-catalyzed transesterification[18–20] and through reversible addition reactions such as the Diels–Alder reaction.[21] This dynamic bond behavior gives CANs the ability to act as a bridge between thermosets and thermoplastics, given that they can be remolded after forming a network while maintaining many useful proprieties associated with thermosets such as mechanical strength and solvent resistance.[11] Specifically, addition-fragmentation chain transfer (AFT), which involves a reversible radical-mediated bond exchange process, has been studied in bulk materials, to synthesize polymer network with excellent stress relaxation characteristics,[22–24] to create physical patterns within or on polymer substrates,[25,26] to control the introduction, exchange, and/or removal of biochemical epitopes in hydrogel networks,[27] and to undergo self-healing.[14] With few exceptions, despite the unique behavior of this type of polymeric materials, their use in real

industrial applications is often limited since CAN's are often relatively soft materials.[28] To improve their material performance, recent effort has been directed towards designing mechanoresponsive CANs-based composites to expand the usage of the re-processible, remoldable and recyclable materials. Organic nanoparticles with aggregation induced emission (AIE) properties based on dynamic bonds have previously been developed.[29–31] Fiber-reinforced composites,[32] carbon nanotube composites,[33] and silica nanocomposites[34] made of a dynamic epoxy resin have been investigated. Also, transesterification-based shape memory composites based on graphene-filled vitrimers were prepared.[35] However, all of these approaches implement the DCC throughout the resin and fail to implement the desired DCC at the polymer-matrix interface where stress is concentrated, contributing to composite failure.

Here, SNPs were functionalized using a silane that had a thiol-terminated AFT moiety capable of photochemical bond exchange that was copolymerized with a thiol-ene resin. The interfacial dynamic covalent chemistry (DCC) employed at the composite interfaces, not only covalently bonds the resins to the filler as is often done with other filler modifications to promote adhesion between the filler and resin, but here this approach also creates composite interfaces capable of stress relaxation and dynamic bond exchange. While DCC approaches such as AFT,[14,15] Diels-Alder,[21,36] transesterification[18] and others have been used extensively to promote healing and other desirable aspects in conventional materials,[11,32,37] the localization of a dynamic covalent bond to the interface has been little if ever explored, particularly relative to controls in which no such bond exchange is possible. The evolution of material properties including toughness, tensile strength, polymerization shrinkage stress and the recovery of the dissipative energy in covalently crosslinked, relatively glassy, photo-polymerized thiol-ene composites was explored for both AI and PI-based composites. The effect of *in situ* interfacial AFT bond exchange during the fracture

process on the fracture toughness as well as the composite failure mechanism was investigated. Furthermore, the effect of interfacial DCC (adaptive interface) was compared with the effectiveness of resin-based DCC (adaptive network). Finally, the AI was combined with the AN to further improve the composite performance.

4.2. Materials and Methods

Materials

Synthesis of 2-Methylene-1,3-Propanedithiol: Allyl dithiol was synthesized according to a previously reported method.[38]

Synthesis of Allyl sulfide (AFT) based silane: A solution of 3-(triethoxysilyl) propyl isocyanate 5.00 g (20.2 mmol, 1.00 equiv) in 200 mL THF with 5 mol% triethylamine as a base catalyst (1.00 mmol, 0.10 g) was added in a round bottom flask and purged under nitrogen. The reaction mixture was allowed to stir for 5 min, followed by a dropwise addition of 2-Methylene-1,3-Propanedithiol 6.08 g (50.5 mmol, 2.50 equiv), then allowed the reaction mixture to stir at room temperature for 24 h. THF was evaporated and the obtained product was purified by column chromatography using a hexane/ethyl acetate mixture (8:2) as eluent and dried *in vacuo* as a colorless oil with 70% yield. ^{1}H NMR (400 MHz, chloroform-*d*, δ): 0.64 (m, 2H), 1.25 (t, 9H), 1.49 (d, 1H), 1.66 (p, 2H), 3.23 (m, 2H), 3.31 (q, 2H), 3.36 (d*t*, 2H), 3.84 (q, 6H) , 5.07 (p, 2H), 5.78 (s, 1H); ^{13}C NMR (101 MHz, chloroform-*d*, δ): 7.73, 14.21, 18.30, 24.13, 31.24, 33.61, 43.40, 58.53, 60.38, 77.23, 117.64, 137.73, 164.24.

Synthesis of the control non-AFT silane: The synthesis of the control non-AFT silane is analogous to the procedure described above for the allyl sulfide (AFT) based silane, where the commercially available 1,3-Propanedithiol replaces the 2-Methylene-1,3-Propanedithiol in the

synthesis above). ^{1}H NMR (400 MHz, chloroform-*d*, δ): 0.64 (m, 2H), 1.24 (t, 9H), 1.35 (t, 1H), 1.66 (p, 2H) 1.94 (m, 2H), 2.68 (q, 2H), 3.02 (t, 2H), 3.31 (q, 2H), 3.84 (q, 6H), 5.78 (s, 1H); ^{13}C NMR (101 MHz, chloroform-*d*, δ): 7.73, 14.21, 18.30, 22.98, 23.08, 28.24, 34.53, 43.66, 58.53, 60.38, 77.23, 166.70.

Synthesis of 2-methylpropane-1,3-di(thioethyl vinyl ether) (MeDTVE) and 2-Methylene-propane-1,3-di(thioethyl vinyl ether) (MDTVE) followed the procedure found in reference.[39]

Filler functionalization

4.00 g of silica particles (Schott, OX50, 40 nm) were first taken in a glass tube and heated at 165 °C under vacuum using a Buchi heater/condenser for 3 h. The dried nanoparticles were then transferred to a 250 mL bottom rounded flask containing 200 mL of anhydrous toluene supplemented with 2.00 g of either AFT based silane or our control non-AFT silane pre-reacted for 10 minutes with 2.00 g of n-propylamine. The reaction mixture was then refluxed at 120 °C for 24 h. After sinalization of nanoparticle, the liquid suspension was centrifuged and the solid pellets collected thoroughly, and washed with toluene (3X ≈25 mL) and methylene chloride (3X ≈25 mL) in two separate washing/centrifugation cycles. Finally, the washed filler particles were dried under vacuum overnight at 70 °C. The thiol functionalized fillers were analyzed by DRIFT FT-IR spectroscopy and thermogravimetry (TGA). The 2 wt% mass loss difference between silanized and unfunctionalized fillers suggests successful functional group grafting on the surface of glass particles in each case (Figure S4). Also, the DRIFT FT-IR characterization provides evidence of silanol group disappearance around 3745 cm^{-1}, implying successful surface modification (Figure S5).

Sample preparation

Stoichiometric mixtures of a PETMP, TATATO (1:1 molar ratio of thiol:ene), with 1 wt% of I819 as visible light photoinitiator, and 2 wt% of I65 as UV photoinitiator, and 5-50 wt% of SNPs, either the AFT-functionalized to generate the AI or the corresponding negative control to generate the PI were prepared. Silanized fillers and resins were blended in a speedmixer (DAC 150 FVZ, Flakteck) to ensure homogenous formulations. Samples were photocured with 400-500 nm visible light at 50 mW/cm^2 for 20 min and then post-cured in an oven at 100 ˚C for 24 h.

Fourier Transform Infrared Spectroscopy

An FTIR spectrometer (Nicolet 6700) connected to a tensometer via fiber optic cables was used to monitor the real-time polymerization kinetics in concert with stress measurements. Samples were placed between two cylindrical quartz rods, and 50 mW/cm^2 light was irradiated from the bottom rod using a light guide connected to a mercury lamp (Acticure 4000, EXFO) with 400-500 nm bandgap filter. The overtone signal of double bonds was monitored at 6160 cm^{-1} during the FT-IR measurements.

Polymerization shrinkage stress measurement

Shrinkage stress was measured via a tensometer using cantilever beam deflection theory (American Dental Association Health Foundation, ADAHF–PRC). A composite paste (1 mm in thickness, 6 mm in diameter) is placed between two cylindrical quartz rods, which were previously treated with a thiol silane. A 50 mW/cm^2 of light was irradiated for 2 min from the bottom rod using a light guide connected to a mercury lamp (Acticure 4000, EXFO) with a 400–500 nm bandgap filter. Polymerization-induced shrinkage of sample exerted a tensile force which caused the deflection of the aluminum beam. A LVDT (linear variable differential transformer) was used

to convert the displacement to shrinkage stress based upon beam calibration constant and cross-sectional area of the sample. For the simultaneous measurement of conversion with shrinkage stress, data was collected continuously for 15 min.

Viscosity measurement

The resin viscosity was measured via a TA instruments ARES rheometer. Each resin was placed between two parallel quartz plates (8 mm in diameter, 0.4 mm in thickness), and the viscosity was monitored at a shear rate of 252 s^{-1}.

Scanning electron microscopy

Scanning electron microscope (Zeiss, Supra 60) was used to investigate the microstructures and the fracture surfaces of composites. Samples were coated with a thin layer of gold to prevent charging before the observation by SEM.

Thermogravimetric analysis

Thermogravimetric analysis (TGA Pyris 1, PerkinElmer) was used to analyze the functionalized silica nanoparticles. Each sample was run in a nitrogen atmosphere (20 ml min^{-1}) from 50 $^{\circ}C$ to 850 $^{\circ}C$ at a heating rate of 10 $^{\circ}C$ min^{-1}.

Three-point bend test

Rectangular bars (2×4×20 mm) and a 3-mm long notch on one edge were used for three-point bend tests to measure fracture toughness. The three-point bend test was performed using a (MTS 858 Mini Bionix II) testing machines. Five specimens of each composition were tested to evaluate

the mechanical tests with displacement rate of 1.0 mm/min. The fracture toughness was calculated using the following equation:

$$K1c = \frac{Pm\ S}{WD\text{^}(\frac{2}{3})} f\left(\frac{a}{w}\right)$$

where a is the crack length and f (a/w) is the polynomial geometrical correction factor given as:

$$f\left(\frac{a}{w}\right) = \frac{3(\frac{a}{w})^{1/2}[1.99 - \left(\frac{a}{w}\right)\left(1 - \frac{a}{w}\right) \times \left(2.15 - \frac{3.93a}{W} + \frac{2.7a^2}{W^2}\right)]}{2(1 + \frac{2a}{W})(1 - \frac{a}{W})^{2/3}}$$

4.3. Results and Discussion

To form an AI composite and examine the influence of DCC at the particle matrix interface on composite behavior, silica nanoparticles (SNPs) were functionalized with an AFT-capable allyl sulfide containing triethoxysilane (synthesis in experimental section), enabling AFT-induced bond exchange upon light exposure in the presence of a suitable radical-generating photoinitiator as illustrated in **Figure 4.1**. For use as a control, SNPs were functionalized with a similar silane also capable of bonding to the resin but not capable of subsequent AFT-mediated bond exchange (PI). The thiol functionalized fillers were analyzed by DRIFT FT-IR spectroscopy and thermogravimetry (TGA) which provided additional evidence of successful functional group attachment to the SNP surface (Figure S4 and Figure S5) at a density of 1.03×10^{-6} mole of AFT silane per m^2 on the nanoparticle surface. In the following experiments, SNPs were dispersed into a resin comprised of a stoichiometric ratio of pentaerythritol tetra(3-mercaptopropionate) PETMP thiol and 1,3,5-triallyl-1,3,5-triazine-2,4,6(1H,3H,5H)-trione (TATATO) alkene that leads to the

formation of a glassy polymer network as the resin phase of the composite. Loading of SNPs is varied to include 5 wt%, 15 wt%, 25 wt%, and 50 wt% of the total composite weight, recognizing that the importance and volume fraction of the interface will rise along with the increase in the filler loading.

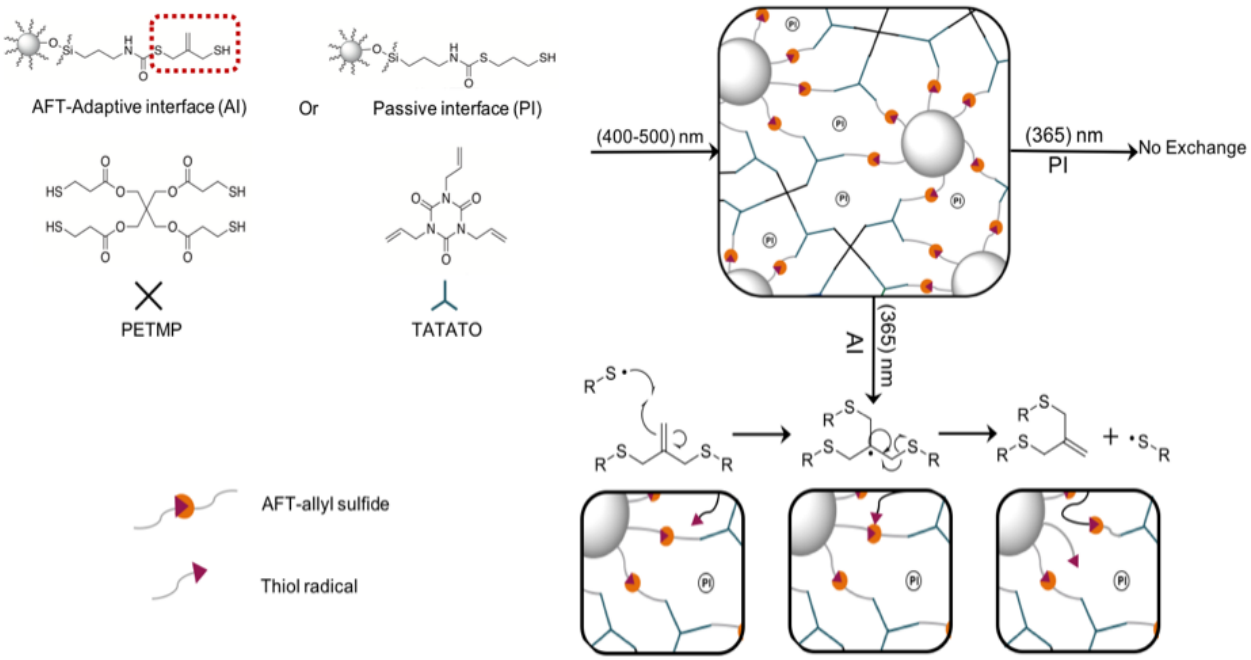

Figure 4.7. Monomers and fillers used in the formulation of the composites to examine the influence of dynamic bond exchange at the SNP-polymer interface. Resins were formulated such that there was a stoichiometric balance of PETMP and TATATO (1:1 SH:ene).

Internal stresses are well known to arise in composites, both within the bulk resin as well as at the particle interface during curing, during the polymerization due to post-gelation volumetric contraction and elastic modulus evolution primarily during vitrification, leading to diminished composite performance and premature failure through initiation of microcracks and interfacial debonding.[40,41] To investigate the effect of dynamic bond exchange at the particle interface on bulk shrinkage stress reduction, a tensometer connected to an FTIR spectrometer via fiber optic cables was used to monitor real-time functional group conversion and the corresponding stress generated due to polymerization shrinkage[40–42] **(Figure 4.2)**. In the radical mediated thiol-ene

polymerization, the AFT process occurred simultaneously with photopolymerization of the thiol-ene monomers to facilitate stress relaxation at the particle interface via bond reconfiguration. Due to the interfacial bond exchange, the AI system containing 25 wt% SNPs showed modestly slower photopolymerization reaction kinetics **(Figure 4.2A)** because the allyl sulfide functionality and the vinyl ether compete in reactions for the thiyl radical, which is consistent with what has been reported in the literature for allyl sulfide containing thiol-ene systems.[22] The residual stress was measured to be 0.9 MPa in the PI sample and 0.5 MPa in the AI system, indicating a significant 45 % reduction in shrinkage stress after curing to equivalent conversions when AFT was present only at the particle interface **(Figure 4.2B)**. Varying the loading of SNPs to 5 wt%, 15 wt%, 25 wt%, and 50 wt% resulted in shrinkage stress decreasing monotonically with increased SNP loading for both AI and PI systems, as shown in **Figure 4.2C**. The reduction in shrinkage stress with increasing particle loading is due to the reduction in overall reactive functional group density, which is responsible for the bulk volumetric shrinkage during polymerization.[43] Both AI and PI systems exhibit fairly similar shrinkage stress at low loading where the contribution from the interface is the least; however, the disparity in shrinkage stress between the two systems becomes progressively more significant at higher loading, such as 25 wt% and 50 wt%, with dramatic reduction of shrinkage stress observed for the AI-based composite when compared to the PI composites. It should be noted that both composite systems exhibit the same tensile modulus for any given SNP loading level **(Figure S4.1)**, which indicates effective covalent attachment between the resin and filler with either interfacial configuration.

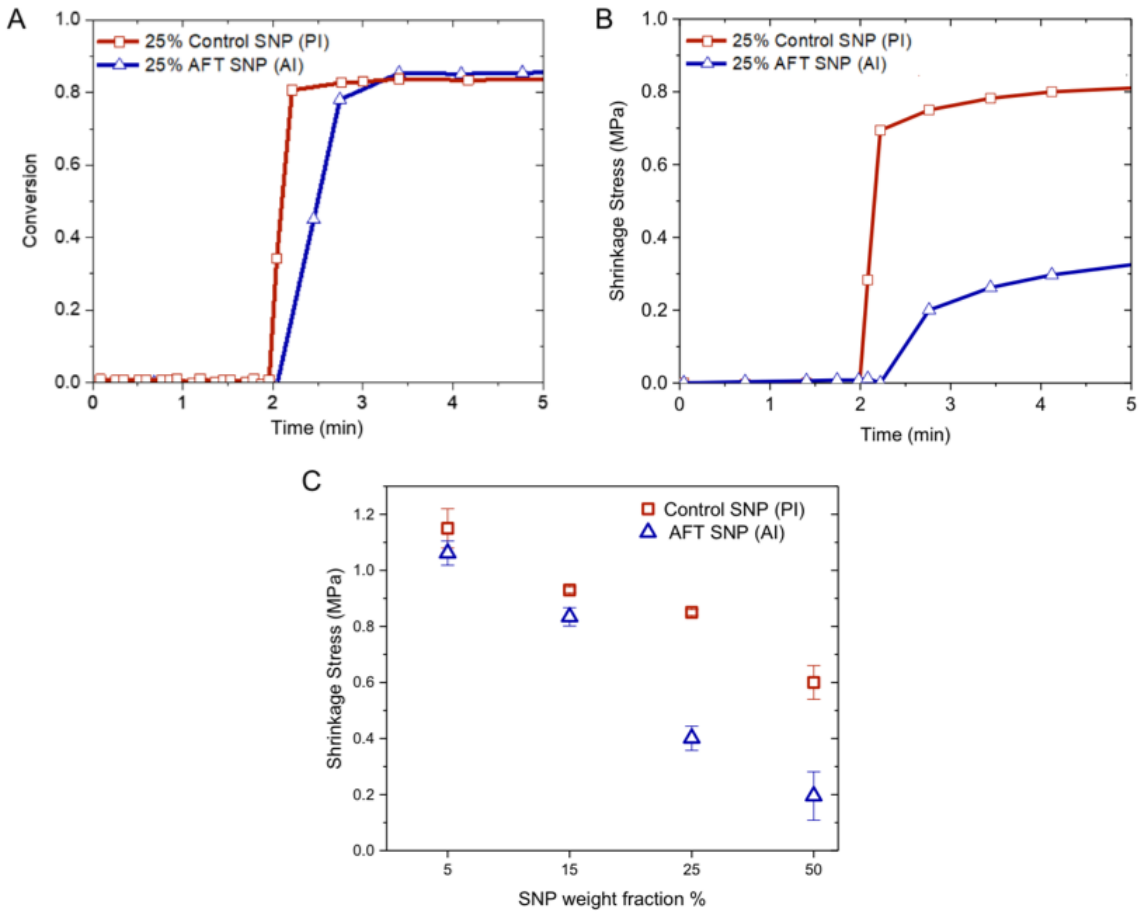

Figure 4.8. A. Polymerization kinetics as measured by FT-NIR. B. *In situ* polymerization stress for a 1:1 PETMP/TATATO sample with 25 wt% of both control SNPs to generate PI (squares) and AFT SNPs to generate AI (triangles) C. The final polymerization shrinkage stress taken after 10 min reaction time for both PI (squares) and AI (triangles) composites as a function of SNPs weight fraction. All samples were placed between two quartz rods, previously treated with a thiol-functional silane and irradiated for 2 min at ambient temperature with 400-500 nm light at 50 mW/cm^2 following 2 min in the dark to establish a baseline measurement.

Interfacial bond exchange is not limited to influencing the shrinkage stress development during curing, and it can be further employed to relieve stress after polymerization during mechanical loading of composites. Accordingly, post-polymerization stress relaxation experiments were conducted on the composites to assess the influence of AI in fully cured, glassy composites. A constant strain of 1 % was applied to all composites, which were then exposed to

365 nm light at a 20 mW/cm^2 intensity for 10 min. The light source served to activate the bond exchange process at the particle interface in the presence of I651 as a latent UV-initiator. **Figure 4.3A** shows that for a fixed SNP loading of 25 wt%, the AI composites relaxed 70 % of the initial stress, while the PI composites relaxed only 11 % of the initial stress. The relaxation exhibited by the PI composite is attributed to segmental motion along chains in the glassy state[44]while the large degree of additional stress relaxation in the AI system is considered to be a result of interfacial bond exchange. At 50 wt% fillers, this represents a 66% increase in the stress relaxation of AI composites relative to the PI composites. Varying the SNP loading in the system results in minimal change in the stress relaxation behavior of the PI samples, but dramatically affects the AI behavior (**Figure 4.3B)**. Specifically, the AI composites relaxed 40% of the initial stress at 5 wt% SNP loading, 55% at 15 wt% SNP loading, 70% at 25 wt% and 80% of the initial stress at 50 wt% SNP loading. These observed trends of more stress relief at higher SNP loading in the AI composite are due to the increase of the interfacial surface area associated with increasing the SNP loading, which then increase the number of exchangeable bonds at the interface relative to the overall composite volume.[1]

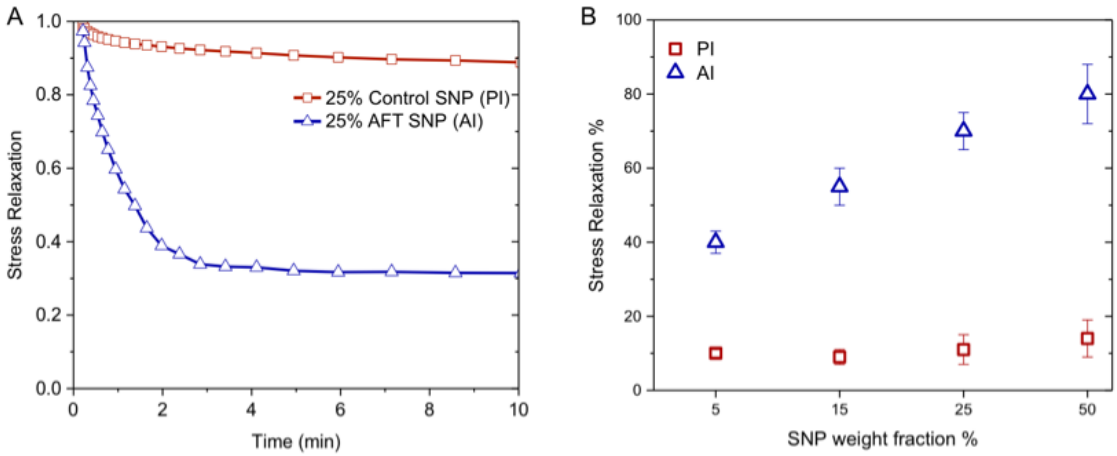

Figure 4.9. A. Photo-induced stress relaxation achieved on fully cured 0.25 mm thick sample, of a 1:1 PETMP/TATATO with 25 wt% of both control SNPs to generate PI (squares) and AFT SNPs to generate AI (triangles), at constant 1% strain. B. Final stress relaxation as a function of SNPs weight fraction. The specimens were irradiated at t=0 with 365 nm, 20 mW cm^2 UV-light for 10 min.

In addition to static testing at a constant strain, samples with varied SNP loading were subjected to a tensile test with a strain ramp of 1 mm/min until failure. Samples were not illuminated during the strain ramp, so bond exchange in the AI composites was confined to the curing stage. Young's modulus increased linearly with increasing nanoparticle weight fractions for PI and AI system **(Figure S4.1)**. The tensile strength **(Figure 4.4A)** and toughness **(Figure 4.4B)** of the PI composite improved with greater SNP loading values up to an optimum value of 15 wt% and then began deteriorating with larger SNP content. This optimal loading value is consistent with the existing literature where the phenomenon has been attributed to the formation of physical defects within nanocomposites during the curing process at higher loadings where particle-particle interaction due to aggregation begins to occur, creating physical defects that act as stress concentrators, weakening the composites.[3,6,45–47] It is therefore interesting to note that the AI-based nanocomposites diverged from this typical behavior. Specifically, tensile strength increased linearly with increasing weight fractions of SNPs, well beyond the optimal 15 wt% seen

in the control, **Figure 4.4A**. Toughness measured in the AI composites increased significantly moving from 5 wt% to 15 wt% filler. Increasing the filler amount beyond 15% did not compromise the composite toughness; 25 wt% and 50 wt% composites exhibit a minor increase in toughness relative to the 15 wt% samples, appearing to achieve a plateau as shown in **Figure 4.4B**. A widespread problem in materials engineering is the general mutual exclusivity of strength and toughness; **Figure 4.4C** highlights the ability of these AI-based composites to defeat this problem and broaden the envelope of attainable properties in this material system.[48] Since a reduction in polymerization shrinkage plays a crucial role in diminishing stress generation and as a result the likelihood of defect formation particularly at interfaces [49], this behavior is obviously related to the significant reduction in the shrinkage stress with increasing the AI-based SNPs loading **(Figure 4.2C)**. As is well-known, at high shrinkage stress, as chains become deformed into less entropically favorable conformations, the energy barrier to chain scission becomes smaller, leading to increased probability of chain scission, which again generates defects.[50,51] On the other hand, having exchangeable bond at the particle interface in the AI composite works to counter this effect by relaxing chain conformation at the interface, delaying chain scission, and therefore reducing the likelihood of crack nucleation. Additionally, after crack nucleation, the significant reduction in the shrinkage stress caused by the AFT bond exchange causes the SNP interfacial zones ahead of the crack tip to be subjected to lower stresses, when compared to the PI that originally exhibited higher stress during the polymerization process. At high particle loading, this stress will be amplified by interactions between the stress fields around the particles, which as a result cause the composite's failure and decreases its ultimate mechanical properties.[6]

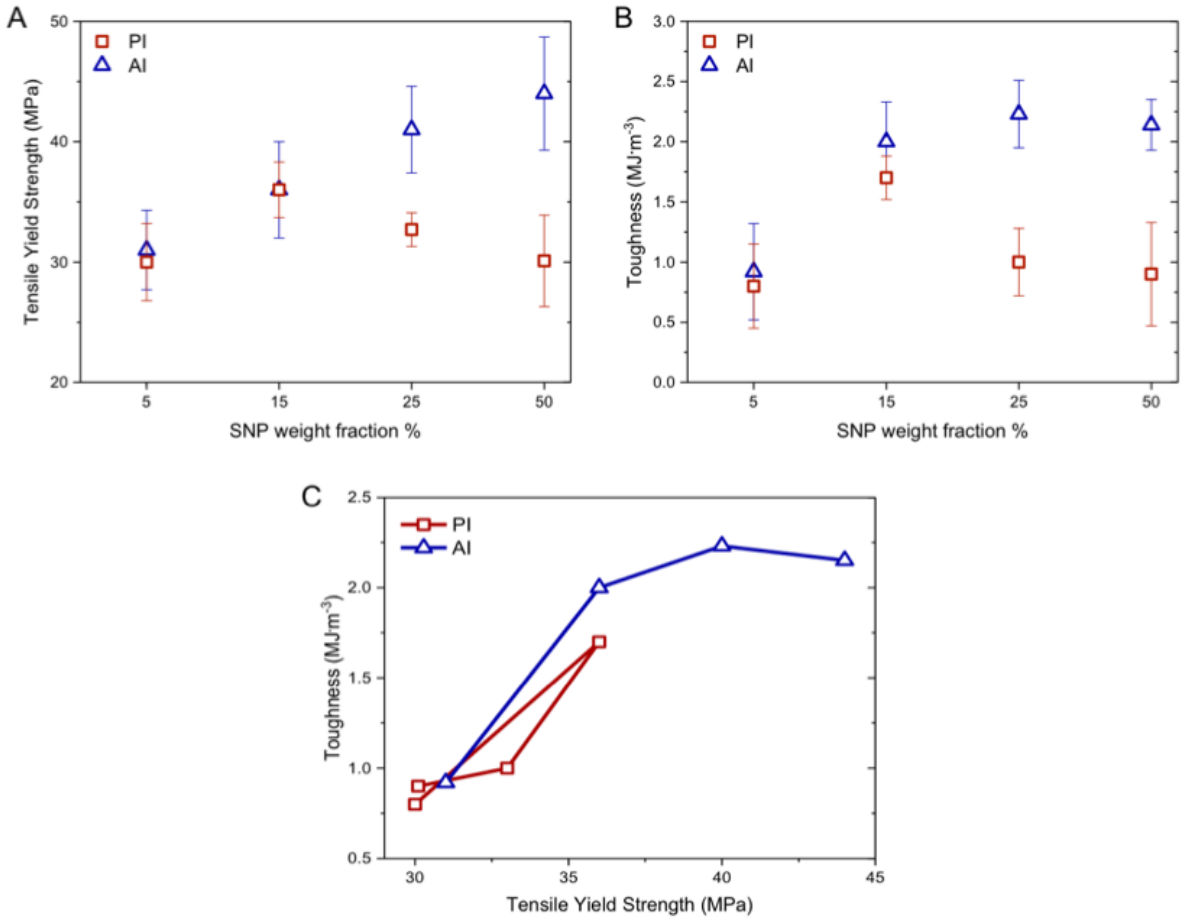

Figure 4.10. The effect of particle weight fraction% on the mechanical properties of PI-based SNPs (squares) and AI-based SNPs (triangles). A. Tensile yield strength (MPa), B. Toughness ($MJ.m^{-3}$), C. Toughness ($MJ.m^{-3}$) versus tensile yield strength (MPa) at 5,15,25 and 50 wt% SNP. Stoichiometric mixtures of PETMP and TATATO (1:1 SH:ene), with 1 mol% of I819 visible light photoinitiator per functionality, 2 mol% of I651, and 5-50 weight percentages of SNPs functionalized with either the AFT silane to generate the AI composite or the control silane to generate the PI composite were prepared then cured with 400-500 nm visible light at $50mW/cm^2$ for 20 min, then post-cured in an oven at 100°C for 24 h.

To investigate the effects of *in situ* interfacial bond exchange on composite failure, fully cured, pre-cracked samples containing 25 wt% SNPs were subjected to 3-point bend tests. The dimensions of each specimen used in the investigation were 2×4×20 mm with a 3-mm long notch on one edge. The fracture toughness value, K_{IC} ($MNm^{-3/2}$), for each specimen was measured at a crosshead speed of 1 mm/min until fracture. **Figure 4.5A** illustrates the behavior of three different

samples subjected to loading: A PI composite, AI composite, and one AI composite exposed to UV-light to enable the AFT *in situ* at the crack tip during loading. As can be seen from **Figure 4.5A**, the AI composite that was exposed to UV-light to induce *in situ* interfacial bond exchange exhibited higher yield strength (10.4 MPa) and fracture toughness (2.3 $MNm^{-3/2}$) than both the unexposed AI composite, which exhibited a 8.2 MPa yield strength and 1.3 $MNm^{-3/2}$ fracture toughness, and the PI composite, which gave the lowest values of both yield strength (5 MPa) and toughness (0.8 $MNm^{-3/2}$). Subsequent scanning electron microscopy (SEM, Zeiss, Supra 60) images were taken of the fractured surfaces **(Figure 4.5B)**. Images reveal that both the PI and the unexposed AI composites contain voids dotted throughout the fracture surface. Cavitation of this nature associated with rigid silica particles has been previously reported in the literature, where stress concentrations around the SNPs initiate particle debonding, followed by plastic deformation via a void-growth mechanism, which is believed to change the stress state in the surrounding matrix and reduces the constraint at the crack tip. These voids were shown to become less numerous by improving the adhesion between the particles and the resin, where the stress is effectively transferred through the particle-polymer interface and reduces the stress state around the SNPs[52–54], which is consistent with the difference in the nature and the number of voids between the PI and the AI composites. These voids are smaller and less numerous on the AI composite, where the particles are subjected to lower stress due to the lower stress that originally built up during the polymerization process when compared to the PI composites. Furthermore, a smoother surface with significantly less exposure of silica nanoparticles along the fracture surface was obtained when *in situ* AFT bond exchange at the particle-polymer interface was triggered during the fracture process, which relieved the triaxial stress that drives the particles cavitation mechanism, demonstrating a reduction of polymer-particle debonding events during failure. This

impressive shift in failure mechanism is not without precedent as previous work has demonstrated an elimination of voids by thermally relaxing stress.[55–57] As a result, a corresponding increase in the toughness was also obtained when *in situ* AFT bond exchange at the particle-polymer interface was triggered during the fracture process. It should be noted that both AI- and PI-based composites showed very similar dispersion of the SNPs using TEM imaging at 25 wt% SNP loading **(Figure S4.2)**.

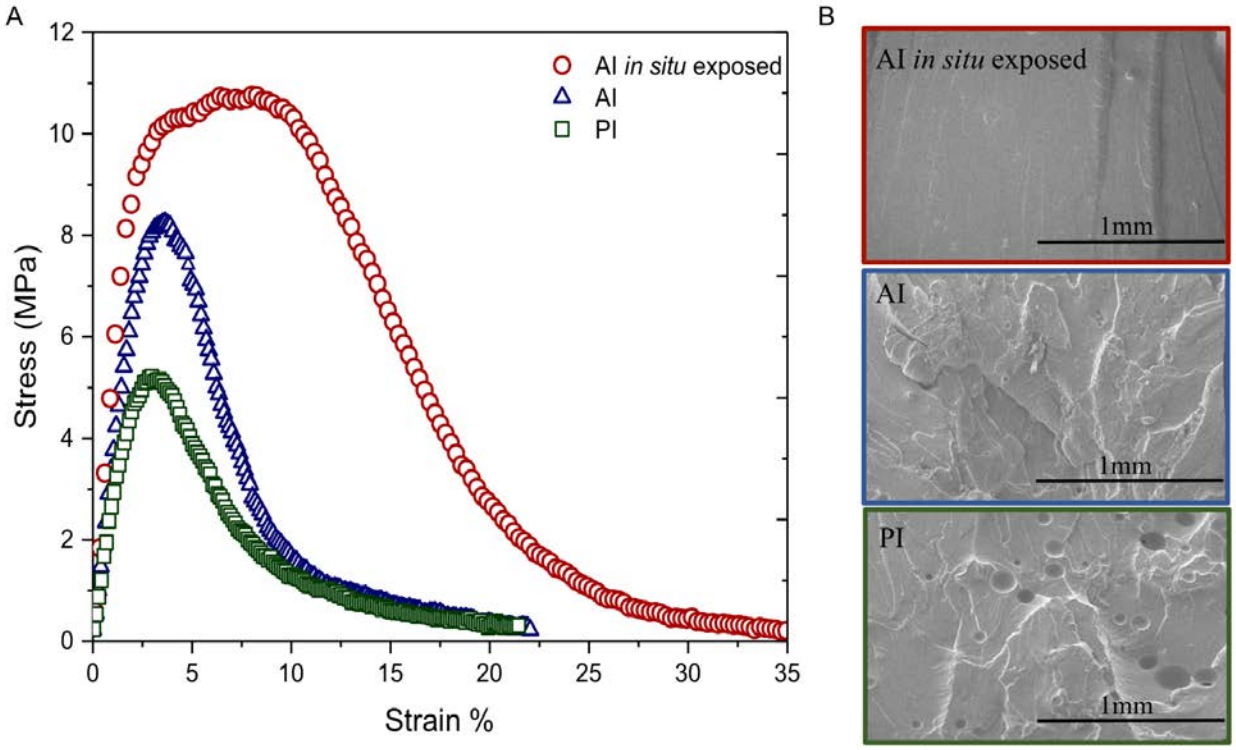

Figure 4.11. A. Fracture test for fully cured, dogbone-shaped PETMP-TATATO-25wt% SNPs coated with: □ PI, △ AI, ○ AI radically triggered with 40 mW/cm^2 of 365nm light through the crack tip, during the 3-point bend test at a displacement rate of 1 mm/min. B. High-resolution scanning electron microscopy (FEG-SEM) images were taken for fractured surfaces of three PETMP-TATATO composites containing: AI radically triggered with 20mW/cm^2 of 365 nm light through the crack tip during the fracturing process, AI based SNPs, PI based SNPs.

Typically, cavitation, delamination, and plastic-shear yielding all contribute to dissipation of mechanical energy during loading.[47] Interestingly, we have now demonstrated that while AI

suppressed the two former dissipating mechanisms during three-point bending **(Figure 4.5)**, it accentuated the latter during stress relaxation tests **(Figure 4.3)**. Noting these competing phenomena naturally leads to questions regarding how these composites will behave when subjected to cyclic loading. In order to explore the influence of interfacial bond exchange in composites subjected to cyclic loading, a 10 N force was ramped with 5 N/min ramping rate for both PI and AI composites, which were then irradiated with UV-light through the crack tips for 30 s, at which point the force was ramped down over a 2 min period. This procedure was repeated for five loading-unloading cycles, and the hysteresis curves are presented in **Figure 4.6A** for the AI and **Figure 4.6B** for the PI composite. As shown, AI based composites systematically exhibit a greater degree of both energy dissipation and non-recoverable strain throughout all five cycles. Bond exchange in these cycles is limited, however, by the photoinitiator consumption. The rate at which photoinitiator is consumed is altered by adjusting the UV intensity applied to the samples.[58]

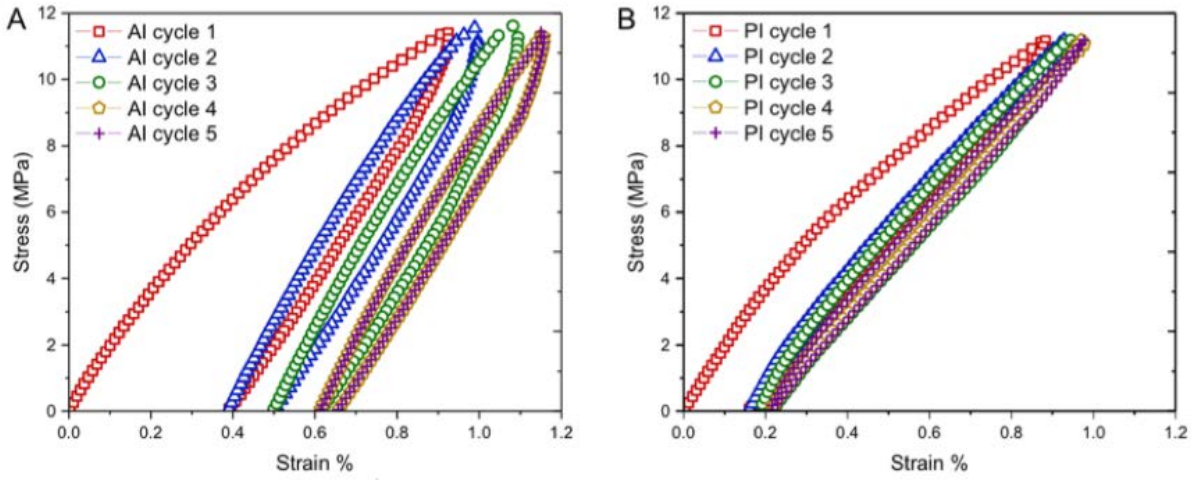

Figure 4.12. Five hysteresis loop cycles during loading of 10 N force then unloading to 0 N at 5N/min rate for PETMP-TATTATO-25wt% of SNPs coated with: A. AI, B. PI. All samples were cured under the same conditions where stoichiometric mixtures of a PETMP, TATATO (1:1 SH:ene), with 1 mole% of I819, 2 mole% of I651, and 25 wt% of SNPs were cured using 400-500 nm visible light at 50mW/cm^2 for 20 minutes, then post-cured in an oven at 100°C for 24 h.

So far, this work has examined composite behavior when AFT is only present and active at the resin-particle interface. Given that AFT has been widely studied in bulk materials, we now compare the effects of interfacial dynamic bond exchange (adaptive interface AI) with bond exchange occurring throughout the resin matrix (adaptive network AN). To do this we use a modified material formulation of the formulation shown in **Figure 4.1**. We employ two different resins, an AN resin comprised of 25 mol% of the alkene forming the composite was supplied by the 2-methylene-propane-1,3-di (thioethyl vinyl ether) AFT-DVE monomer to facilitate bond exchange throughout the polymer network, and the non-AN resin using the control, nonfunctional analog alkene **(Scheme 4.1)**. We also employ two different silanes for functionalizing particles, either an AFT-silane to generate the AI or non-AFT silane to generate the PI. Four different permutations were then examined: 1. A control composite which does not contain any AFT-exchangeable bonds in the polymer backbone nor at the SNPs surface (PN-PI), 2. AI-based composite containing AFT-moieties only at the SNPs surface coming from AFT-based silane (PN-AI), 3. AN-based composite containing AFT moieties only in the polymer backbone coming from AFT-DVE monomer (AN-PI), 4. Composite based on both AI and AN by introducing AFT moieties in both the polymer backbone and at the surface of SNPs (AN-AI). The four formulations produce equivalently crosslinked networks with similar T_g's of 30 °C, and tensile moduli of 1300-1500 MPa at room temperature **(SI Figure S4.3** & **Table S4.1**).

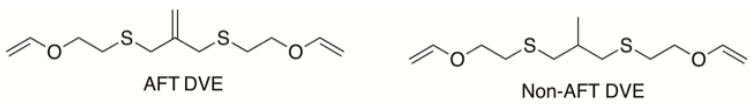

Scheme 4.1. 2-Methylene-propane-1,3-di (thioethyl vinyl ether) (AFT-DVE) monomer and the negative control analogue 2-methylpropane-1,3-di (thioethyl vinyl ether) (non-AFT).

For each of the four formulated composites, real-time polymerization kinetics of the functional group conversion and the corresponding stress generated due to polymerization shrinkage were monitored **(Figure 4.7A)**. After curing, tensile tests were performed to compare the effects of interfacial dynamic bond exchange with bond exchange occurring throughout the resin on the mechanical properties of the composites **(Figure 4.7B)**. As **Figure 4.7A** shows, the composite that does not contain any exchangeable bonds exhibits the highest degree of shrinkage stress, 0.7 MPa, while the formulation containing exchangeable bonds both throughout the network and at the particle interface (AN-AI) exhibits the lowest degree of shrinkage stress, only 0.2 MPa. While this substantial difference is to be expected[34], a truly surprising result is observed when comparing samples that limit AFT capabilities to either the resin (AN) or the interface (AI). **Figure 4.7B** shows that the PN-AI composite where AFT is limited to the interface exhibit similar values of toughness and tensile strength to AN-PI composite where AFT occurs only in the resin despite having an order of magnitude fewer dynamic bonds. This result highlights the importance of interfacial stress relaxation in polymeric composites: Thermosetting resins with standard silica fillers exhibit an enhancement of mechanical properties comparable to those obtained in composites with dynamic, chemically complex resins by functionalizing the filler with CANs-capable silane. Such an approach can be applied to a wide spectrum of resin/filler combinations far beyond the proof of concept examples examined here.

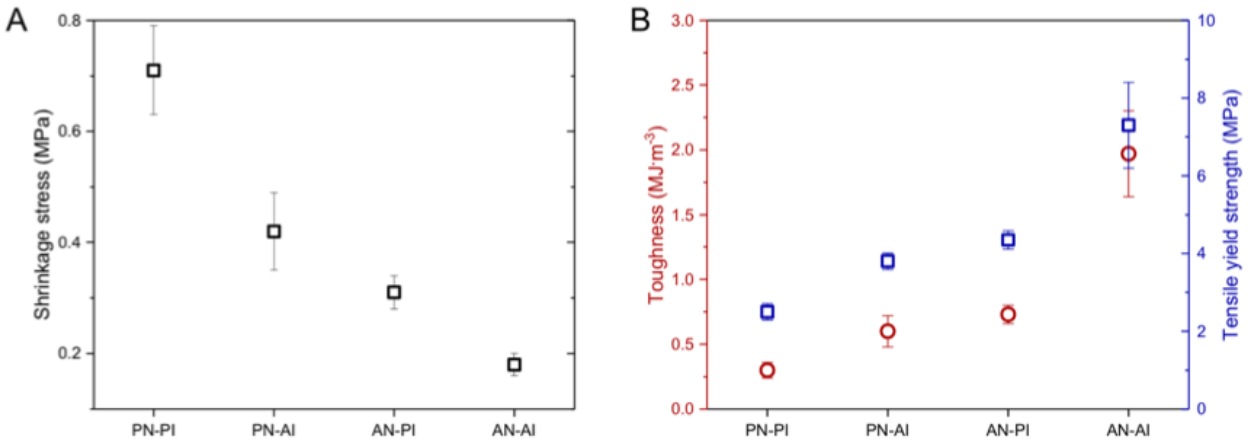

Figure 4.7. A. Final polymerization shrinkage stress taken after 10 min reaction time as a function of the double bond conversion via tensometer. B. Material properties: Toughness ($MJ.m^{-3}$) (red circles) and Tensile yield strength (MPa) (blue squares) of four composites: (i) PN-PI composite with no exchangeable bonds, (ii) PN-AI composite with interfacial bond exchange, (iii) AN-PI composite containing exchangeable bond in the polymer network but not at the interface, and (iv) AN-AI composite containing exchangeable bonds both in the polymer backbone and at the resin-filler interface. The resin contained PETMP as the thiol monomer and a stoichiometrically balanced (relative to functional groups) quantity of an allyl and vinyl ether mixture, itself composed of 75 mol% (relative to ene functional groups) TATATO and 25% of either the AFT or non-AFT DVE, with 1 mole% of I819, 2 mol% of I651, and 25 wt% of SNPs were cured using 400-500 nm visible light at $50mW/cm^2$ for 20 min. Tensile test was conducted on dogbone-shaped sample with strain rate 1mm/min.

4.4. Conclusion

In summary, we demonstrate that surface modification with a DCC bond exchanging silane, specifically AFT-based moieties, mitigates the deleterious interfacial stress concentration that is ubiquitous in composites in which the composite phases have significantly different stiffness. The resulting interfacial stress relaxation is achieved with significant benefits to the composite performance, including improvements in toughness, tensile strength, polymerization shrinkage stress, and the recovery of the dissipative energy when subjected to cyclic loading. During the radical photopolymerization of composites, the process of AFT occurred simultaneously with polymerization leading to a relaxation of the stress at the interface via

localized bond reconfiguration. As a result, significant reductions in shrinkage stress were achieved. The influence of interfacial post-polymerization stress relaxation in composites subjected to mechanical loading was also demonstrated. Additionally, a reduction of particle debonding events during the composites failure and a corresponding increase in the toughness were obtained when *in situ* AFT interfacial bond exchange was triggered during the fracture process. Besides the fact that AFT-exchange is limited by the consumption of photoinitiator, nanocomposites also have limited UV light penetration especially for optically thick specimens or while mechanical loads are being applied; however, this preliminary investigation provides a new platform technology to improve the mechanical performance of thermosetting composites simply by introducing an adaptive yet secure interface to their formulation. This work is readily extended to other DCCs and CANs and applied to a wide spectrum of resin/filler combinations beyond what has been examined here.

4.5. Acknowledgments

The authors acknowledge financial support from the National Science Foundation (NSF DMR 1310528) and the National Institutes of Health (NIH 1U01DE023777). Publication of NIST, an agency of the US government, not subject to copyright. Certain commercial equipment, instruments, or materials are identified in this paper in order to specify the experimental procedure adequately. Such identification does not imply recommendation or endorsement by NIST, nor does it imply that the materials or equipment identified are necessarily the best available for the purpose.

4.6. References

(1) Zheng, Y.; Zheng, Y.; Ning, R. Effects of Nanoparticles SiO2 on the Performance of Nanocomposites. *Mater. Lett.* **2003**, *57* (19), 2940–2944.

(2) Kojima Yoshitsugu; Usuki Arimitsu; Kawasumi Masaya; Okada Akane; Fukushima Yoshiaki; Kurauchi Toshio; Kamigaito Osami. Mechanical Properties of Nylon 6-Clay Hybrid. *J. Mater. Res.* **1993**, *8* (5), 1185–1189.

(3) Fu, S. Y.; Feng, X. Q.; Lauke, B.; Mai, Y. W. Effects of Particle Size, Particle/Matrix Interface Adhesion and Particle Loading on Mechanical Properties of Particulate-Polymer Composites. *Compos. Part B Eng.* **2008**, *39* (6), 933–961.

(4) Üstündag, E.; Dragoi, D.; Clausen, B.; Brown, D.; Bourke, M. A. M.; Balch, D. K.; Dunand, D. C. Internal Stresses in Bulk Metallic Glass Matrix Composites. **2001**, *644* (4), 1–6.

(5) Eiras, D.; Pessan, L. A. Mechanical Properties of Polypropylene/Calcium Carbonate Nanocomposites. *Mater. Res.* **2009**, *12* (4), 517–522.

(6) Sun, S.; Li, C.; Zhang, L.; Du, H. L.; Burnell-Gray, J. S. Effects of Surface Modification of Fumed Silica on Interfacial Structures and Mechanical Properties of Poly(Vinyl Chloride) Composites. *Eur. Polym. J.* **2006**, *42* (7), 1643–1652.

(7) Wkiner, K. A.; Springer-, E.; Erikison, K.; Asoy, J. Colin George Whitesides. **1987**, *240*, 1987–1988.

(8) Iwan, M.; Andryszewski, T.; Wydryszek, M.; Fialkowski, M. Fabrication of Nanocomposites by Covalent Bonding between Noble Metal Nanoparticles and Polymer Matrix. *RSC Adv.* **2015**, *5* (86), 70127–70138.

(9) Kinloch, A. J.; Mohammed, R. D.; Taylor, A. C.; Eger, C.; Sprenger, S.; Egan, D. The Effect of Silica Nano Particles and Rubber Particles on the Toughness of Multiphase Thermosetting Epoxy Polymers. *J. Mater. Sci.* **2005**, *40* (18), 5083–5086.

(10) Cramer, N. B.; Stansbury, J. W.; Bowman, C. N. Recent Advances and Developments in Composite Dental Restorative Materials. *J. Dent. Res.* **2011**, *90* (4), 402–416.

(11) Kloxin, C. J.; Bowman, C. N. Covalent Adaptable Networks: Smart, Reconfigurable and Responsive Network Systems. *Chem. Soc. Rev.* **2013**, *42* (17), 7161–7173.

(12) Scott, T. F.; Schneider, A. D.; Cook, W. D.; Bowman, C. N. Photoinduced Plasticity in Cross-Linked Polymers. *Science* **2005**, *308* (5728), 1615–1617.

(13) Cox, L. M.; Sun, X.; Wang, C.; Sowan, N.; Killgore, J. P.; Long, R.; Wu, H. A.; Bowman, C. N.; Ding, Y. Light-Stimulated Permanent Shape Reconfiguration in Cross-Linked Polymer Microparticles. *ACS Appl. Mater. Interfaces* **2017**, *9* (16), 14422–14428.

(14) Amamoto, Y.; Kamada, J. pd.; Otsuka, H.; Takahara, A.; Matyjaszewski, K. Photoinduced Self-Healing of Covalently Cross-Linked Polymers through Reshuffling of Trithiocarbonate Units. *Angew. Chemie - Int. Ed.* **2011**, *50* (7), 1660–1663.

(15) Nicolaÿ, R.; Kamada, J.; Van Wassen, A.; Matyjaszewski, K. Responsive Gels Based on a Dynamic Covalent Trithiocarbonate Cross-Linker. *Macromolecules* **2010**, *43* (9), 4355–4361.

(16) Chung, C. M.; Roh, Y. S.; Cho, S. Y.; Kim, J. G. Crack Healing in Polymeric Materials via Photochemical [2+2] Cycloaddition. *Chem. Mater.* **2004**, *16* (21), 3982–3984.

(17) Amamoto, Y.; Otsuka, H.; Takahara, A.; Matyjaszewski, K. Self-Healing of Covalently Cross-Linked Polymers by Reshuffling Thiuram Disulfide Moieties in Air under Visible Light. *Adv. Mater.* **2012**, *24* (29), 3975–3980.

(18) Capelot, M.; Montarnal, D.; Tournilhac, F.; Leibler, L. Metal-Catalyzed Transesterification for Healing and Assembling of Thermosets. *J. Am. Chem. Soc.* **2012**, *134* (18), 7664–7667.

(19) Solid, L. D.; Hrubesh, L. W.; Chan, H. M.; Grenestedt, J. L.; Harmer, M. P.; Caram, H. S.; Roy, S. K.; Handbook, P. T.; Raton, B.; Ashby, M. F.; et al. Silica-Like Malleable Materials From. *Science* **2011**, *334*, 965–968.

(20) Lyon, G. B.; Cox, L. M.; Goodrich, J. T.; Baranek, A. D.; Ding, Y.; Bowman, C. N. Remoldable Thiol–Ene Vitrimers for Photopatterning and Nanoimprint Lithography. *Macromolecules* **2016**, 1281.

(21) Chen, X.; Dam, M. A.; Ono, K.; Mal, A.; Shen, H.; Nutt, S. R.; Sheran, K.; Wudl, F. A Thermally Re-Mendable Cross-Linked Polymeric Material. *Science* **2002**, *295* (5560), 1698–1702.

(22) Kloxin, C. J.; Scott, T. F.; Bowman, C. N. Stress Relaxation via Addition−Fragmentation Chain Transfer in a Thiol-Ene Photopolymerization. *Macromolecules* **2009**, *42* (7), 2551–2556.

(23) Park, H. Y.; Kloxin, C. J.; Abuelyaman, A. S.; Oxman, J. D.; Bowman, C. N. Stress Relaxation via Addition–Fragmentation Chain Transfer in High T g , High Conversion Methacrylate-Based Systems. *Macromolecules 45* (14), 5640

(24) Mu, X.; Sowan, N.; Tumbic, J. a.; Bowman, C. N.; Mather, P. T.; Qi, H. J. Photo-Induced Bending in a Light-Activated Polymer Laminated Composite. *Soft Matter* **2015**, *11* (13), 2673–2682.

(25) Kloxin, C. J.; Scott, T. F.; Park, H. Y.; Bowman, C. N. Mechanophotopatterning on a Photoresponsive Elastomer. *Adv. Mater.* **2011**, *23* (17), 1977–1981.

(26) Cox, L. M.; Li, Z.; Sowan, N.; Nair, D.; Xiao, J.; Bowman, C. N.; Ding, Y. Reconfigurable Surface Patterns on Covalent Adaptive Network Polymers Using Nanoimprint Lithography. *Polymer* **2014**, *55* (23), 5933–5937.

(27) Gandavarapu, N. R.; Azagarsamy, M. A.; Anseth, K. S. Photo-Click Living Strategy for Controlled, Reversible Exchange of Biochemical Ligands. *Adv. Mater.* **2014**, *26* (16), 2521–2526.

(28) Denissen, W.; Winne, J. M.; Du Prez, F. E. Vitrimers: Permanent Organic Networks with Glass-like Fluidity. *Chem. Sci.* **2015**, *7*, 30–38.

(29) Zhang, X.; Wang, K.; Liu, M.; Zhang, X.; Tao, L.; Chen, Y.; Wei, Y. Polymeric AIE-Based Nanoprobes for Biomedical Applications: Recent Advances and Perspectives. *Nanoscale* **2015**, *7* (27), 11486–11508.

(30) Jiang, R.; Liu, M.; Li, C.; Huang, Q.; Huang, H.; Wan, Q.; Wen, Y.; Cao, Q. yong; Zhang, X.; Wei, Y. Facile Fabrication of Luminescent Polymeric Nanoparticles Containing Dynamic Linkages via a One-Pot Multicomponent Reaction: Synthesis, Aggregation-Induced Emission and Biological Imaging. *Mater. Sci. Eng. C* **2017**, *80*, 708–714.

(31) Wan, Q.; Liu, M.; Xu, D.; Huang, H.; Mao, L.; Zeng, G.; Deng, F.; Zhang, X.; Wei, Y. Facile Fabrication of Amphiphilic AIE Active Glucan via Formation of Dynamic Bonds: Self Assembly, Stimuli Responsiveness and Biological Imaging. *J. Mater. Chem. B* **2016**, *4* (22), 4033–4039.

(32) Ruiz de Luzuriaga, A.; Martin, R.; Markaide, N.; Rekondo, A.; Cabañ ero, G.; Rodrí guez, J.; Odriozola, I. Epoxy Resin with Exchangeable Disulfide Crosslinks to Obtain Reprocessable, Repairable and Recyclable Fiber-Reinforced Thermoset Composites. *Mater. Horizons* **2016**, 241–247.

(33) Yang, Y.; Pei, Z.; Zhang, X.; Tao, L.; Wei, Y.; Ji, Y. Carbon Nanotube–Vitrimer Composite for Facile and Efficient Photo-Welding of Epoxy. *Chem. Sci.* **2014**, *5*, 3486–3492.

(34) Legrand, A.; Souli-Ziakovic, C. Silica-Epoxy Vitrimer Nanocomposites. *Macromolecules* **2016**, *49* (16), 5893–5902.

(35) Yang, Z.; Wang, Q.; Wang, T. Dual-Triggered and Thermally Reconfigurable Shape Memory Graphene-Vitrimer Composites. *ACS Appl. Mater. Interfaces* **2016**, *8* (33), 21691–21699.

(36) Sheridan, R. J.; Bowman, C. N. Understanding the Process of Healing of Thermoreversible Covalent Adaptable Networks. *Polym. Chem.* **2013**, *4* (18), 4974–4979.

(37) Kloxin, C. J.; Scott, T. F.; Adzima, B. J.; Bowman, C. N. Covalent Adaptable Networks (CANs): A Unique Paradigm in Cross-Linked Polymers. *Macromolecules* **2010**, *43* (6), 2643–2653.

(38) Evans, R. A.; Rizzardo, E. Free-Radical Ring-Opening Polymerization of Cyclic Allylic Sulfides. 2. Effect of Substituents on Seven- and Eight-Membered Ring Low Shrink Monomers. *Macromolecules* **2000**, *33* (18), 6722–6731.

(39) Kloxin, C. J.; Scott, T. F.; Bowman, C. N. Stress Relaxation via Addition−Fragmentation Chain Transfer in a Thiol-Ene Photopolymerization. *Macromolecules* **2009**, *42* (7), 2551–2556.

(40) Schneider, L. F. J.; Cavalcante, L. M.; Silikas, N. Shrinkage Stresses Generated during Resin-Composite Applications: A Review. *J. Dent. Biomech.* **2010**, *1* (1), 131630–131630.

(41) Song, H. B.; Sowan, N.; Shah, P. K.; Baranek, A.; Flores, A.; Stansbury, J. W.; Bowman, C. N. Reduced Shrinkage Stress via Photo-Initiated Copper(I)-Catalyzed Cycloaddition Polymerizations of Azide-Alkyne Resins. *Dental Materials*. Elsevier Inc. June 25, 2016.

(42) Shah, P. K.; Stansbury, J. W. Role of Filler and Functional Group Conversion in the Evolution of Properties in Polymeric Dental Restoratives. *Dent. Mater.* **2014**, *30* (5), 586–593.

(43) Gonalves, F.; Azevedo, C. L. N.; Ferracane, J. L.; Braga, R. R. BisGMA/TEGDMA Ratio and Filler Content Effects on Shrinkage Stress. *Dent. Mater.* **2011**, *27* (6), 520–526.

(44) Capaldi, F. M.; Boyce, M. C.; Rutledge, G. C. Molecular Response of a Glassy Polymer to Active Deformation. **2004**, *45*, 1391–1399.

(45) Ou, Y.; Yang, F.; Yu, Z.-Z. *A New Conception on the Toughness of Nylon 6/Silica Nanocomposite Prepared via in Situ Polymerization*; **1998**; Vol. 36.

(46) Tsai, J. L.; Hsiao, H.; Cheng, Y. L. Investigating Mechanical Behaviors of Silica Nanoparticle Reinforced Composites. *J. Compos. Mater.* **2010**, *44* (4), 505–524.

(47) Young, R. J.; Maxwell, D. L.; Kinloch, A. J. The Deformation of Hybrid-Particulate Composites. *J. Mater. Sci.* **1986**, *21* (2), 380–388.

(48) Ritchie, R. O. The Conflicts between Strength and Toughness. *Nat. Mater.* **2011**, *10* (11), 817–822.

(49) Queiroz, G.; Universidade, M. M.; Universidade, M. M. Evaluation of Linear Polymerization Shrinkage , Flexural Strength and Modulus of Elasticity of Dental Composites. *Dent. Mater.* **2010**, *13*, 51–55.

(50) Odell, J. a.; Keller, a.; Rabin, Y. Flow-Induced Scission of Isolated Macromolecules. *J. Chem. Phys.* **1988**, *88* (6), 4022–4028.

(51) Michler, G. H.; Von Schmeling, H. H. K. B. The Physics and Micro-Mechanics of Nano-Voids and Nano-Particles in Polymer Combinations. *Polym.* **2013**, *54* (13), 3131–3144.

(52) Huang, Y.; Kinloch, A. J. The Toughness of Epoxy Polymers Containing Microvoids 1330 POLYMER , 1992 , Volume 33 , Number 6 Toughness of Epoxy Polymers. *Technology* **1991**, 1991–1993.

(53) Hsieh, T. H.; Kinloch, A. J.; Masania, K.; Taylor, A. C.; Sprenger, S. The Mechanisms and Mechanics of the Toughening of Epoxy Polymers Modi Fi Ed with Silica Nanoparticles. *Polymer* **2010**, *51* (26), 6284–6294.

(54) Hsieh, T. H.; Kinloch, A. J.; Masania, K.; Sohn Lee, J.; Taylor, A. C.; Sprenger, S. The Toughness of Epoxy Polymers and Fibre Composites Modified with Rubber Microparticles and Silica Nanoparticles. *J. Mater. Sci.* **2010**, *45* (5), 1193–1210.

(55) Kinloch, A. J.; Taylor, C. The Toughening of Cyanate-Ester Polymers. Part I Physical Modification Using Particles, Fibres and Woven-Mats. *J. Mater. Sci.* **2002**, *37* (3), 433–460.

(56) Guild, F. J.; Kinloch, A. J.; Taylor, A. C. Particle Cavitation in Rubber Toughened Epoxies: The Role of Particle Size. *J. Mater. Sci.* **2010**, *45* (14), 3882–3894.

(57) Zhang, H.; Tang, L. C.; Zhang, Z.; Friedrich, K.; Sprenger, S. Fracture Behaviours of in Situ Silica Nanoparticle-Filled Epoxy at Different Temperatures. *Polymer* **2008**, *49* (17), 3816–3825.

(58) Chatani, S.; Kloxin, C. J.; Bowman, C. N. The Power of Light in Polymer Science: Photochemical Processes to Manipulate Polymer Formation, Structure, and Properties. *Polym. Chem.* **2014**, *5* (7).

4.7. Supporting Information

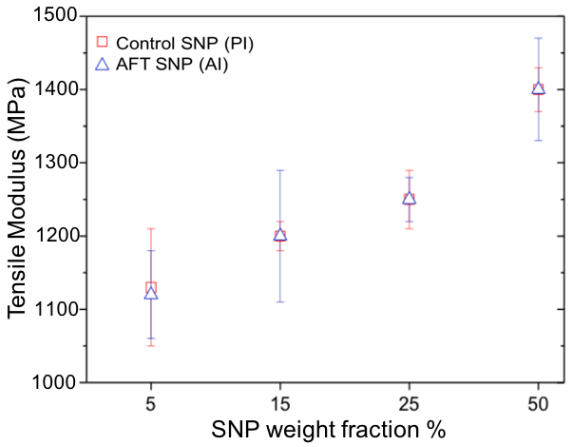

Figure S4.1. Tensile young's modulus for both PI (squares) and AI (triangles) composites as a function of SNPs weight fraction. Resins were formulated such that there was stoichiometric balance of a PETMP, TATTATO (1:1 SH:ene). Polymerization was conducted with 1 wt% of I819 (bis(2,4,6-trimethylbenzoyl)-phenylphosphineoxide) visible light photoinitiator, and 2 wt% of I65 (2,2-Dimethoxy-1,2-diphenylethan-1-one). Samples were photocured with (400-500) nm visible light at 50 mW/cm^2 for 20 min and then post-cured in an oven at 100°C for 24 h.

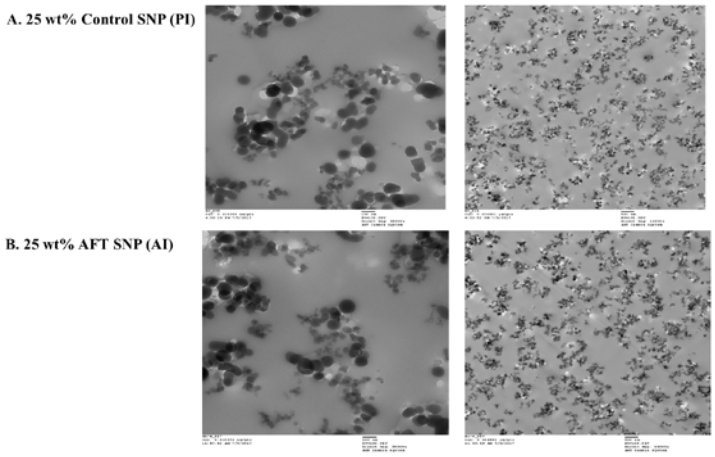

Figure S4.2. High-resolution scanning electron microscopy (TEM) images were taken for surfaces of PETMP-TATATO composites containing: A. 25 wt% control SNP (PI), B. 25 wt% AFT SNP (AI). Resins were formulated such that there was stoichiometric balance of a PETMP, TATTATO (1:1 SH:ene). Polymerization was conducted with 1 wt% of I819 (bis(2,4,6-trimethylbenzoyl)-phenylphosphineoxide) visible light photoinitiator, and 2 wt% of I65 (2,2-Dimethoxy-1,2-diphenylethan-1-one). Samples were photocured with (400-500) nm visible light at 50 mW/cm^2 for 20 min and then post-cured in an oven at 100°C for 24 h.

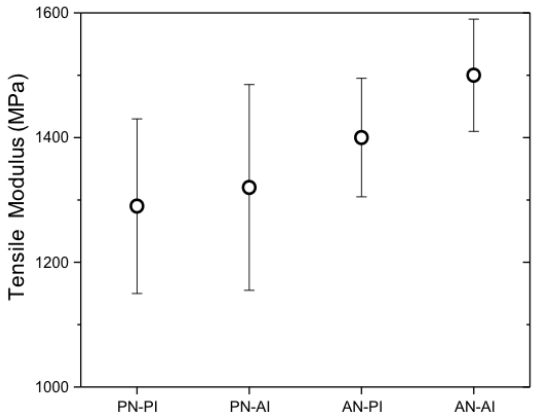

Figure S4.3. Tensile young's modulus of four composites: (i) PN-PI composite with no exchangeable bonds, (ii) PN-AI composite with interfacial bond exchange, (iii) AN-PI composite containing exchangeable bond in the polymer network but not at the interface, and (iv) AN-AI composite containing exchangeable bonds both in the polymer backbone and at the resin-filler interface. The resin contained PETMP as the thiol monomer and a stoichiometrically balanced (relative to functional groups) quantity of an allyl and vinyl ether mixture, itself composed of 75 mol% (relative to ene functional groups) TATATO and 25% of either the AFT or non-AFT DVE, with 1 mole% of I819, 2 mol% of I651, and 25 wt% of SNPs were cured using 400-500 nm visible light at 50mW/cm^2 for 20 min. Tensile test was conducted on dogbone-shaped sample with strain rate 1mm/min.

Table S4.1. Viscosity at shear rate 250 s^{-1}, glass transition temperature and storage modulus (MPa) at T_g + 30˚C of four different composite formulations.

Sample	Viscosity (Pa·s)	T_g˚C	Storage modulus (MPa)
PN-PI	1	28±2	17±3
PN-AI	1	27±2	20±2
AN-PI	1	25±2	20±5
AN-AI	1	27±2	21±3

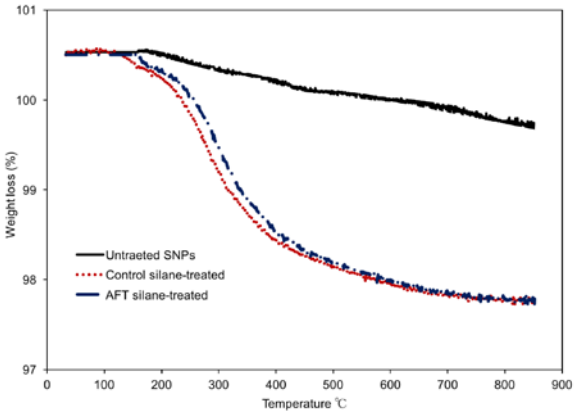

Figure S4.4. Thermogravimetric analysis on glass microparticles before, and after silanization with AFT silane (AI) and control silane (PI). The 2 % weight difference between treated and untreated particles suggests successful silane grafting on the glass surface. Based on this result, calculation yields approximately $1.03*10^{-6}$ mole of AFT silane per m^2 on the nanoparticle surface and $1.05*10^{-6}$ mole of control silane per m^2 on the nanoparticle surface.

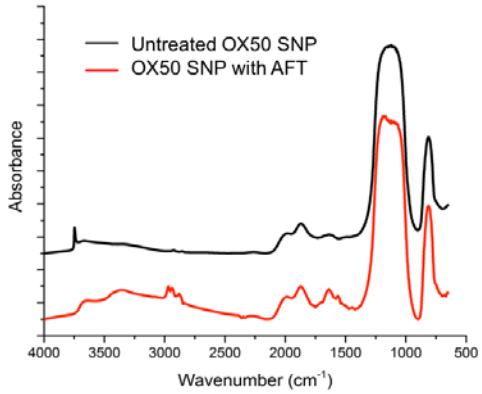

Figure S4.5. Diffuse reflectance infrared fourier transform spectroscopy (DRIFTS) analysis of untreated (top, black line) and AFT functionalized (bottom, red line) silicon dioxide nanoparticles. Silanol peak disappearance is evident at 3745 cm^{-1}. Also, the IR signals of the organic layer grafted on the particle surface are apparent in the range 2800-3100 cm^{-1}.

Chapter 5

Enhancing the Toughness of Composites via Dynamic Thiol-Thioester Exchange (TTE) at the Resin-Filler Interface*

Due to a mismatch in mechanical moduli, the interface between constituent materials in a composite is the primary locus for crack nucleation due to stress concentration. Relaxation of interfacial stresses, without modifying the properties of constituent materials, is a potent means of improving composite performance with broad appeal. Herein, we develop a new type of adaptive interface that utilizes thiol-thioester exchange (TTE) at the filler-polymer interface. Specifically, dynamic covalent bonds sequestered at material interfaces are reversibly exchanged in the presence of thioester moieties, excess thiol and a base/nucleophile catalyst. Employing this active interface effectively mitigates deleterious growth of interfacial stresses, thereby enhancing the composite's mechanical performance in terms of reductions in polymerization shrinkage stress and improvement in toughness. Specifically, activating interfacial TTE in an otherwise static matrix, resulted in 45% reduction in the polymerization stress, 50% post polymerization stress relaxation and drastically increased toughness relative to control composites incapable of TTE bond exchange but otherwise identical.

*Manuscript in preparation.

5.1. Introduction

Polymers reinforced with rigid fillers (such as glass beads, silica and alumina particles) are widely used in many engineering fields due to the flexibility they provide in targeting desired physical and mechanical properties. Nanocomposites are of particular interest when designing composites of higher stiffness, due to the enormous surface area associated with nanofillers.[1,2] It is well known that the interfacial region in such polymers concentrates stresses due to the common mismatch in mechanical moduli between constituent materials, which negatively impacts the overall mechanical properties.[3] Accordingly, several decades of work have been directed towards reducing the interfacial stress, improving stress transfer between fillers and the matrix, and examining impacts of filler size, content and the adhesive strength.[2] Despite these efforts, alleviating the concentration of interfacial stresses in order to prevent premature composite failure and improve crack-growth resistance is an ongoing challenge. Inspired by this limitation, recent developments in dynamic polymer composites have showcased the incorporation of dynamic covalent chemistries (DCCs). The presence of DCC-capable moieties in the resin formulation leads to chemical bond reshuffling and promotes stress relaxation while maintaining connectivity of the polymer network. These dynamic networks exhibit static thermoset properties under ordinary circumstances but reversibly rearrange covalent bonds, often in response to an externally applied stimulus.[4,5]

Recently, mechanoresponsive DCC-based composites, such as addition fragmentation chain transfer (AFT) based dental composites,[6,7] transesterification-based epoxy composites,[8,9] and disulfide-based vitrimer composites,[10] have been developed. A unique adaptive interface platform was introduced to effectively mitigate the interfacial stress and improve the overall mechanical properties by localizing AFT moieties only at the matrix-filler interface. However,

composites with AFT-active filler are capable of undergoing stress relaxation at the interface only during light exposure which is required for generating short-lived radicals, thus offering minimal capacity for stress relaxation over the lifetime of the composite or in areas where light exposure is limited (e.g., optically thick).[11]

To address AFT's shortcomings, a perpetual, light independent interfacial DCC mechanism is examined here: the anion-mediated thiol-Thioester Exchange (TTE) reaction. Exchange reactions involving thioesters have been effectively utilized to develop native chemical ligation (NCL)[12], degradable hydrogel networks,[13] synthetic sequence-controlled polymers,[14] and to increase refractive indices in bulk polymers.[15] However, the dynamic behavior in such crosslinked networks was not explored until Worrell et al. published the first work introducing TTE reaction as a new class of covalent adaptable networks (CANs) that enable rapid, continuous ambient temperature stress relaxation.[16] This exchange reaction only proceeds under the condition that free thiol, thioester, and base/nucleophile as a catalyst are all present in the network. The exchange reaction happens when the unreacted thiol groups are deprotonated by basic catalysts, which generates thiolate anions that then attack the carbonyl functional groups to form a short-lived symmetrical intermediate, followed by the regeneration of the thioester and thiolate anion (**Figure 5.1A**). If any of these three elements are missing, the polymer behaves as a typical crosslinked elastomer.[16] While this dynamic exchange reaction has been demonstrated in bulk materials,[16,17] using this phenomenon to relax interfacial stresses has never been achieved.

Therefore, following the successful demonstration by Worrell et al. indicating the efficiency of the TTE reactions[16] and the exceptional efficiency of interface-limited DCC processes in composites,[11] herein silica nanoparticles (SNP) were functionalized using a silane that had a TTE moiety capable of bond exchange and dispersed into a thiol-ene resin. By localizing

TTE to the resin filler interface, adaptive interfaces capable of stress relaxation and dynamic bond exchange were created (**Figure 5.1A**). This behavior manifests as enhanced stress relaxation and improved mechanical properties. Due to the long catalytic lifetime of base/nucleophile catalysts, such system undergo continuous exchange reaction of covalent bonds and continue to relax the interfacial stress over the lifetime of the composite. Strikingly, *in situ* interfacial bond exchange is observed to directly impact fracture processes, delaying crack propagation and displaying unique failure mechanisms in TTE-enabled composites.

5.2. Materials and Methods

Materials

Pentaerytritol tetrakis(3-mercaptopropionate) (PETMP), Triallyl-1,3,5-triazine-2,4,6-(1H,3H,5H)-trione (TATATO), 1,4-diazabicyclo[2.2.2]octane (DABCO), and propylamine were purchased from Sigma-Aldrich. Irgacure 819 (bis(2,4,6-trimethylbenzoyl)-phenylphosphineoxide) was obtained from BASF. Schott glass (mean particle size 40 nm) untreated were generously donated by Evonik Silicas and used as the inorganic fillers. Prior to implementation and as described later, these fillers were subsequently functionalized with thiol group for inclusion and copolymerization in the composite. All chemicals were used as received. The thioester-diacrylate[20] was synthesized using methods reported elsewhere.

Filler Functionalization

4 g of silica particles (Schott, OX50, 40 nm) were first taken in a glass tube and heated at 165 °C under vacuum using a Buchi heater/condenser for 3 h. The dried nanoparticles were then transferred to a 250 mL bottom rounded flask containing 200 mL of anhydrous toluene

supplemented with 2 g of (3-Mercaptopropyl) trimethoxysilane prereacted for 10 min with 2 g of n-propylamine. The reaction mixture was then refluxed at 120 °C for 24 h. After sinalization of nanoparticle, the liquid suspension was centrifuged and the solid pellets collected thoroughly, and washed with toluene (3× ≈ 25 mL) and methylene chloride (3× ≈ 25 mL) in two separate washing/centrifugation cycles. The washed filler particles were dried under vacuum overnight at 70 °C. Then 2 g of the dried thiol functionalized fillers were reacted with 0.7 g thioester diacrylate in DCM in presence of 3 mL TEA base at R.T overnight. After silanaization of nanoparticle was washed with DCM (1× ≈ 25 mL), toluene (2× ≈ 25 mL) and DMSO (2× ≈ 25 mL), and dried under vacuum overnight at 70 °C. The functionalized particles were analyzed by DRIFT FT-IR spectroscopy and TGA. The mass loss difference between silanized and unfunctionalized fillers suggests successful functional group grafting on the surface of glass particles in each case. Also, the DRIFT FT-IR characterization provides evidence of silanol group disappearance around 3745 cm^{-1}, and the appearance of the thioester group around 1700 cm^{-1} implying successful surface modification.

Fourier Transform Infrared Spectroscopy

An FT-IR spectrometer (Nicolet 6700) connected to a tensometer via fiber optic cables was used to monitor the real-time polymerization kinetics in concert with stress measurements. Samples were placed between two cylindrical quartz rods, and 300 mW cm^{-2} light was irradiated from the bottom rod using a light guide connected to a mercury lamp (Acticure 4000, EXFO) with 400–500 nm bandgap filter. The overtone signal of double bonds between 6250–6096 cm^{-1} was monitored during the FT-IR measurements.

Polymerization Shrinkage Stress Measurement

Shrinkage stress was measured via a tensometer using cantilever beam deflection theory (American Dental Association Health Foundation, ADAHF–PRC). A composite paste (1 mm in thickness, 6 mm in diameter) was placed between two cylindrical quartz rods, which were previously treated with a methacrylate functional silane to promote bonding at the glass surface/ resin interface. A 300 mW cm^{-2} of light was irradiated from the bottom rod using a light guide connected to a mercury lamp (Acticure 4000, EXFO) with a 400–500 nm bandgap filter. Polymerization-induced shrinkage of sample exerted a tensile force which caused the deflection of the aluminum beam. A linear variable differential transformer was used to convert the displacement to shrinkage stress based upon beam calibration constant and cross-sectional area of the sample. For the simultaneous measurement of conversion with shrinkage stress, data were collected continuously for 10 min (n=3).

Thermogravimetric Analysis

TGA (Pyris 1, PerkinElmer) was used to analyze the functionalized silica nanoparticles. Each sample was run in a nitrogen atmosphere (20 mL min^{-1}) from 50 to 850 °C at a heating rate of 10 °C min^{-1}.

Fracture test

We adopted single edge notch geometry for the fracture test as shown in Fig. 5.3(A). The sample consisted of a rectangular thin sheet with width w=22mm and height h=20mm. An initial crack with length a=5mm was introduced at the edge of the sample by a blaze. In order to perform the Digital Image Correlation (DIC), a speckle grey distribution pattern that deforms along with the sample is required to calculate displacements and strains with accuracy. To obtain such a pattern,

we sprayed the sample surface with black dots as shown in Fig S5.3. Then the sample was mounted on a mechanical test machine (Intron 5965) for fracture test. First the sample was subjected to a tensile displacement at a fixed strain rate of 0.025/min until the global strain reached to 0.03. Next, the sample was relaxed by holding the global strain at 0.03 for 5mins for Control sample and 3 mins for TTE sample. Then, a same loading rate 0.025/min was applied until the crack stated to propagate. The stain history is shown in Fig 5.3(A). During the test, the video recording was performed with a CCD camera (Canon EOS 6D DSLR along with Canon 100mm F/2.8L Macro Lens).

Digital image correlation

The DIC software used in this study was Ncorr, an open source code written in MATLAB. Ncorr has ability to obtain the displacement and strain fields by analyzing input reference and current images based on the DIC algorithm. For the reference image, we extracted the first frame from video as the initial configuration. For the current images, since there are three stages for loading history, we extracted frames every 6s before relaxation, every 1min during relaxation and every 10s after relaxation as deformed configurations. After specifying three important parameters (subset radius, subset spacing and strain radius) following the instructions provided by Nccor, we were able to obtain the displacement and strain fields for the fracture test. More details on the code are available in at the website (http://www.ncorr.com/).

Three-point-bending test

Rectangular bars (2×4×20 mm) and 2 uneven notches (3-mm long notch and 1.5 mm short notch) on one edge were used for three-point bend tests to measure fracture toughness. The three-point bend test was performed using a (MTS 858 Mini Bionix II) testing machines. Five specimens of

each composition were tested to evaluate the mechanical tests with displacement rate of 1.0 mm/min.

Tensile Testing

It was performed using an MTS Exceed E42 universal testing machine with a 500N load cell to give the engineering stress–strain curve, the Young's modulus (determined from the initial linear elastic region of the stress–strain curve), the yield stress (the stress at the maximum), the elongation to break, and the toughness (as measured from the area under the stress–strain curve). Dogbone samples were cut or molded (for brittle specimens) with a 3.15 mm width and 0.1 mm thickness, however the gage length was ≈15 mm. The specimens were clamped in the grip areas and tested under uniaxial tensile loading at displacement rate 0.0001 s^{-1}.

5.3. Results and Discussion

To develop a TTE-based adaptive interface and examine its influence on composite behavior, SNPs were functionalized using a silane that had a thioester moiety capable of bond exchange and dispersed with 10 wt% particle loading into photopolymerizable thiol-ene resin, as illustrated in **Figure 5.1**. The static resin was comprised of a triene monomer (1,3,5-triallyl-1,3,5-triazine-2,4,6(1H,3H,5H)-trione (TATATO)) and a tetrathiol (pentaerythritol tetra (3-mercaptopropionate (PETMP)) with 10% excess thiol and 2wt% 1,4-diazabicyclo[2.2.2]octane (DABCO) nucleophile (**Figure 5.1B**). An identical control sample, unable to undergo TTE bond exchange through the elimination of the TTE moiety from the interface or the catalyst necessary for the bond exchange was also formulated. The control composite exhibited a similar T_g and

storage modulus at ambient conditions ($T_g \approx 60$ °C, **Figure S5.1**), which allows us to decouple the effects caused by the interfacial bond-exchange process.

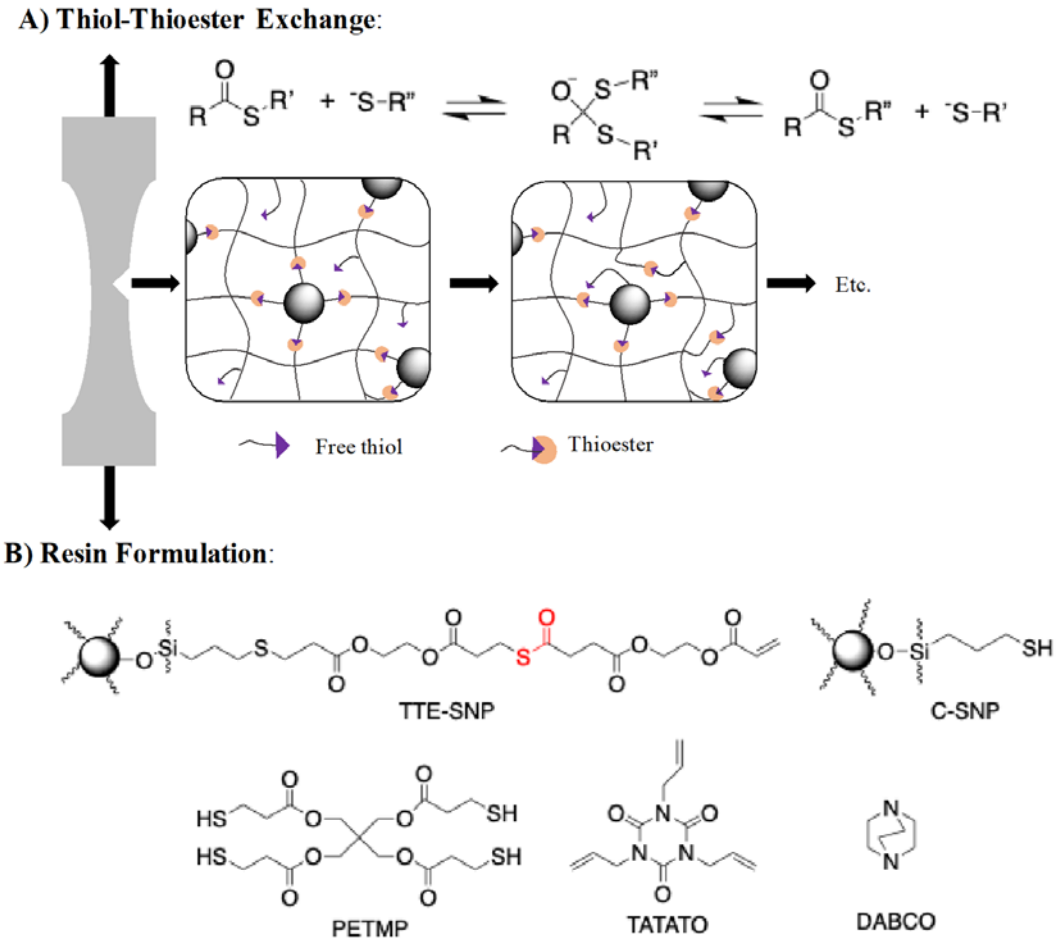

Figure 5.5. A) Mechanism and illustration for TTE at the SNP-polymer interface. B) Monomers and fillers used in the formulation of the composites. Resins were formulated of PETMP and TATATO (1.1:1 SH:ene), 2 wt% DABCO and 10 wt% of SNPs, either TTE or the corresponding control. Polymerization was initiated with 1 wt% of I819 (bis(2,4,6-trimethylbenzoyl)-phenylphosphineoxide) visible light photoinitiator, and photocured with 400–500 nm visible light at 50 mW cm^{-2} for 5 min on each side and then postcured in an oven at 60 °C for 4 h.

Residual stress is known to arise during polymerization, due to post-gelation volumetric contraction and elastic modulus development primarily during vitrification, leading to reduced mechanical performance and premature failure.[20,21] The design of mechanically robust glassy networks with low polymerization-induced shrinkage stress at quantitative conversion is

particularly demanding in the application of bulk materials. To investigate the effect of interfacial TTE bond exchange on shrinkage stress reduction within a composite system, the real-time polymerization kinetics, and the corresponding stress generated due to the shrinkage on both control and TTE-capable composites were monitored *via* an FTIR spectrometer connected to a tensometer. **Figure 5.2A** shows the evolution of shrinkage stress of the TTE composite as compared to the shrinkage stress developed in the analogue control at equivalent conversion. A significant (45%) reduction in the polymerization shrinkage stress was achieved in the composites with activated TTE at the particles interface as compared with the TTE-free composites used in the control experiment at equivalent 90% conversion (**Figure 5.2A**). While interfacial relaxation should intuitively be capable of reducing shrinkage stress, the dramatic improvement here is enabled by the high surface area to volume ratio of SNPs.

To assess the influence of TTE bond exchange in fully cured, glassy composites (T_g = 60 °C as measured in DMA) and examine the ability of interfacial TTE bond exchange to relieve stress during mechanical loading, stress relaxation experiments were conducted by applying a constant 1% tensile strain to both TTE-based and control composites at ambient temperature. Composites with activated TTE at the particle interface exhibited a significant 50% stress relaxation within 30 minutes even though the bulk resin is not capable of any DCC. In contrast, the control composites showed minimal stress relaxation, typical of glassy thermosets (**Figure 5.2B**). This ability to relax stresses is a key demonstration of the ability of interfacial dynamic bond exchange to enhance composite performance when under mechanical loading.

To examine the influence of interfacial bond exchange on the strength and toughness of glassy composites under mechanical loading, tensile testing was conducted with a constant strain rate of 0.0001 s^{-1} until failure. Composites with activated TTE at the interface exhibited

significantly higher tensile strength and 3-4 times greater toughness than the control composite (**Figure 5.2C & Table S5.1**). Interestingly, in addition to the dramatic increase in toughness, different failure modes were also observed in the control and TTE-activated samples. The control samples showed a typical brittle failure mode for a glassy composite, where at the peak stress, a crack appeared and catastrophically propagated across the sample, providing no early indication of upcoming failure. However, a different failure mode was observed in the TTE samples, where an initial crack formed and then propagated across the sample as would normally be observed in the control, but the crack propagation was eventually arrested, and the stress plateaued. Subsequent increases in stress nucleated a second crack on the opposite side of the sample. The two cracks then merged and the sample failed catastrophically (**Figure 5.3C**). This shift in fracture behavior along with the corresponding increase in the toughness relative to control samples is related to ongoing interfacial stress relaxation of chain deformations during tensile loading. During tensile tests, the energetic barrier to chain scission in the polymer resin reduces, generating defects and leading to failure.[22,23] Having exchangeable bonds at the particle interface in TTE composite acts to counter this effect by relaxing chain conformation, reducing the stress at the crack tip that drives the crack propagation, and hence delaying failure.

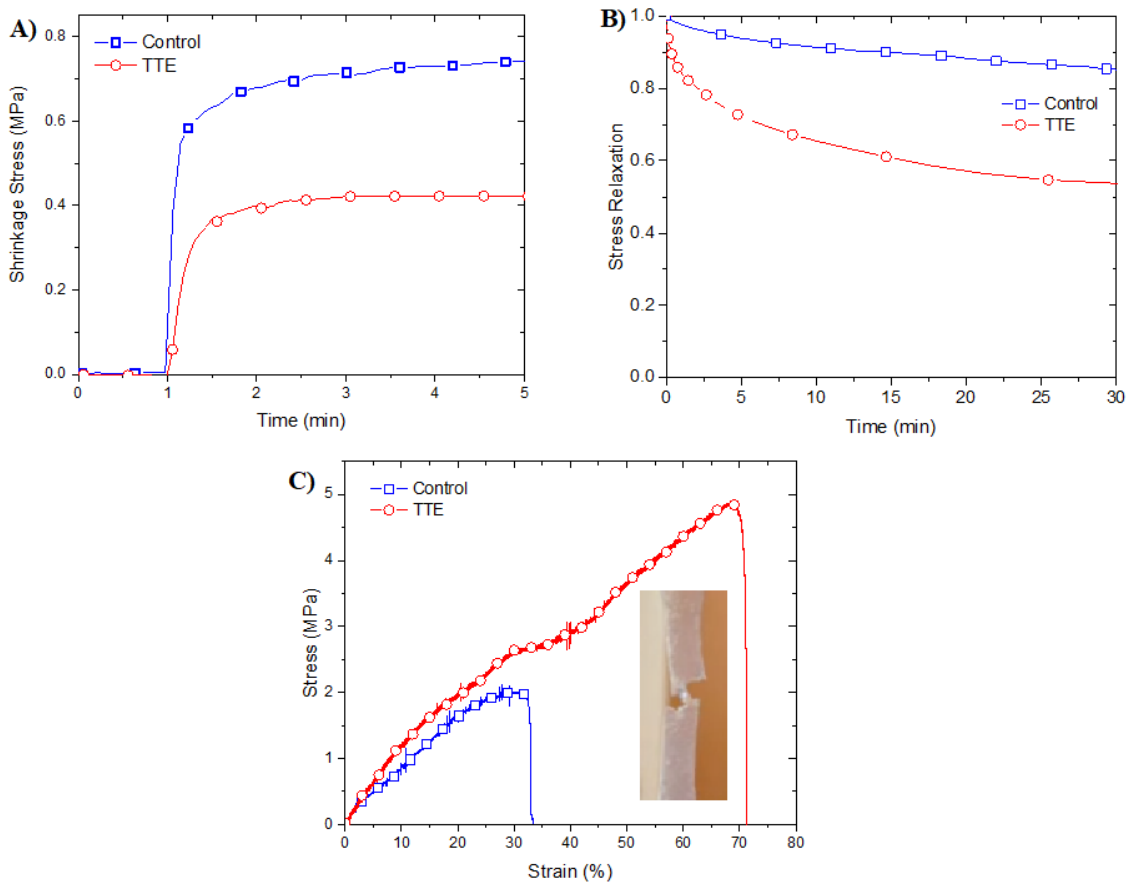

Figure 5.6. A) In situ polymerization stress of both control (squares) and TTE (circles) composites. Samples were placed between two quartz rods, previously treated with a thiol-functional silane and irradiated for 5 min at ambient temperature with 400–500 nm light at 50 mW cm^{-2} following 1 min in the dark to establish a baseline measurement. B) Stress relaxation achieved on fully cured 0.25 mm thick sample, of control (squares) and TTE (circles) composite at constant 1% strain. C) Tensile test for fully cured, dogbone-shaped of both control and TTE-enabled composites at a displacement rate 0.0001 s^{-1}.

Motivated by the different failure mechanisms observed in tensile experiments, notched samples of control and TTE-activated composites (**Figure 5.3A**) were used to study how TTE affects the deformation of a pre-existing crack before it starts to propagate. As shown in **Figure 5.3B**, initially the notched TTE and control samples exhibited similar compliance, but the notched TTE sample was able to sustain a higher peak force than the control. Digital Image Correlation (DIC) was used to map the strain fields in both notched samples. Results of the normal strain

component ε_{yy} along the tensile direction, shown in **Figure 5.3C**, revealed a striking difference. In the control sample, a significant concentration of ε_{yy} near the crack tip emerged as the external loading increased, which manifests severely amplified stress at the crack tip. The crack tip stress concentration causes localized material failure and hence crack propagation.[24] In contrast, the ε_{yy} field in the TTE sample was more diffusive, as reflected in the lower strain at the crack tip but higher strain far ahead of the crack tip as compared to the control sample. This result suggests that the TTE process was able to alleviate crack tip strain concentration through stress relaxation, which led to crack tip blunting and delocalized material failure, reminiscent of the toughening effects of plasticity in metals.[25] The DIC experiment was repeated for other TTE and control samples and similar observations were found (**Figure S5.2**). To quantify the toughening effect of TTE, the Griffith fracture criterion were applied to the notched samples, i.e., whether a crack can propagate or not is governed by a competition between the energy release rate G and the fracture energy Γ (unit: J/m^2).[25] The former, G, is the energy available to drive crack propagation per unit area and represents structural effects such as the external loading and sample geometry. The latter, Γ, defined as the energy required to advance the crack by a unit area, describing the material's resistance to fracture. Initiation of crack propagation occurs when G exceeds Γ. Since the TTE and control composites can be approximated as linear elastic materials with about the same modulus before unloading occurs, G can be evaluated using the crack opening displacement (**Figure S5.3**). The critical value G_c at the onset of crack propagation is taken as the fracture energy. Using this method, G_c for the TTE sample in **Figure 5.3** was found to be 550 J/m^2, over twice that of G_c for the control (260 J/m^2).

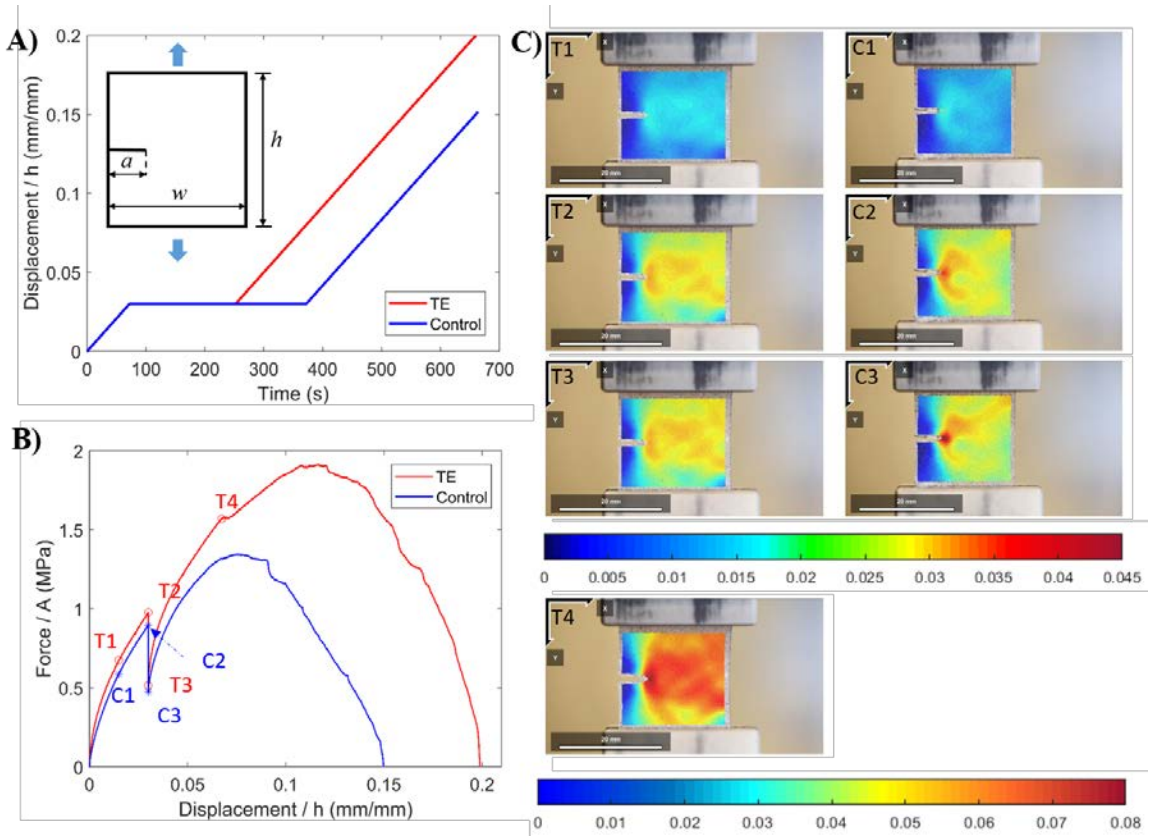

Figure 5.7. Single edge notch fracture test using the (A) Control and (B) TTE samples. Spatial distribution of the vertical normal strain components ε_{yy}, measured using DIC, right before crack propagation (marked by the red dots in the nominal stress versus strain plot) is shown.

The notched sample tests in **Figure 5.3** focus on the crack deformation before propagation. To highlight further the effect of the TTE adaptive interfaces on the crack propagation behavior, three-point bending tests were performed on a two-notch sample where one notch is double the length of the other, with a crosshead speed of 1 mm/min until fracture (**Figure 5.4A)**. The dimensions of each specimen used in the investigation were 2 × 4 × 20 mm^3 with 3 mm and 1.5 mm cracks on one edge. The control composite failed in a brittle manner, with propagation of the longer crack happening at 10% strain (1.1 mm displacement) as shown in **Figure 5.4A-1**. In contrast, by activating the TTE at the resin/filler interface, the failure process became more ductile. **Figure 5.4A-1** show that in TTE-activated samples the initial crack propagation also began at the

tip of the longer crack, but the propagation was slow compared to the control and was eventually arrested. As the displacement loading continued to increase, the shorter crack began to propagate and ultimately caused failure. The arrest of the longer crack resulted in ≈ 3 times the total energy (6.1 ± 0.9 (MJ/m^3)) being absorbed before material failure when compared to the control (1.9 ± 0.5 (MJ/m^3)) (**Table S5.2**).

Morphology of fractured surfaces were characterized by utilizing a Micro X-ray Computed Tomography (MXCT, ZEISS Xradia 520 Versa) to capture post-mortem images of the cracks in control and TTE composites. As shown in **Figure 5.4A-2**, the control sample failed by continuous crack growth at the initially longer crack, before the shorter crack even started to grow, while fractured surfaces of TTE indicate that the initially longer crack propagated for only ≈ 100 μm then stopped growing and the shorter one catastrophically propagated to cause the ultimate failure (**Figure 5.4A-2)**.

The difference in crack propagation behavior in the TTE and control samples is interpreted by considering how the energetic driving force *G* and resistance Γ change as the crack propagates. The change in *G* is governed by structural effects such as external loading conditions, sample geometry and crack length. On the other hand, Γ typically increases upon crack propagation in materials with hysteretic behavior due to the expansion of a dissipation zone around the crack tip, known as crack growth resistance.[25] For the control composite, the concentrated crack tip strain field and the brittle fracture mode imply that the increase in Γ upon crack propagation should be insignificant. Therefore, the fact that the longer crack in the control sample propagated catastrophically suggests that *G* should increase with crack length, i.e., structurally the test geometry in **Figure 5.4A** favors continuous growth of the longer crack. Since the TTE and control samples are subjected to the same geometry and loading condition, structural effects should also

favor continuous growth of the longer crack in the TTE sample. However, the longer crack in the TTE composite was arrested, implying that Γ must also increase with crack length. This phenomenon, attributed to the TTE-induced stress relaxation and energy dissipation at the crack tip,[26,27] can stabilize the propagation of the longer crack if it surpasses the structural effects for *G* that favor continuous growth.

Another peculiar observation in the TTE sample is that the shorter crack took over the propagation after the longer crack was arrested. **Figure 5.4A-2** reveals that the shorter crack propagated at an angle with the original direction, indicating an interplay between Mode-I (tensile) and Mode-II (in-plane shear) in the local stress field.[25] A detailed analysis on the propagation of the shorter crack would require knowledge regarding the mixed-mode dependence of the fracture energy and is not pursued here. Instead, the fact that the short crack was able to propagate indicates that the stress field around its tip did not experience significant relaxation by the TTE reaction during the propagation of the long crack. Based on this argument, we hypothesize that higher stress leads to faster TTE-induced relaxation by increasing the reaction kinetics. Initially The higher stress at the longer crack accelerates the relaxation which eventually leads to its arrest. During this process, the shorter crack did not experience the same extent of stress relaxation, which allowed it to propagate after the arrest of the long crack. To verify this hypothesis, the time history of stress relaxation at three different fixed strain levels was measured (**Figure 5.4B)**. Accelerated relaxation rate was noticed by increasing the strain levels from 0.2% to 2% to 4%. At 0.2% strain 35% stress relaxation was achieved in 10 minutes, while the same degree of relaxation was achieved in 30 s at 4% strain, which clearly support our hypothesis. In addition, cyclic loading at three different stress levels, 0.5 MPa, 2 MPa and 4 MPa up to 3 loading-unloading cycles was performed. The ratio between the dissipative energy and the released energy was calculated at the three stress levels

and is presented in **Figure S5.4**. Higher stress levels systematically resulted in higher ratios of dissipative energy to the released energy, due to the accelerated, more efficient bond exchange, congruent with **Figure 5.3B**.

To investigate how TTE bond exchange affects the polymer composites at long time scales, a cyclic loading to 2 MPa stress was applied on both TTE and control composites, followed by unloading and reloading of the stress until the composite's failure. The hysteresis curves are presented in **Figure 5.4C & Figure S5.5**. Upon load release, TTE based composites systematically exhibit a greater degree of both energy dissipation and non-recoverable strain when compared to the control. Additionally, the TTE composite was found to survive more than 20 cycles without observable crack nucleation while the control composites were only able to survive 3-4 such cycles **Figure S5.4**. The cyclic loading tests, interpreted as an accelerated fatigue experiment, suggest that the resin/filler interfacial relaxation leads to longer composite lifetime.

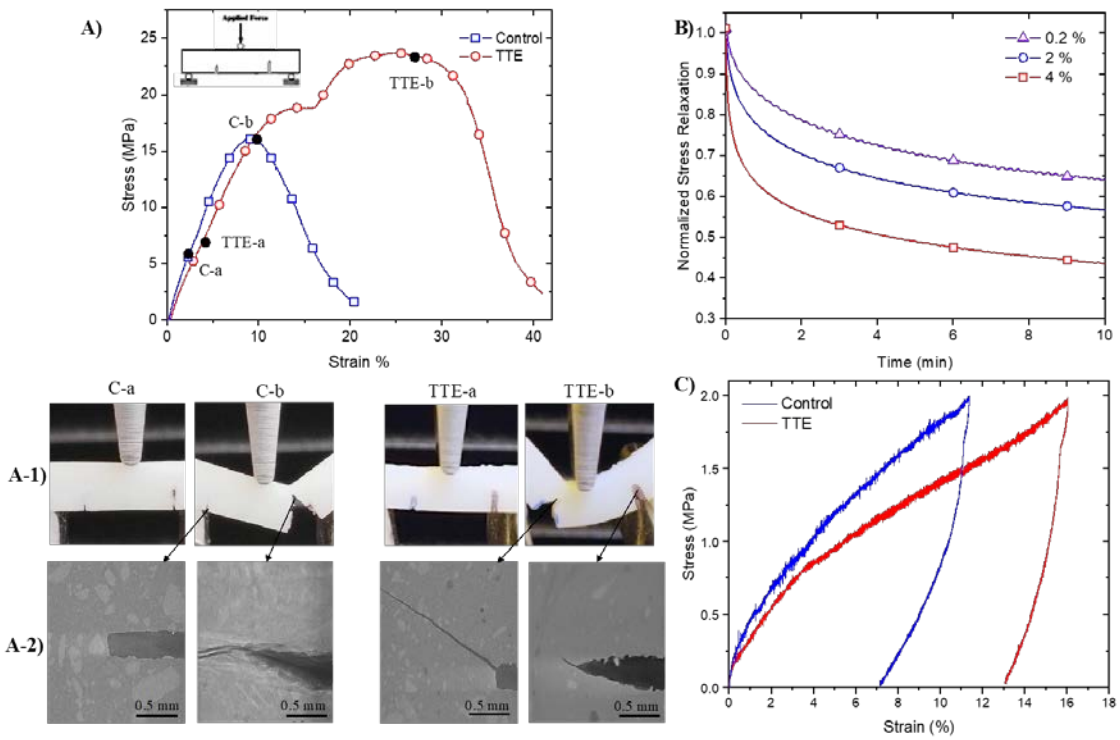

Figure 5.4. A) Stress-strain profiles from fracture of double-notched composite specimens for: Control composites (blue square) and dynamic TTE-enabled interface (red circle) at a displacement rate 1 mm/min. A-1) Images of the two uneven notches before and after failure. The non-dynamic control, as with other conventioanl materials, fails at the large notch whereas the TTE-enabled material initially yields at the large notch up to approximately 15% strain after which the small notch grows and is the locus of failure. A-2) Micro X-ray Computed Tomography (MXCT) images of fractured surfaces of the two cracks for both control and TTE-enabled composites. C) Stress relaxation of TTE composite at different strain (0.2% (purple triangle), 2% (blue circle) and 4% (red square)). C) First hysteresis loop cycle during loading of 2 MPa stress then unloading to 0 MPa at 0.0001 s^{-1} rate for both control and TTE enabled composite.

5.4. Conclusions

The efficiency of TTE bond exchange as a new light independent, interfacial DCC mechanism that can undergo continues bond reshuffling through the lifetime of polymer composites was examined here. As evidenced above, this platform significantly improves the composite's mechanical performance by relaxing the interfacial stress, despite the presence of TTE only at the interface with very low concentration. Activating TTE bond exchange at the polymer-particle interface enables the composites to significantly increase the degree of interfacial stress

relaxation, resulting in 45% reduction in polymerization stress, 50% stress relaxation when fully cured, glassy composite is under mechanical loading, 3-4 times improvement in the toughness, and a fundamental shifting of the failure mechanism. Achieving this behavior represents a transformative technology to continuously relax the stress concentration at the polymer-filler interface with broad potential for applications in materials with different constituents, especially in opaque composites or when composites are under mechanical loading.

5.5. Acknowledgments

The authors acknowledge financial support from the National Science Foundation (NSF DMR 1310528) and the National Institutes of Health (NIH 1U01DE023777). Additional thanks to Shane Fraizer and for assistance in performing Micro X-ray Computed Tomography experiment (MXCT).

5.6. Supporting Information

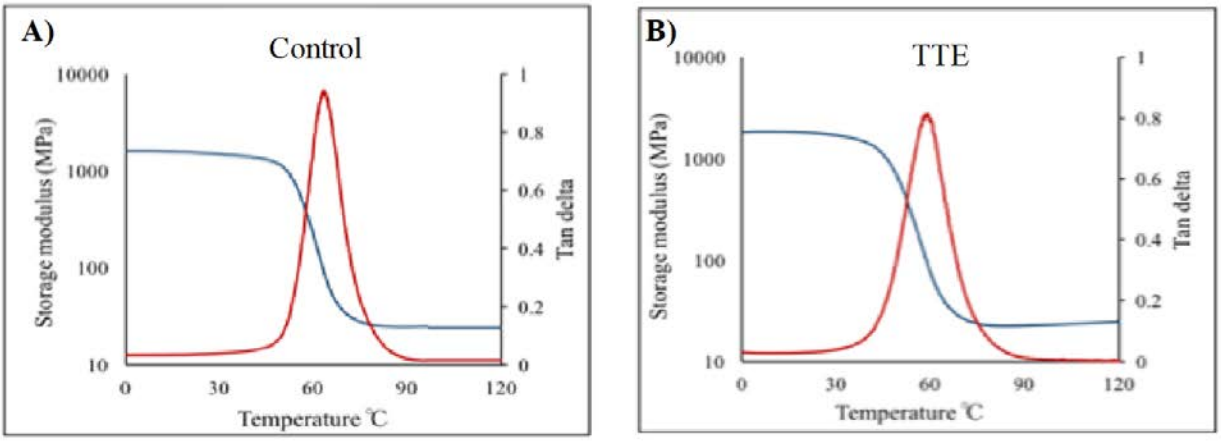

Figure S5.6. The tan δ curves and storage modulus curves of control-based and TTE based composites, obtained from DMTA measurements at 1 Hz.

Table S5.1. Mechanical properties of both control TTE based composites obtained from tensile testing at 0.0001 s^{-1} displacement rate.

	Tensile strength (MPa)	Elongation at break (%)	Toughness (MJ/m^3)
Control	3 ± 0.3	35 ± 4	0.5 ± 0.1
TTE	6 ± 1	55 ± 10	1.9 ± 0.4

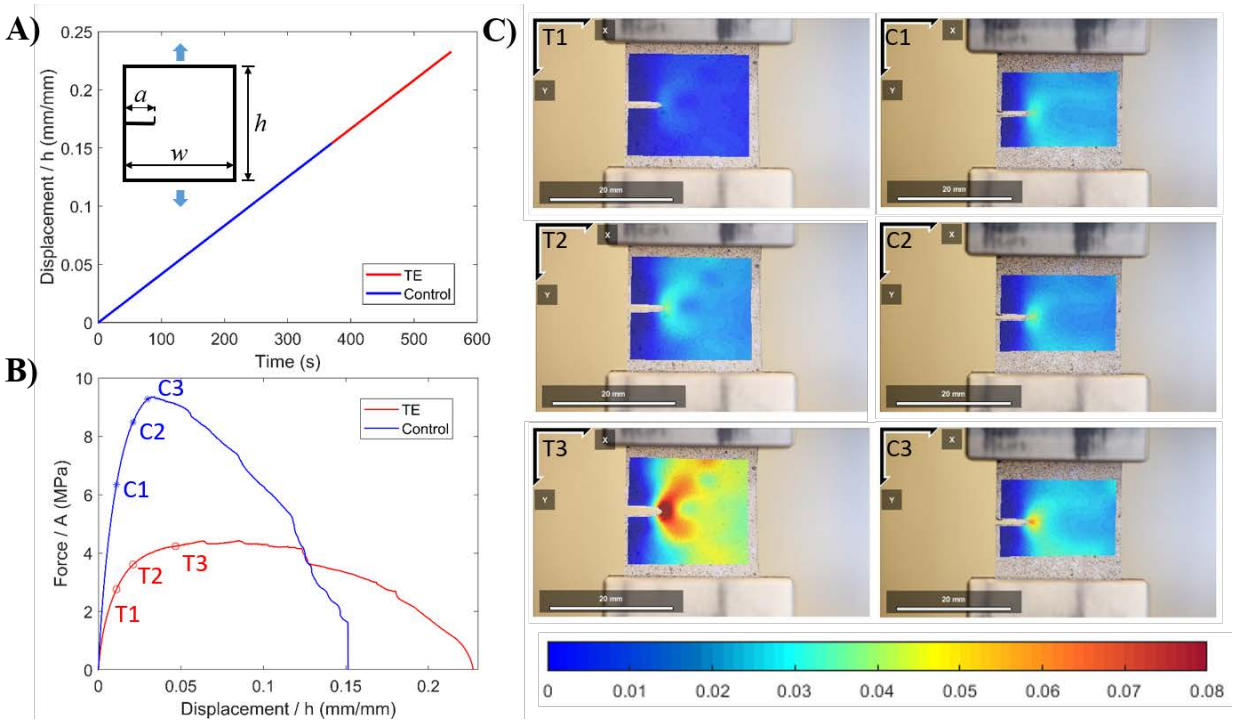

Figure S5.7. Notched sample tension and DIC data for another set of sample.

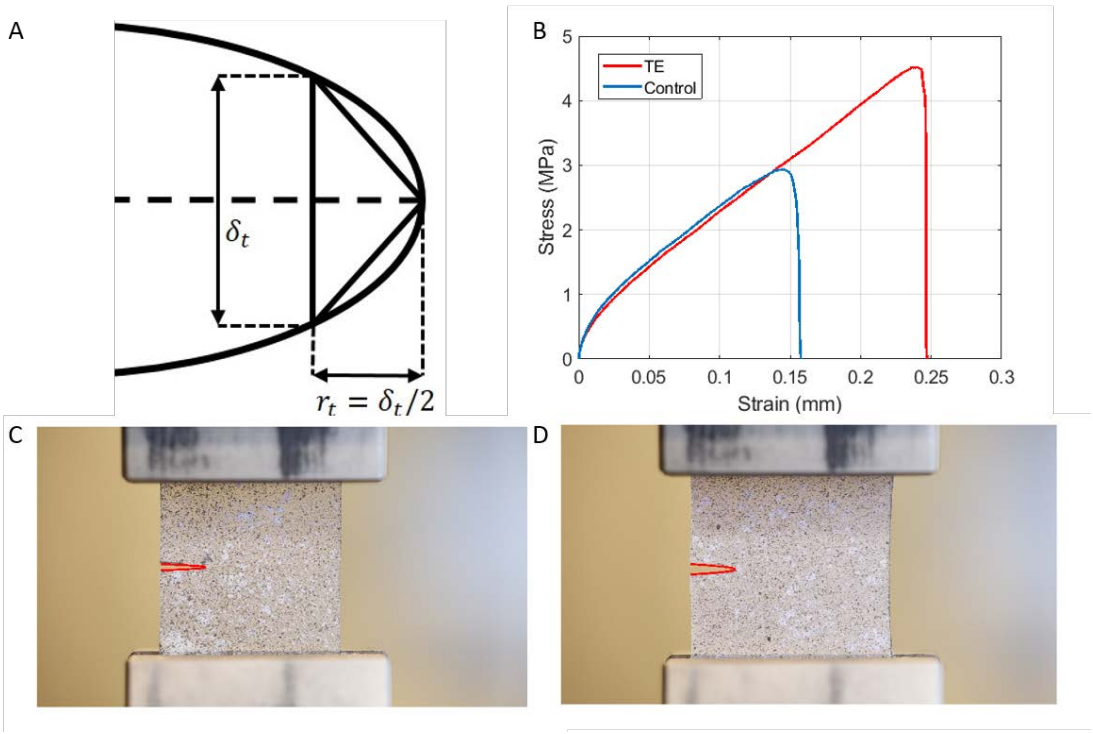

Figure S5.8. Evaluation of fracture energy G_c based on the crack opening displacement.

Table S5.2. Mechanical properties of 2-notches samples of both control and TTE based composite under 3-point bend test.

	Maximum stress (MPa)	Elongation at break (%)	Toughness (MJ/m^3)
Control	12 ± 3	10 ± 8	1.9 ± 0.5
TTE	28 ± 6	30 ± 10	6.1 ± 0.9

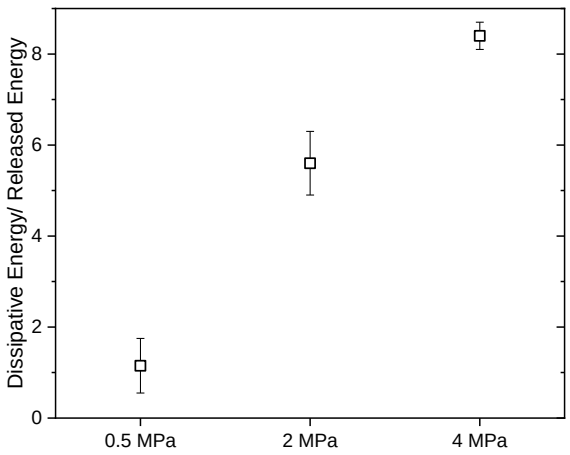

Figure S5.9. The ratio between the dissipative energy and the released energy of TTE based composites upon applying cyclic loading up to 3 stress level 0.5 MPa, 2 MPa and 4 MPa followed by release of the stress.

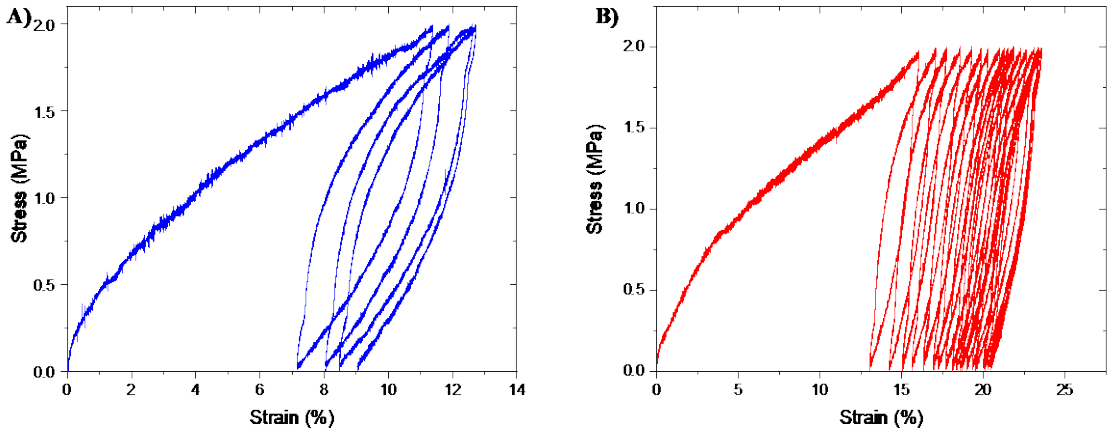

Figure S5.10. Hysteresis loop cycles during loading of 2 MPa stress then unloading to 0 MPa at 0.1 mm min^{-1} rate for both control and TTE enabled composite.

5.7. References

(1) Chen, Q.; Chasiotis, I.; Chen, C.; Roy, A. Nanoscale and Effective Mechanical Behavior and Fracture of Silica Nanocomposites. *Compos. Sci. Technol.* **2008**, *68* (15–16), 3137–3144.

(2) Fu, S. Y.; Feng, X. Q.; Lauke, B.; Mai, Y. W. Effects of Particle Size, Particle/Matrix

Interface Adhesion and Particle Loading on Mechanical Properties of Particulate-Polymer Composites. *Compos. Part B Eng.* **2008**, *39* (6), 933–961.

(3) Eiras, D.; Pessan, L. A. Mechanical Properties of Polypropylene/Calcium Carbonate Nanocomposites. *Mater. Res.* **2009**, *12* (4), 517–522.

(4) Kloxin, C. J.; Bowman, C. N. Covalent Adaptable Networks: Smart, Reconfigurable and Responsive Network Systems. *Chem. Soc. Rev.* **2013**, *42* (17), 7161–7173.

(5) Kloxin, C. J.; Scott, T. F.; Adzima, B. J.; Bowman, C. N. Covalent Adaptable Networks (CANs): A Unique Paradigm in Cross-Linked Polymers. *Macromolecules* **2010**, *43* (6), 2643–2653.

(6) Park, H. Y.; Kloxin, C. J.; Abuelyaman, A. S.; Oxman, J. D.; Bowman, C. N. Stress Relaxation via Addition–Fragmentation Chain Transfer in High T g , High Conversion Methacrylate-Based Systems. *Macromolecules 45* (14), 5640-5646

(7) Park, H. Y.; Kloxin, C. J.; Fordney, M. F.; Bowman, C. N. Stress Reduction and T g Enhancement in Ternary Thiol-Yne-Methacrylate Systems via Addition-Fragmentation Chain Transfer. *Macromolecules* **2012**, *45* (14), 5647–5652.

(8) Yang, Z.; Wang, Q.; Wang, T. Dual-Triggered and Thermally Reconfigurable Shape Memory Graphene-Vitrimer Composites. *ACS Appl. Mater. Interfaces* **2016**, *8* (33), 21691–21699.

(9) Legrand, A.; Souli-Ziakovic, C. Silica-Epoxy Vitrimer Nanocomposites. *Macromolecules* **2016**, *49* (16), 5893–5902.

(10) Ruiz de Luzuriaga, A.; Martin, R.; Markaide, N.; Rekondo, A.; Cabañ ero, G.; Rodrí guez, J.; Odriozola, I. Epoxy Resin with Exchangeable Disulfide Crosslinks to Obtain Reprocessable, Repairable and Recyclable Fiber-Reinforced Thermoset Composites. *Mater. Horizons* **2016**, 241–247.

(11) Sowan, N.; Cox, L. M.; Shah, P. K.; Song, H. B.; Stansbury, J. W.; Bowman, C. N. Dynamic Covalent Chemistry at Interfaces: Development of Tougher, Healable Composites through Stress Relaxation at the Resin-Silica Nanoparticles Interface. *Adv. Mater. Interfaces* **2018**, 1800511.

(12) Nilsson, B. L.; Soellner, M. B.; Raines, R. T. Ynthesis Of. **2005**, 91–118.

(13) Ghobril, C.; Charoen, K.; Rodriguez, E. K.; Nazarian, A.; Grinstaff, M. W. Angewandte A Dendritic Thioester Hydrogel Based on Thiol – Thioester Exchange as a Dissolvable Sealant System for Wound Closure. **2013**, 14070–14074.

(14) Price, J. L.; Hadley, E. B.; Steinkruger, J. D.; Gellman, S. H. NIH Public Access. **2011**, *49* (2), 368–371.

(15) Liu, J.; Ueda, M. High Refractive Index Polymers: Fundamental Research and Practical Applications. *J. Mater. Chem.* **2009**, *19* (47), 8907.

(16) Worrell, B. T.; McBride, M. K.; Lyon, G. B.; Cox, L. M.; Wang, C.; Mavila, S.; Lim, C.-H.; Coley, H. M.; Musgrave, C. B.; Ding, Y.; et al. Bistable and Photoswitchable States of Matter. *Nat. Commun.* **2018**, *9* (1), 2804.

(17) Wang, C.; Mavila, S.; Worrell, B. T.; Xi, W.; Goldman, T. M.; Bowman, C. N. Productive Exchange of Thiols and Thioesters to Form Dynamic Polythioester-Based Polymers. **2018**.

(18) Podgórski, M.; Worrell, B. T.; Sinha, J.; Mcbride, M. K.; Bowman, C. N. Thermal Metamorphosis in (Meth)Acrylate Photopolymers: Stress Relaxation, Reshaping, and Second-Stage Reaction . *Macromolecules* **2019**, *52*, 8114–8123.

(19) ASTM D638-02a, Standard Test Method for Tensile Properties of Plastics, ASTM International, West Conshohocken, 2002.

(20) Schneider, L. F. J.; Cavalcante, L. M.; Silikas, N. Shrinkage Stresses Generated during Resin-Composite Applications: A Review. *J. Dent. Biomech.* **2010**, *1* (1), 131630–131630.

(21) Song, H. B.; Sowan, N.; Shah, P. K.; Baranek, A.; Flores, A.; Stansbury, J. W.; Bowman, C. N. Reduced Shrinkage Stress via Photo-Initiated Copper(I)-Catalyzed Cycloaddition Polymerizations of Azide-Alkyne Resins. *Dental Materials*. Elsevier Inc. June 25, 2016.

(22) Odell, J. a.; Keller, a.; Rabin, Y. Flow-Induced Scission of Isolated Macromolecules. *J. Chem. Phys.* **1988**, *88* (6), 4022–4028.

(23) Michler, G. H.; Von Schmeling, H. H. K. B. The Physics and Micro-Mechanics of Nano-Voids and Nano-Particles in Polymer Combinations. *Polym.* **2013**, *54* (13), 3131–3144.

(24) Adriaensens, P.; Storme, L.; Carleer, R.; Vanderzande, D.; Gelan, J.; Litvinov, V. M.; Marissenf, R. Visualization of Tensile Stress Induced Material Response at a Crack Tip in Polymers under Critical Load by NMR Imaging. *Macromolecules* **2000**, *33* (13), 4836–4841.

(25) Zehnder, A. T. *Fracture Mechanics*; Springer US, 2012.

(26) Qi, Y.; Caillard, J.; Long, R. Journal of the Mechanics and Physics of Solids Fracture Toughness of Soft Materials with Rate-Independent Hysteresis. *J. Mech. Phys. Solids* **2018**, *118*, 341–364.

(27) Zhang, T.; Lin, S.; Yuk, H.; Zhao, X. Predicting Fracture Energies and Crack-Tip Fields of Soft Tough Materials. *Extrem. Mech. Lett.* **2015**, *4*, 1–8.

Chapter 6

Dynamic Covalent Chemistry (DCC) in Dental Restorative Materials: Implementation of a DCC-Based Adaptive Interface (AI) at the Resin-Filler Interface for Improved Performance*

Dental restorative composites have been extensively studied with a goal to improve material performance. However, stress induced microcracks from polymerization shrinkage, thermal and other stresses along with the low fracture toughness of methacrylate-based composites remain significant problems. Herein, the study focuses on applying a dynamic covalent chemistry (DCC)-based adaptive interface to conventional BisGMA/TEGDMA (70:30) dental resins by coupling moieties capable of thiol-thioester (TTE) DCC to the resin-filler interface as a means to induce interfacial stress relaxation and promote interfacial healing. Silica nanoparticles (SNP) are functionalized with TTE-functionalized silanes to covalently bond the interface to the network while simultaneously facilitating relaxation of the filler-matrix interface via DCC. The functionalized particles were incorporated into the otherwise static conventional BisGMA/TEGDMA (70:30) dental resins. The role of interfacial bond exchange to enhance dental composite performance in response to shrinkage and other stresses, flexural modulus and toughness was investigated. Shrinkage stress was monitored with a tensometer coupled with FTIR spectroscopy. Flexural modulus/strength and flexural toughness were characterized in three-point bending on a universal testing machine. A reduction of 30% in shrinkage stress was achieved when interfacial TTE bond exchange was activated while not only maintaining but also enhancing mechanical properties of the composite. These enhancements include a 60% increase in Young's modulus, 33% increase in flexural strength and 35% increase in the toughness, relative to

composites unable to undergo DCC but otherwise identical in composition. Furthermore, by combining interfacial DCC with resin-based DCC, an 80% reduction of shrinkage-induced stress is observed in a thiol-ene system “equipped” with both types of DCC mechanisms relative to the composite without DCC in either the resin or at the resin–filler interface. This behavior highlights the advantages of utilizing the DCC at the resin-filler interface as a stress-relieving mechanism that is compatible with current and future developments in the field of dental restorative materials, nearly independent of the type of resin improvements and types that will be used, as it can dramatically enhance their mechanical performance by reducing both polymerization and mechanically applied stresses throughout the composite lifetime.

*Manuscript Submitted

6.1. Introduction

Conventional dental restorative composites are mechanically stiff, highly-crosslinked networks formulated from inorganic fillers dispersed in photocured dimethacrylate resins.[1–3] Despite significant advances in composite development, premature restoration failure remains problematic. Though there are other factors such as secondary decay and hydrolytic degradation that influence the composite performance and lifetime; the often premature failure of these materials is at least in part attributed to the mechanical failure of the composite in response to stresses that arise both during and after placement.[1,2,4,5] Typically, inorganic fillers are used in dental composite to enhance the composite's mechanical performance including strength, wear resistance, thermal expansion coefficient and polymerization-induced volumetric shrinkage. However, high filler loadings in dental composites significantly affect their viscosity and hinder photopolymerization kinetics due to light scattering. Additionally, the inorganic filler is also a source for large stress gradients due to the modulus and thermal expansion mismatch between the filler and the resin matrix.[1,2,4] This stress, along with polymerization shrinkage stress and mechanically applied stress, are believed by many to cause serious clinical issues such as microcracking at the restoration-tooth interface and microleakage, and reduce the restoration's lifetime.[1,3,4,6–8] Therefore, the successful relaxation of any and all stresses that arise or are applied to the restoration is critical but it is anticipated that stress relaxation at the particle-resin interface would be of particular importance in improving the composite performance. In one approach, several ideas have been directed towards reducing shrinkage stress of dental restoratives while maintaining all other desirable material properties while other researchers have examined the effect of the type, size distribution, loading content and surface modification of the filler on composites properties.[4,7,8] Efforts have been directed to facilitate improvements in dental

composites by reducing the reactive group concentration,[9–11], modifying dimethacrylate monomer formulations,[12,13] and exploring alternative polymerization techniques, such as thiol-ene reaction,[3,14] ring-opening polymerizations,[5] copper(I)-catalyzed azide-alkyne cycloadditions (CuAAC).[2,15]

Recently, covalent adaptable networks (CANs) such as those based on reversible addition fragmentation chain transfer (RAFT) have been successfully implemented in dense networks and as resin phase in dental composites to eliminate stresses that arise from polymerization shrinkage and external loading, by enabling dynamic bond exchange in the polymer backbone while conserving the overall covalently bonded structure **(Figure 6.1A)**. However, while RAFT is simultaneously compatible with the current light induced radical-mediated methacrylate polymerization methodologies that are clinically practiced, this approach often results in a modification of material properties such as Young's modulus, T_g, and fracture toughness.[16,17] Therefore, improving the performance of conventional dental resins by alleviating the interfacial stresses through DCC approaches that target the particle-resin interface without deteriorating the mechanical properties of the polymerized material remains an unachieved goal.

To this end, a previous study has developed RAFT-containing adaptive interfaces that covalently bonded silica nanoparticles to a static thiol-ene resin and enabled bond exchange exclusively at the resin-filler interface.[18] As the interfacial region between the organic resin and inorganic fillers is known to concentrate stresses and nucleate crack formation, isolating the bond exchange to occur exclusively at the interfacial region enables stress relaxation where the stress is concentrated and significantly improved the composite's performance **(Figure 6.1B)**. Particularly, since implementation of a RAFT adaptive interface demonstrated its capability to reduce stress and improve material properties in an inert thiol-ene composite,[18] here, we apply the adaptive

interface concept to a conventional dental resin by introducing thiol-thioester (TTE) moieties that promote resin-filler bonding and persistent stress relaxation at the filler-resin interface, without altering the resin formulation. A fundamental difference between the RAFT and TTE DCC processes is that the RAFT-based approach is only active in facilitating bond exchange during the polymerization in the presence of the radicals that also cause polymerization. The TTE process is base or nucleophile catalyzed and as such, the bond exchange process in these composites is hypothesized to persist long after the initial polymerization is complete. As such, it is expected that interfacial stresses that arise after the polymerization, e.g., due to thermal expansion mismatch, would also be capable of relaxing. Further, the TTE approach does not require a thiyl radical to catalyze the exchange reaction and is thus compatible with multimethacrylate resin polymerizations.

The thiol-thioester exchange reaction (TTE) has been introduced recently as a new class of CANs that undergo dynamic bond exchange and enable rapid stress relaxation at ambient conditions in the presence of free thiols, thioesters, and a base/nucleophile catalyst. This reaction involves the exchange of one thioester link for another, mediated by a thiolate anion that is generated from a base or nucleophile reacting with a thiol[19] **(Figure 6.1A)**.

Here, silica nanoparticles functionalized with a TTE-containing silane are introduced into BisGDMA/TEGDMA (70:30) dental resins in the presence of a nucleophilic catalyst in order to induce the stress relaxation mechanism at the interface of the polymer and the filler. TTE-capable moieties undergo continuous bond cleavage and reformation reversibly, in the presence of a base/ nucleophile, leading to network relaxation and stress elimination while conserving the overall network connectivity. Material properties, including polymerization-induced shrinkage stress, flexural modulus, strength and toughness of TTE-based dental composites, are explored and

compared with control composites that consist of a similar silane but without the DCC moieties.

Furthermore, as prior work has shown that combining an RAFT-interface with an RAFT-resin results in synergistic effects on mechanical properties such as strength and toughness, here, the two types of DCC approaches were combined, in the resin and at the resin-filler interface. RAFT to be radically triggered within the resin matrix during polymerization with TTE to be triggered exclusively at the interface between the silica particle and the matrix to further enhance composite performance. This approach enables the stress relaxation in both locations; within the composite resin and at the resin-filler interface and provides for long term stress relaxation throughout the entire life of the composite via long catalytic lifetime of base/nucleophile-initiated TTE reactions, while only activating the RAFT-based exchange when polymerization stresses are generated, i.e. during the light exposure. Testing on polymerization-induced shrinkage stress and post-polymerization stress relaxation is conducted and compared with control composites by eliminating the appropriate DCC functional groups or catalysts.

6.2. Materials and Methods

Materials

2,2-Bis[4-(2-hydroxy-3-methacrylyloxypropoxy) phenyl] propane (Bis-GMA) and triethylene glycol dimethacrylate (TEGDMA) (Esstech, Essington, PA, USA) were purchased from Esstech (Essington, PA, USA) as a premixed monomer mixture in 70:30 mass ratio. Pentaerytritol tetrakis(3-mercaptopropionate) (PETMP), Triethyleneglycol-Divinylether (TEGDVE), 1,4-diazabicyclo[2.2.2]octane (DABCO), 3-chloro-2-chloromethyl-1-propene, potassium ethyl xanthogenate, ethylene diamine, and propylamine were purchased from Sigma-Aldrich. Irgacure

819 (bis(2,4,6-trimethylbenzoyl)- phenylphosphineoxide) was obtained from BASF. Schott glass (mean particle size 40 nm) untreated were generously donated by Evonik Silicas, and used as the inorganic fillers. Prior to implementation and as described later, these fillers were subsequently functionalized with thiol group for inclusion and copolymerization in the composite. All chemicals were used as received. The thioester-diacrylate[20] and 2-methylene-propane-1,3-di (thioethyl vinyl ether) (MDTVE-AFT)[21] were synthesized using methods reported elsewhere.

Filler Functionalization

4 g of silica particles (Schott, OX50, 40 nm) were first taken in a glass tube and heated at 165 °C under vacuum using a Buchi heater/condenser for 3 h. The dried nanoparticles were then transferred to a 250 mL bottom rounded flask containing 200 mL of anhydrous toluene supplemented with 2 g of (3-Mercaptopropyl) trimethoxysilane prereacted for 10 min with 2 g of n-propylamine. The reaction mixture was then refluxed at 120 °C for 24 h. After sinalization of nanoparticle, the liquid suspension was centrifuged and the solid pellets collected thoroughly, and washed with toluene (3× ≈ 25 mL) and methylene chloride (3× ≈ 25 mL) in two separate washing/centrifugation cycles. The washed filler particles were dried under vacuum overnight at 70 °C. Then 2 g of the dried thiol functionalized fillers were reacted with 0.7 g thioester diacrylate in DCM in presence of 3 mL TEA base at R.T overnight. After sinalization of nanoparticle was washed with DCM (1× ≈ 25 mL), toluene (2× ≈ 25 mL) and DMSO (2× ≈ 25 mL), and dried under vacuum overnight at 70 °C. The functionalized particles were analyzed by DRIFT FT-IR spectroscopy and TGA. The mass loss difference between silanized and unfunctionalized fillers suggests successful functional group grafting on the surface of glass particles in each case. Also, the DRIFT FT-IR characterization provides evidence of silanol group disappearance around 3745

cm^{-1}, and the appearance of the thioester group around 1700 cm^{-1} implying successful surface modification.

Fourier Transform Infrared Spectroscopy

An FT-IR spectrometer (Nicolet 6700) connected to a tensometer via fiber optic cables was used to monitor the real-time polymerization kinetics in concert with stress measurements. Samples were placed between two cylindrical quartz rods, and 300 mW cm^{-2} light was irradiated from the bottom rod using a light guide connected to a mercury lamp (Acticure 4000, EXFO) with 400–500 nm bandgap filter. The overtone signal of double bonds between 6250–6096 cm^{-1} was monitored during the FT-IR measurements.

Polymerization Shrinkage Stress Measurement

Shrinkage stress was measured via a tensometer using cantilever beam deflection theory (American Dental Association Health Foundation, ADAHF–PRC). A composite paste (1 mm in thickness, 6 mm in diameter) was placed between two cylindrical quartz rods, which were previously treated with a methacrylate functional silane to promote bonding at the glass surface/ resin interface. A 300 mW cm^{-2} of light was irradiated from the bottom rod using a light guide connected to a mercury lamp (Acticure 4000, EXFO) with a 400–500 nm bandgap filter. Polymerization-induced shrinkage of sample exerted a tensile force which caused the deflection of the aluminum beam. A linear variable differential transformer was used to convert the displacement to shrinkage stress based upon beam calibration constant and cross-sectional area of the sample. For the simultaneous measurement of conversion with shrinkage stress, data were collected continuously for 10 min (n=3).

Thermogravimetric Analysis

TGA (Pyris 1, PerkinElmer) was used to analyze the functionalized silica nanoparticles. Each sample was run in a nitrogen atmosphere (20 mL min^{-1}) from 50 to 850 °C at a heating rate of 10 °C min^{-1}.

Three-point flexural test

Three-point bend (MTS 858 Mini Bionix II) with a strain rate of 0.1 mm min^{-1} and a span of 20 mm was used to obtain properties of the composites (n=5). Samples sandwiched between two glass slides and polymerization was initiated with 1 wt% of I819, and photocured with 400–500 nm visible light at 50 mW cm^{-2} for 5 min on each side to ascertain uniform conversions throughout the sample thickness and then postcured in an oven at 60 °C for 4 h. Flexural tests were performed 24 hours after initial cure. Composite sample dimensions were 2/2.5/10 mm (n=5). Functional group conversion was recorded via FTIR spectra prior to and after the polymerization.

6.3. Results and Discussion

Silica nanoparticles (SNP) were synthesized from thiol-functionalized nanoparticles treated with diacrylate thioesters, that through DCC mechanisms promote resin-filler bonding and interfacial stress relaxation as illustrated in **Figure 6.1B**. The synthesis and functionalization processes are explained further in the Experimental Section. For use as a control, SNPs were functionalized with a thiol containing silane (3-mercaptopropyl trimethoxysilane) also capable of bonding to the resin but not capable of TTE- bond exchange by following previously published methods.[2] The functionalized fillers were analyzed by diffuse reflectance infrared Fourier transform spectroscopy (DRIFTS) and thermogravimetric analysis (TGA) which provided additional evidence of successful functional group attachment to the SNP surface. In the following

experiments, 15 wt% SNP were dispersed into BisGMA/TEGDMA (70:30) dental resins containing 15 wt% PETMP to serve as a free thiol and 1 wt% DABCO nucleophilic catalyst, as illustrated in **Figure 6.1C**. Polymerization was initiated with 1 wt% of I819 (bis(2,4,6-trimethylbenzoyl)-phenylphosphineoxide) visible light photoinitiator, and photocured with 400–500 nm visible light then postcured in an oven at 60 °C for 4 h, which leads to the formation of a glassy polymer network (T_g as measured in DMA ≈ 110 °C). Thermo-mechanical properties of both TTE- and control BisGMA/TEGDMA composites, such as T_g and storage modulus at 40 ˚C, are reported in **Table 6.1**. The TTE- and control BisGMA/TEGDMA composites showed similar T_g values, suggesting that the functional group conversion within each composites system is nearly equivalent, validating that this sample is an appropriate control.

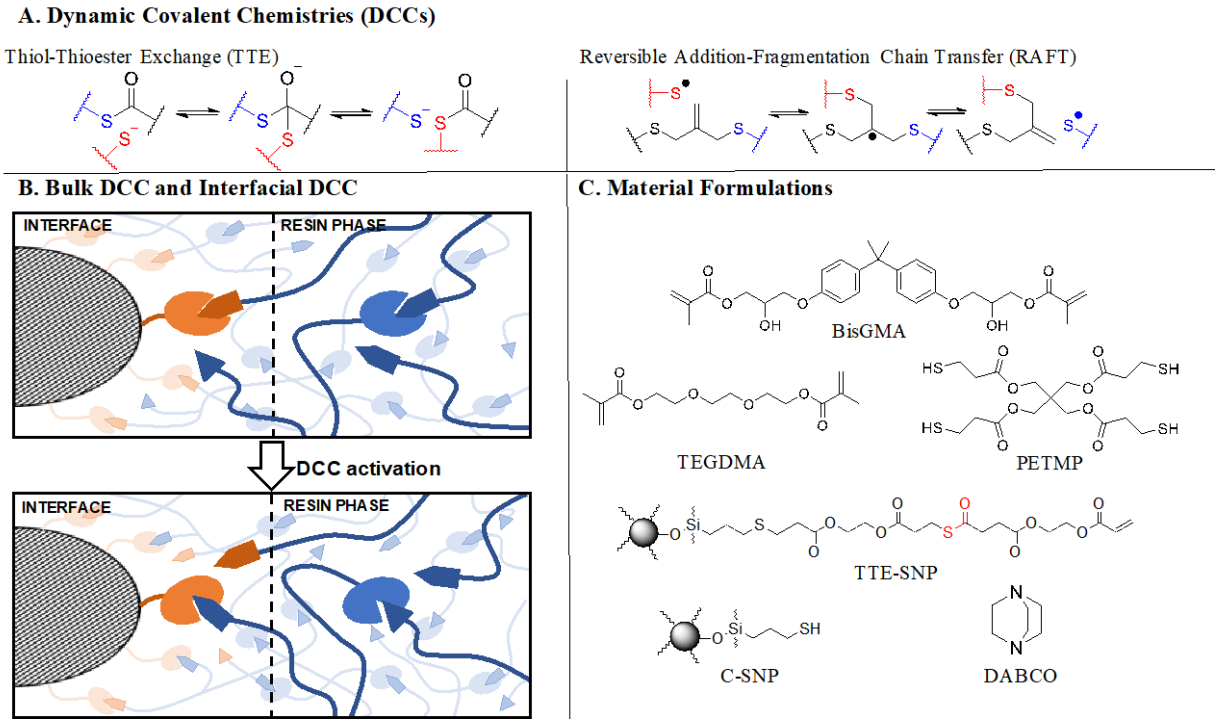

Figure 6.2. A) Mechanisms for thiol-thioester exchange (TTE) and Reversible addition-fragmentation chain transfer (RAFT) as examples for dynamic covalent chemistries (DCCs). B) Illustration of TTE bond exchange in the resin phase and at the filler interface enables stress relaxation. As stress accumulates, TTE bond rearrangement occur between a free thiol and thioester linkage. This bond exchange enables stress relaxation without a sacrifice of crosslinking density or filler attachment to the network. C) Monomers and fillers used for this study.

An FTIR spectrometer connected to a tensometer via fiber optic cables was utilized to investigate the effect of interfacial TTE bond exchange on bulk shrinkage stress, which is known to be one of the primary causes of failure for dental materials. Internal stress is well known to develop during the polymerization reaction due to postgelation volumetric contraction and elastic modulus evolution, which usually leads to premature failure through initiation of microcracks and interfacial debonding. The incorporation of TTE-functionalized nanoparticles within the BisGMA/TEGDMA resin resulted in a material with more than 30 % lower shrinkage stress as compared with the thioester-free nanoparticles used in the control experiment at equivalent 80 % conversion (**Figure 6.2A & B**), while preserving the ability to relax interfacial stress for an extended period following polymerization. This outcome is due to the persistent presence of thiolate species, which enable exchange, and thus post-polymerization relaxation.

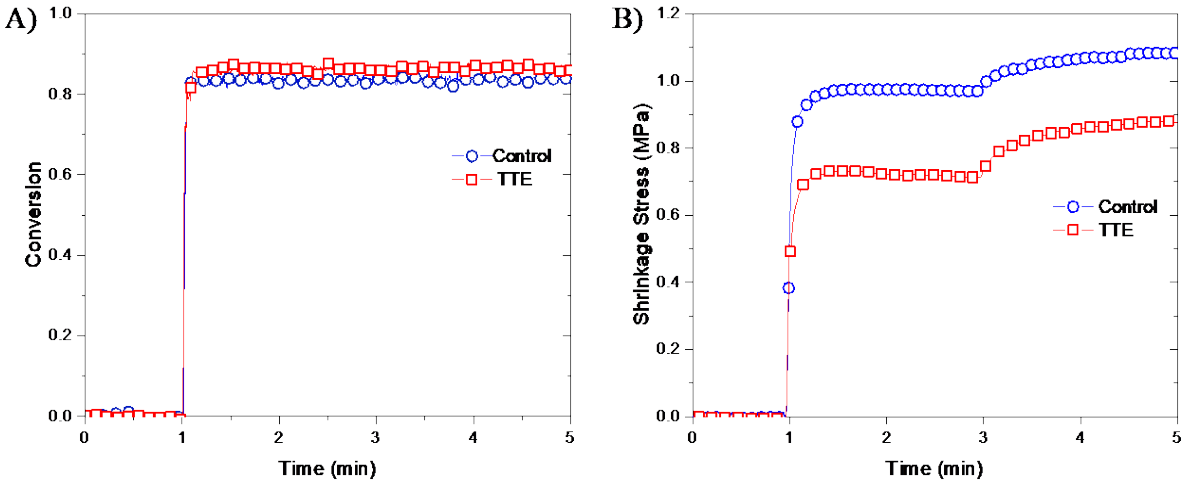

Figure 6.2. A) Polymerization kinetics as measured by FT-IR as a function of the disappearance of C=C functional group at 6165 cm^{-1}. B) In situ polymerization shrinkage stress for control composites (blue circle) and TTE- composites (red square) conversion using a tensometer coupled with the FTIR. All samples were placed between two quartz rods, previously treated with a methacrylate-functional silane and irradiated for 3 min at ambient temperature with 300 mW/cm^2 of 400–500 nm light.

As an indication of the benefits of the continuous post polymerization stress relaxation and to investigate its effects on composite failure, mechanical properties including flexural modulus, flexural strength, and flexural toughness of both TTE- and control BisGMA/TEGDMA resins/ composites were analyzed via three-point bend tests performed on a universal testing machine (MTS) as presented in **Figure 6.3** and **Table 6.1**. **Figure 6.3A** displays a representative stress–strain curve of the TTE composites in comparison with the control composite. The flexural modulus (or Young's modulus) calculated from the initial slope of the stress–strain curve dramatically increased from approximately 2.5 GPa to 4 GPa, when TTE bond exchange was activated at the interface, leading to 33% improvement in the flexural strength value (120 ± 8 MPa) as compared with the control composites (90 ± 3 MPa), **Figure 6.3B** and **Table 6.1**. Due to the increased elastic modulus of the TTE- composites, the composites exhibited even higher flexural toughness (2.6 ± 0.3 MJm^{-3}), as compared with the control composites (2.0 ± 0.2 MJm^{-3}) at equivalent strain. This improvement in flexural toughness is related to the reduction in the shrinkage stress as well as the post polymerization stress relaxation that will continue to occur over the lifetime of the composite because of the persistent catalyst, which enables stress relaxation and healing at the interface, improving the mechanical properties of the dental restorative material.

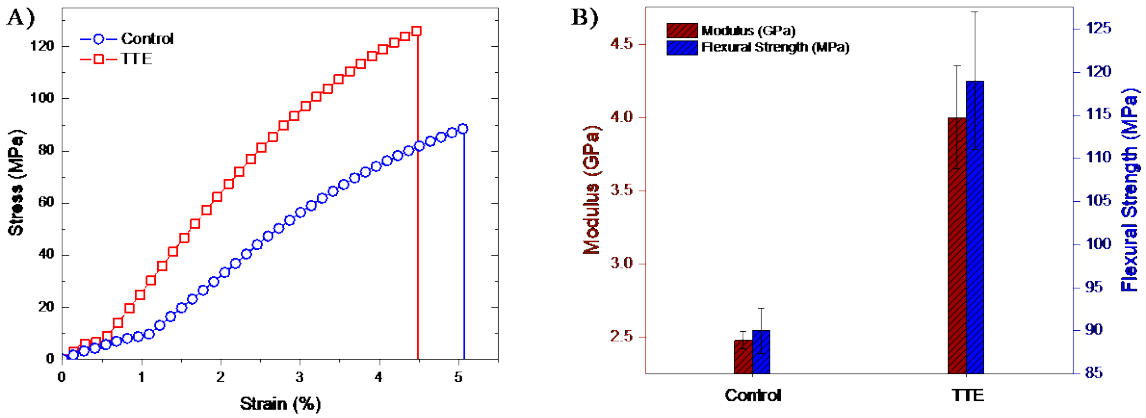

Figure 6.3. A) Stress-strain profiles from 3-point bend test for both control composites (blue circle) and dynamic TTE-enabled interface (red square) at a displacement rate of 0.1 mm/min. B) Modulus (red columns) and flexural strength obtained from 3-point bend test for both control and TTE composites. Sample dimensions: 2 mm thick bars, 20 mm span. Resins were formulated of BisGMA/TEGDMA (70:30) mixture with 15 wt% PETMP, 1 wt% DABCO and 15 wt% of SNP, either TTE or the corresponding control. Polymerization was initiated with 1 wt% of I819, and photocured with 400–500 nm visible light at 50 mW cm^{-2} for 5 min on each side and then postcured in an oven at 60 °C for 4 h.

Table 6.1. Comparison of TTE- and control composite glass transition temperature (T_g), storage modulus at 40 ˚C, flexural modulus, flexural strength, flexural toughness from the three-point bend testing.

	T_g (˚C)	Storage Modulus at 40 ˚C	Modulus (GPa)	Flexural strength (MPa)	Flexural toughness (MJ/m^3)
Control	110 ± 3	2.4 ± 0.4	2.5 ± 0.1	90 ± 3	2.0 ± 0.2
TE	107 ± 1	2.3 ± 0.2	4.0 ± 0.3	120 ± 8	2.6 ± 0.3

Given that RAFT has been widely studied in bulk dental materials, and following this successful demonstration of the exceptional efficiency of interface-limited TTE exchange processes in composites, here, TTE exchange is utilized in tandem with RAFT. RAFT is radically triggered within the resin matrix during the polymerization process while the TTE is triggered exclusively at the interface between the silica particle and the matrix to provide long term stress relaxation throughout the life of the composite.

Specifically, the resin formulations presented in **Figure 6.4A** is utilized in this study. The resin formulation is based on thiol-ene networks comprised of a divinyl AFT (2-methylene-propane-1,3-di(thioethyl vinyl ether) (MDTVE)) or non-AFT (Triethyleneglycol-Divinylether (TEGDVE)) and PETMP (added in 0.15 mol excess), with TTE based fillers that also are capable of relaxing stress in the presence of the catalyst (DABCO). Control experiments in which no stress relaxation is enabled through elimination of the RAFT functional groups or the TTE catalyst are also included.

To investigate the interaction of interfacial and bulk dynamic chemistries, polymerization-induced shrinkage stress was measured for each of the four formulated composites, with and without RAFT in the resin and with and without thioester exchange at the interface (**Figure 6.4B**). As **Figure 6.4B** shows, the composite that does not contain any exchangeable bonds exhibits the highest degree of shrinkage stress, 0.8 MPa, while around 90% shrinkage stress reduction is observed in the formulation "equipped" with both types of DCC mechanisms are activated, both throughout the network and at the particle interface. By decoupling the bond exchange to be exclusively effective at the particle interface or throughout the resin; 40% and 75% reductions in shrinkage stress were achieved, respectively. This behavior indicates a synergistic effect to dramatically reduce shrinkage stress when both interfacial and bulk dynamic chemistries are simultaneously active. As such, it is expected to lead to noticeable improvement in the mechanical properties and fracture resistance when utilized in dental restoratives.

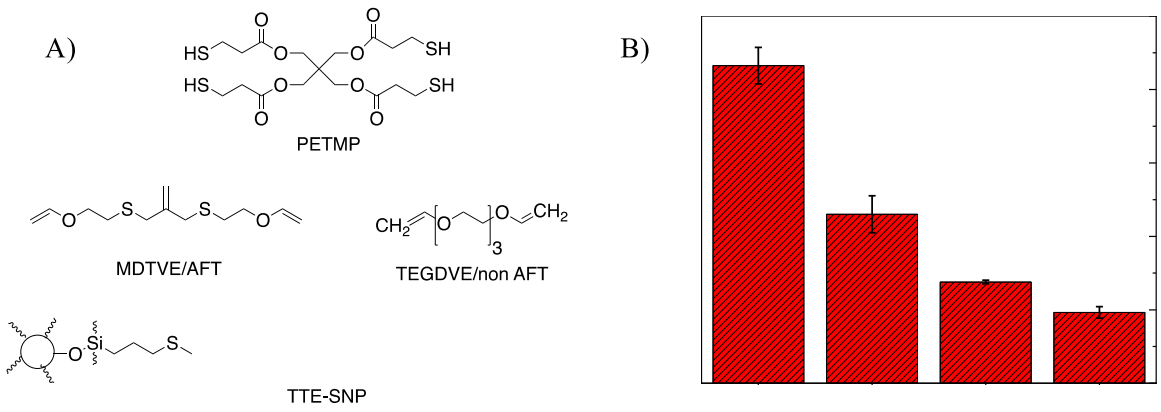

Figure 6.4. A) Monomers and fillers used in the formulation of the composites to examine the influence of combining RAFT resin with TTE at the SNP-polymer interface. B) Final polymerization shrinkage stress taken after 5 min reaction time at equivalent 100% conversion, as a function of the double bond conversion via tensometer in thiol-ene composites: No DCC: non-AFT resin/thioester SNPs, no catalyst; Interfacial TTE: non-AFT resin/thioester SNPs, with DABCO added; Resin based AFT only: AFT resin/thioester SNPs, no catalyst; Both DCCs: AFT resin/thioester SNP, DABCO added. Each composition contained 10 wt.% SNPs, 1 wt.% IR819, and was irradiated with 50 mW/cm^2 light intensity of 400-500 nm. Two mixtures contained DABCO (1 wt.%).

6.4. Conclusions

In summary, the TTE reaction has been implemented for the first time at the resin-filler interface in conventional dental composites and was demonstrated to enable interfacial stress relaxation of these critical, highly stressed regions. This relaxation mechanism persists due to the catalytic mechanism, even in the absence of any DCC in the resin phase, which leads to significant improvement in composite performance including 30% reduction in polymerization stress, 60% improvement in flexural modulus, and 40% improvement in the flexural strength.

This approach represents a fundamental shift in dental composites by relaxing interfacial stresses while improving mechanical properties, which would be of significant clinical value for extending the lifetime of dental restorations.

6.5. Acknowledgments

The authors acknowledge financial support from the National Institutes of Health (NIH 1U01DE023777).

6.6. References

(1) Schneider, L. F. J.; Cavalcante, L. M.; Silikas, N. Shrinkage Stresses Generated during Resin-Composite Applications: A Review. *J. Dent. Biomech.* **2010**, *1* (1), 131630–131630.

(2) Moszner, N.; Salz, U. Recent Developments of New Components for Dental Adhesives and Composites. *Macromol. Mater. Eng. 2007*, **2007**, *292*, 245–271.

(3) Podgórski, M.; Becka, E.; Claudino, M.; Shah, P. K.; Stansbury, J. W.; Bowman, C. N. Ester-Free Thiol – Ene Dental Restoratives — Part A : *Dent. Mater.* **2015**, *31* (11), 1255–1262.

(4) Cramer, N. B.; Stansbury, J. W.; Bowman, C. N. Recent Advances and Developments in Composite Dental Restorative Materials. *J. Dent. Res.* **2011**, *90* (4), 402–416.

(5) Ms, S.; Auj, Y.; S. A. Physicomechanical Evaluation of Low-Shrinkage Dental Nanocomposites Based on Silsesquioxane Cores. *European Journal of Oral Sciences* **2007**, 230–238.

(6) Drummond, J. L. Materials. **2009**, *87* (8), 710–719.

(7) Shah, P. K.; Stansbury, J. W. Role of Filler and Functional Group Conversion in the Evolution of Properties in Polymeric Dental Restoratives. *Dent. Mater.* **2014**, *30* (5), 586–593.

(8) Gonalves, F.; Azevedo, C. L. N.; Ferracane, J. L.; Braga, R. R. BisGMA/TEGDMA Ratio and Filler Content Effects on Shrinkage Stress. *Dent. Mater.* **2011**, *27* (6), 520–526.

(9) Liu, J.; Howard, G. D.; Lewis, S. H.; Barros, M. D.; Stansbury, J. W. A Study of Shrinkage Stress Reduction and Mechanical Properties of Nanogel-Modified Resin Systems. *Eur. Polym. J.* **2012**, *48* (11), 1819–1828.

(10) Moraes, R. R.; Garcia, J. W.; Barros, M. D.; Lewis, S. H.; Pfeifer, C. S.; Liu, J.; Stansbury, J. W. Control of Polymerization Shrinkage and Stress in Nanogel-Modified Monomer and Composite Materials. *Dent. Mater.* **2011**, *27* (6), 509–519.

(11) Carioscia, J. A.; Lu, H.; Stanbury, J. W.; Bowman, C. N. Thiol-Ene Oligomers as Dental Restorative Materials. **2005**, 1137–1143.

(12) Klee, J. E.; Schneider, C.; Ho, D.; Burgath, A.; Frey, H.; Mu, R. Hyperbranched Polyesters and Their Application in Dental Composites : Monomers for Low Shrinking Composites. **2001**, *354*, 346–354.

(13) Chung, C.; Kim, J.; Kim, M.; Kim, K.; Kim, K. Development of a New Photocurable Composite Resin with Reduced Curing Shrinkage. **2002**, *18*, 174–178.

(15) Song, H. B.; Sowan, N.; Shah, P. K.; Baranek, A.; Flores, A.; Stansbury, J. W.; Bowman, C. N. Reduced Shrinkage Stress via Photo-Initiated Copper(I)-Catalyzed Cycloaddition Polymerizations of Azide-Alkyne Resins. *Dental Materials*. 25, 2016.

(16) Park, H. Y.; Kloxin, C. J.; Fordney, M. F.; Bowman, C. N. Stress Reduction and T g Enhancement in Ternary Thiol-Yne-Methacrylate Systems via Addition-Fragmentation Chain Transfer. *Macromolecules* **2012**, *45* (14), 5647–5652.

(17) Park, H. Y.; Kloxin, C. J.; Abuelyaman, A. S.; Oxman, J. D.; Bowman, C. N. Stress Relaxation via Addition–Fragmentation Chain Transfer in High T g , High Conversion Methacrylate-Based Systems. *Macromolecules 45* (14), 5640-5646

(18) Sowan, N.; Cox, L. M.; Shah, P. K.; Song, H. B.; Stansbury, J. W.; Bowman, C. N. Dynamic Covalent Chemistry at Interfaces: Development of Tougher, Healable Composites through Stress Relaxation at the Resin-Silica Nanoparticles Interface. *Adv. Mater. Interfaces* **2018**, 1800511.

(19) Worrell, B. T.; McBride, M. K.; Lyon, G. B.; Cox, L. M.; Wang, C.; Mavila, S.; Lim, C.-H.; Coley, H. M.; Musgrave, C. B.; Ding, Y.; et al. Bistable and Photoswitchable States of Matter. *Nat. Commun.* **2018**, *9* (1), 2804.

(20) Podgórski, M.; Worrell, B. T.; Sinha, J.; Mcbride, M. K.; Bowman, C. N. Thermal Metamorphosis in (Meth)Acrylate Photopolymers: Stress Relaxation, Reshaping, and Second-Stage Reaction . *Macromolecules* **2019**, *52*, 8114–8123.

(21) Kloxin, C. J.; Scott, T. F.; Bowman, C. N. Stress Relaxation via Addition−Fragmentation Chain Transfer in a Thiol-Ene Photopolymerization. *Macromolecules* **2009**, *42* (7), 2551–2556.

Chapter 7

Conclusions and Future Recommendations

This thesis is focused on the development of novel CAN materials that are capable of dynamic bond exchange at ambient temperature, while maintaining outstanding mechanical properties. Two types of step growth "click" reactions, copper-catalyzed azide-alkyne cycloaddition (CuAAC) and thiol-ene photopolymerizations, were utilized to form glassy polymer networks. Two types of CAN reactions, photo-induced RAFT and anion-mediated TTE, were incorporated either in the monomer backbones or in the interface of silica nanoparticles (SNP). First, the resin phase stress relaxation in the glassy state was investigated by exploring the stress relaxation capacity of RAFT-based CuAAC polymers upon light activation. Next, adaptive interfaces (AI) platform was developed by coupling DCC moieties at the resin-filler interface to promote interfacial stress relaxation in the glassy state. This was achieved by implementing DCC at the resin-filler interface by surface functionalization of SNP. The resulting evolution of composite performance including toughness and shrinkage stress was explored and compared with a control system without DCC at the interface. Further, the TTE-AI concept was further implemented to the conventional dental composites to enhance flexural modulus and toughness and reduce polymerization stress. Lastly, RAFT and TTE were incorporated in both the resin matrix and at the resin-filler interface to further enhance the performance of composites. The remainder of this chapter is devoted to summarizing the findings and proposing future work.

7.1. Resin phase stress relaxation in the glassy state

As shown in chapter 3, crosslinked polymer networks capable of network reconfiguration not only in the rubbery state but also within the glassy state were prepared by incorporating RAFT moieties into the backbone of photo-initiated CuAAC polymer networks. Upon light activation, RAFT-based CuAAC networks showed enhanced stress relaxation with rapid exchange rate, both for small deformation and post-yielding large deformation as compared to analogous control networks without RAFT moieties. Successful mechano-patterning and an object with complex 3D shape of glassy CuAAC films was achieved at ambient condition. Further, improvement in the tensile toughness upon RAFT activation as well as rejuvenation of mechanical and thermodynamic characteristics in physically-aged samples were demonstrated.

The aging and UV-induced "rejuvenation" in the AS-AK2 CuAAC network are also evident in density measurement (**Figure 7.1,** measured by multi-pycnometer). After 72 h of physical aging, the density of AS-AK2 based and control CuAAC samples increases from 1.05 g/cm^3 to 1.3 g/cm^3 and from 1.0 g/cm^3 to 1.26 g/cm^3, respectively. Such an increase (> 20%) is significantly higher than normally observed in physical aging of polymers.[33,34] With 2 min of UV exposure on the aged samples, the density of AS-AK3-CuAAC decreases to 1.13 g/cm^3, while control CuAAC shows no density change (**Figure 7.1**). This significant change in the density support the hypothesis that the glassy state of the CuAAC networks contain higher degrees of free volume, which enables local segment mobility that is sufficient for the bond-exchange process to occur. However, accurate investigation on free volume changes upon ageing by ellipsometry should be done. The future recommendations also include molecular analysis on aged triazole-based polymer films such as polarized IR spectroscopy and X-Ray to observe the effect of triazole functional groups on ageing and stress relaxation. Additionally, Fluorescence recovery after

photobleaching (FRAP) experiment is recommended to be conducted as a mean to approve that activating the dynamic bonds would modify transport in glassy CuAAC networks.

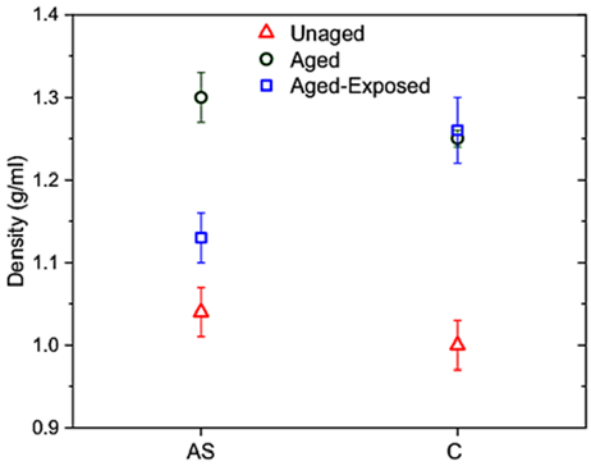

Figure 7.1: Pycnometer density measurement for AS-AK2 and C-AK2 samples before ageing, after 3 days of ageing, and after 3 days of ageing but subsequent exposure to 5 mW/cm^2 UV-light before the density measurement.

7.2. Develop adaptive interfaces (AI) to promote interfacial stress relaxation

As the interfacial region between the organic resin and an inorganic filler is known to concentrate stresses and nucleate crack formation, isolating the bond exchange to occur exclusively at the interfacial region enables stress relaxation where the stress is concentrated and significantly improved composite's performance. As discussed in both Chapter 4 and 5, novel adaptive interface (AI) platform was established to effectively mitigate the interfacial stress and improve the overall mechanical properties without altering the resin formulation. First, radical mediated RAFT-containing AI that covalently bonded silica nanoparticles to a static thiol-ene resin was developed, and its capability to reduce stress and improve material properties in an inert thiol-ene composite was demonstrated. However, composites with RAFT-active filler are capable of undergoing stress relaxation at the interface only during light exposure, which limited the capacity

for stress relaxation over the lifetime of the composite or in optically thick material. Thus, the anion-mediated TTE was examined as a perpetual, light independent interfacial DCC mechanism.

Next in chapter 6, the adaptive interface concept was applied to a conventional dental resin by introducing TTE moieties that promote resin-filler bonding and persistent stress relaxation at the filler-resin interface and was demonstrated to enable significant improvement in composite performance. Lastly, the two types of DCC approaches were combined, one in the resin and the other at the resin-filler interface. This approach enabled the stress relaxation in both locations, the resin matrix and the interfacial region of composite and showed significant reduction in the shrinkage stress.

This work is readily envisioned to be extendable to other DCCs and applied to a wide spectrum of resin/filler combinations beyond what has been examined here. Especially, since numerous applications will benefit from enhanced mechanical performance that results from a reduction in interfacial stress. Future recommendations include investigating the rheological behavior of AI composites and further mechanical testing including fracture and fatigue testing. For TTE composites, the elimination of free thiol from the resin formulation is also recommended especially for dental composites. Further, the effect of various types of base/nucleophile catalysts, catalyst loadings, filler loadings, and filler sizes on the rate of bond exchange process and the resulting stress relaxation should be studied systematically.

Bibliography

Adriaensens, P.; Storme, L.; Carleer, R.; Vanderzande, D.; Gelan, J.; Litvinov, V. M.; Marissenf,R. Visualization of Tensile Stress Induced Material Response at a Crack Tip in Polymers under Critical Load by NMR Imaging. *Macromolecules* **2000**, *33* (13), 4836–4841.

Adzima, B. J.; Tao, Y.; Kloxin, C. J.; DeForest, C. a; Anseth, K. S.; Bowman, C. N. Spatial and Temporal Control of the Alkyne-Azide Cycloaddition by Photoinitiated Cu(II) Reduction. *Nat. Chem.* **2011**, *3* (3), 256–259.

Alzahrani, A. A.; Saed, M.; Yakacki, C. M.; Song, H. B.; Sowan, N.; Walston, J. J.; Shah, P. K.; McBride, M. K.; Stansbury, J. W.; Bowman, C. N. Fully Recoverable Rigid Shape Memory Foam Based on Copper-Catalyzed Azide-Alkyne Cycloaddition (CuAAC) Using a Salt Leaching Technique. *Polym. Chem.* **2018**, *9* (1), 121–130.

Amamoto, Y.; Kamada, J. pd.; Otsuka, H.; Takahara, A.; Matyjaszewski, K. Photoinduced Self-Healing of Covalently Cross-Linked Polymers through Reshuffling of Trithiocarbonate Units. *Angew. Chemie - Int. Ed.* **2011**, *50* (7), 1660–1663.

Amamoto, Y.; Otsuka, H.; Takahara, A.; Matyjaszewski, K. Self-Healing of Covalently Cross-Linked Polymers by Reshuffling Thiuram Disulfide Moieties in Air under Visible Light. *Adv. Mater.* **2012**, *24* (29), 3975–3980.

ASTM D638-02a, Standard Test Method for Tensile Properties of Plastics, ASTM International,

West Conshohocken, 2002.

Baranek, A.; Song, H. B.; Mcbride, M.; Finnegan, P.; Bowman, C. N. Thermomechanical Formation − Structure − Property Relationships in Photopolymerized Copper-Catalyzed Azide − Alkyne (CuAAC) Networks. **2016**.

Capaldi, F. M.; Boyce, M. C.; Rutledge, G. C. Molecular Response of a Glassy Polymer to Active Deformation. **2004**, *45*, 1391–1399.

Capelot, M.; Montarnal, D.; Tournilhac, F.; Leibler, L. Metal-Catalyzed Transesterification for Healing and Assembling of Thermosets. *J. Am. Chem. Soc.* **2012**, *134* (18), 7664–7667.

Carioscia, J. A.; Lu, H.; Stanbury, J. W.; Bowman, C. N. Thiol-Ene Oligomers as Dental Restorative Materials. **2005**, 1137–1143.

Cash, J. J.; Kubo, T.; Bapat, A. P.; Sumerlin, B. S. Room-Temperature Self-Healing Polymers Based on Dynamic-Covalent Boronic Esters. *Macromolecules* **2015**, *48* (7), 2098–2106.

Chatani, S.; Kloxin, C. J.; Bowman, C. N. The Power of Light in Polymer Science: Photochemical Processes to Manipulate Polymer Formation, Structure, and Properties. *Polym. Chem.* **2014**, *5* (7).

Chen, Q.; Chasiotis, I.; Chen, C.; Roy, A. Nanoscale and Effective Mechanical Behavior and Fracture of Silica Nanocomposites. *Compos. Sci. Technol.* **2008**, *68* (15–16), 3137–3144.

Chen, X.; Dam, M. A.; Ono, K.; Mal, A.; Shen, H.; Nutt, S. R.; Sheran, K.; Wudl, F. A Thermally Re-Mendable Cross-Linked Polymeric Material. *Science* **2002**, *295* (5560), 1698–1702.

Chung, C.; Kim, J.; Kim, M.; Kim, K.; Kim, K. Development of a New Photocurable Composite Resin with Reduced Curing Shrinkage. **2002**, *18*, 174–178.

Chung, C.; Roh, Y. ; Cho, S.; Kim, J. Crack Healing in Polymeric Materials via Photochemical [2+2] Cycloaddition. *Chem. Mater.* **2004**, *16* (21), 3982–3984.

Coote, M. L.; Henry, D. J. Effect of Substituents on Radical Stability in Reversible Addition Fragmentation Chain Transfer Polymerization: An Ab Initio Study. *Macromolecules* **2005**, *38* (4), 1415–1433.

Cox, L. M.; Li, Z.; Sowan, N.; Nair, D.; Xiao, J.; Bowman, C. N.; Ding, Y. Reconfigurable Surface Patterns on Covalent Adaptive Network Polymers Using Nanoimprint Lithography. *Polymer* **2014**, *55* (23), 5933–5937.

Cox, L. M.; Sun, X.; Wang, C.; Sowan, N.; Killgore, J. P.; Long, R.; Wu, H. A.; Bowman, C. N.; Ding, Y. Light-Stimulated Permanent Shape Reconfiguration in Cross-Linked Polymer Microparticles. *ACS Appl. Mater. Interfaces* **2017**, *9* (16), 14422–14428.

Cramer, N. B.; Bowman, C. N. Kinetics of Thiol – Ene and Thiol – Acrylate Photopolymerizations with Real-Time Fourier Transform Infrared. **2001**, 3311–3319.

Cramer, N. B.; Stansbury, J. W.; Bowman, C. N. Recent Advances and Developments in Composite Dental Restorative Materials. *J. Dent. Res.* **2011**, *90* (4), 402–416.

Crivello, J. V.; Reichmanis, E. Photopolymer Materials and Processes for Advanced Technologies. *Chem. Mater.* **2014**, *26* (1), 533–548.

Denissen, W.; Rivero, G.; Nicolaÿ, R.; Leibler, L.; Winne, J. M.; Du Prez, F. E. Vinylogous Urethane Vitrimers. *Adv. Funct. Mater.* **2015**, *25* (16), 2451–2457.

Denissen, W.; Winne, J. M.; Du Prez, F. E. Vitrimers: Permanent Organic Networks with Glass-like Fluidity. *Chem. Sci.* **2015**, *7*, 30–38.

Desroches, M.; Caillol, S.; Lapinte, V.; Boutevin, B.; Charles, I.; Montpellier, G.; Cnrs-um-enscm-um, U. M. R.; Om, E. I. A. M. S.; De, R.; Normale, E.; et al. Synthesis of Biobased Polyols by Thiol À Ene Coupling from Vegetable Oils. **2011**, 2489–2500.

Di, D. D.; Fokin, V. V; Finn, M. G. Click Chemistry in Materials Synthesis. Adhesive Polymers from Copper-Catalyzed Azide-Alkyne. **2004**, 4392–4403.

Drummond, J. L. Materials. **2009**, *87* (8), 710–719.

Durner, J.; Spahl, W.; Zaspel, J.; Schweikl, H.; Hickel, R.; Reichl, F. Eluted Substances from Unpolymerized and Polymerized Dental Restorative Materials and Their Nernst Partition Coefficient. **2009**, *6*, 91–99.

Eiras, D.; Pessan, L. A. Mechanical Properties of Polypropylene/Calcium Carbonate Nanocomposites. *Mater. Res.* **2009**, *12* (4), 517–522.

Evans, R. A.; Rizzardo, E. Free-Radical Ring-Opening Polymerization of Cyclic Allylic Sulfides. 2. Effect of Substituents on Seven- and Eight-Membered Ring Low Shrink Monomers. *Macromolecules* **2000**, *33* (18), 6722–6731.

Ferracane, J. L. Resin-Based Composite Performance : Are There Some Things We Can ' t Predict ? *Dent. Mater.* **2012**, *29* (1), 51–58.

Finn, P. M. G.; Fokin, V.; Hein, J. E.; Fokin, V. V. Copper-Catalyzed Azide–Alkyne Cycloaddition (CuAAC) and beyond: New Reactivity of Copper(I) Acetylides. *Chem. Soc. Rev.* **2010**, *39* (4), 1302–1315.

Fortman, D. J.; Brutman, J. P.; Cramer, C. J.; Hillmyer, M. A.; Dichtel, W. R. Mechanically Activated, Catalyst-Free Polyhydroxyurethane Vitrimers. *J. Am. Chem. Soc.* **2015**, *137* (44), 14019–14022.

Fu, S. Y.; Feng, X. Q.; Lauke, B.; Mai, Y. W. Effects of Particle Size, Particle/Matrix Interface Adhesion and Particle Loading on Mechanical Properties of Particulate-Polymer Composites. *Compos. Part B Eng.* **2008**, *39* (6), 933–961.

Gandavarapu, N. R.; Azagarsamy, M. A.; Anseth, K. S. Photo-Click Living Strategy for Controlled, Reversible Exchange of Biochemical Ligands. *Adv. Mater.* **2014**, *26* (16), 2521–2526.

Ganesh, K.; Nagarajan, R.; D. J. L. Rate of Gas Transport in Glassy Polymers: A Free Volume Based Predictive Model. *Ind. Eng. Chem. Res.* **1992**, *31*, 746–755.

Gauss, P.; Ligon-auer, S. C.; Griesser, M.; Gorsche, C.; Svajdlenkova, H.; Koch, T.; Moszner, N.; Liska, R. The Influence of Vinyl Activating Groups on b -Allyl Sulfone-Based Chain Transfer Agents for Tough Methacrylate Networks. **2016**, 1417–1427.

Ghobril, C.; Charoen, K.; Rodriguez, E. K.; Nazarian, A.; Grinstaff, M. W. Angewandte A Dendritic Thioester Hydrogel Based on Thiol – Thioester Exchange as a Dissolvable Sealant System for Wound Closure. **2013**, 14070–14074.

Gonalves, F.; Azevedo, C. L. N.; Ferracane, J. L.; Braga, R. R. BisGMA/TEGDMA Ratio and Filler Content Effects on Shrinkage Stress. *Dent. Mater.* **2011**, *27* (6), 520–526.

Gong, T.; Adzima, B. J.; Baker, N. H.; Bowman, C. N. Photopolymerization Reactions Using the Photoinitiated Copper (I)-Catalyzed Azide-Alkyne Cycloaddition (CuAAC) Reaction. *Adv. Mater.* **2013**, *25*, 2024–2028.

Gong, T.; Adzima, B. J.; Bowman, C. N. A Novel Copper Containing Photoinitiator, Copper(. *Chem. Commun.* **2013**, *49* (72), 7950–7952.

Guild, F. J.; Kinloch, A. J.; Taylor, A. C. Particle Cavitation in Rubber Toughened Epoxies: The Role of Particle Size. *J. Mater. Sci.* **2010**, *45* (14), 3882–3894.

Hoyle, C. E.; Lowe, A. B.; Bowman, C. N. Thiol-Click Chemistry: A Multifaceted Toolbox for Small Molecule and Polymer Synthesis. *Chem. Soc. Rev.* **2010**, *39* (4), 1355.

Hsieh, T. H.; Kinloch, A. J.; Masania, K.; Sohn Lee, J.; Taylor, A. C.; Sprenger, S. The Toughness of Epoxy Polymers and Fibre Composites Modified with Rubber Microparticles and Silica Nanoparticles. *J. Mater. Sci.* **2010**, *45* (5), 1193–1210

Hsieh, T. H.; Kinloch, A. J.; Masania, K.; Taylor, A. C.; Sprenger, S. The Mechanisms and Mechanics of the Toughening of Epoxy Polymers Modi Fi Ed with Silica Nanoparticles. *Polymer* **2010**, *51* (26), 6284–6294.

Huang, Y.; Kinloch, A. J. The Toughness of Epoxy Polymers Containing Microvoids *Technology* **1991**, *33*, 1991–1993.

Iwan, M.; Andryszewski, T.; Wydryszek, M.; Fialkowski, M. Fabrication of Nanocomposites by Covalent Bonding between Noble Metal Nanoparticles and Polymer Matrix. *RSC Adv.* **2015**, *5* (86), 70127–70138.

Jeffrey, G.; Bruce, P. R. *Thermosets*; Major Reference Works; 2017.

Jiang, R.; Liu, M.; Li, C.; Huang, Q.; Huang, H.; Wan, Q.; Wen, Y.; Cao, Q. yong; Zhang, X.; Wei, Y. Facile Fabrication of Luminescent Polymeric Nanoparticles Containing Dynamic Linkages via a One-Pot Multicomponent Reaction: Synthesis, Aggregation-Induced Emission and Biological Imaging. *Mater. Sci. Eng. C* **2017**, *80*, 708–714.

Johnson, J. A.; Finn, M. G.; Koberstein, J. T.; Turro, N. J. Construction of Linear Polymers , Dendrimers , Networks , and Other Polymeric Architectures by Copper-Catalyzed Azide-Alkyne Cycloaddition ‘“ Click ”’ Chemistry. **2008**, 1052–1072.

Kinloch, A. J.; Mohammed, R. D.; Taylor, A. C.; Eger, C.; Sprenger, S.; Egan, D. The Effect of Silica Nano Particles and Rubber Particles on the Toughness of Multiphase Thermosetting Epoxy Polymers. *J. Mater. Sci.* **2005**, *40* (18), 5083–5086.

Kinloch, A. J.; Taylor, C. The Toughening of Cyanate-Ester Polymers. Part I Physical Modification Using Particles, Fibres and Woven-Mats. *J. Mater. Sci.* **2002**, *37* (3), 433–460.

Klee, J. E.; Schneider, C.; Ho, D.; Burgath, A.; Frey, H.; Mu, R. Hyperbranched Polyesters and Their Application in Dental Composites : Monomers for Low Shrinking Composites. **2001**, *354* (June 2000), 346–354.

Kloxin, C. J.; Bowman, C. N. Covalent Adaptable Networks: Smart, Reconfigurable and Responsive Network Systems. *Chem. Soc. Rev.* **2013**, *42* (17), 7161–7173.

Kloxin, C. J.; Scott, T. F.; Adzima, B. J.; Bowman, C. N. Covalent Adaptable Networks (CANs): A Unique Paradigm in Cross-Linked Polymers. *Macromolecules* **2010**, *43* (6), 2643–2653.

Kloxin, C. J.; Scott, T. F.; Bowman, C. N. Stress Relaxation via Addition−Fragmentation Chain Transfer in a Thiol-Ene Photopolymerization. *Macromolecules* **2009**, *42* (7), 2551–2556.

Kloxin, C. J.; Scott, T. F.; Park, H. Y.; Bowman, C. N. Mechanophotopatterning on a Photoresponsive Elastomer. *Adv. Mater.* **2011**, *23* (17), 1977–1981.

Kojima Yoshitsugu; Usuki Arimitsu; Kawasumi Masaya; Okada Akane; Fukushima Yoshiaki; Kurauchi Toshio; Kamigaito Osami. Mechanical Properties of Nylon 6-Clay Hybrid. *J. Mater. Res.* **1993**, *8* (5), 1185–1189.

Kolb, H. C.; Finn, M. G.; Sharpless, K. B. Click Chemistry: Diverse Chemical Function from a Few Good Reactions. *Angew. Chemie - Int. Ed.* **2001**, *40* (11), 2004–2021.

Legrand, A.; Souli-Ziakovic, C. Silica-Epoxy Vitrimer Nanocomposites. *Macromolecules* **2016**, *49* (16), 5893–5902.

Leung, D.; Bowman, C. N. Reducing Shrinkage Stress of Dimethacrylate Networks by Reversible Addition – Fragmentation Chain Transfer. **2012**, 198–204.

Ligon-Auer, S. C.; Schwentenwein, M.; Gorsche, C.; Stampfl, J.; Liska, R. Toughening of Photo-Curable Polymer Networks: A Review. *Polym. Chem.* **2016**, *7* (2), 257–286.

Liu, J.; Howard, G. D.; Lewis, S. H.; Barros, M. D.; Stansbury, J. W. A Study of Shrinkage Stress Reduction and Mechanical Properties of Nanogel-Modified Resin Systems. *Eur. Polym. J.* **2012**, *48* (11), 1819–1828.

Liu, J.; Ueda, M. High Refractive Index Polymers: Fundamental Research and Practical Applications. *J. Mater. Chem.* **2009**, *19* (47), 8907.

Lyon, G. B.; Cox, L. M.; Goodrich, J. T.; Baranek, A. D.; Ding, Y.; Bowman, C. N. Remoldable Thiol–Ene Vitrimers for Photopatterning and Nanoimprint Lithography. *Macromolecules* **2016**, 281.

McBride, M. K.; Gong, T.; Nair, D. P.; Bowman, C. N. Photo-Mediated Copper(I)-Catalyzed Azide-Alkyne Cycloaddition (CuAAC) “Click” Reactions for Forming Polymer Networks as Shape Memory Materials. *Polym.* **2014**, *55* (23), 5880–5884.

McBride, M. K.; Worrell, B. T.; Brown, T.; Cox, L. M.; Sowan, N.; Wang, C.; Podgorski, M.; Martinez, A. M.; Bowman, C. N. Enabling Applications of Covalent Adaptable Networks. **2019**, *10*, 175.

Michler, G. H.; Von Schmeling, H. H. K. B. The Physics and Micro-Mechanics of Nano-Voids and Nano-Particles in Polymer Combinations. *Polym.* **2013**, *54* (13), 3131–3144.

Moraes, R. R.; Garcia, J. W.; Barros, M. D.; Lewis, S. H.; Pfeifer, C. S.; Liu, J.; Stansbury, J. W. Control of Polymerization Shrinkage and Stress in Nanogel-Modified Monomer and Composite Materials. *Dent. Mater.* **2011**, *27* (6), 509–519.

Moszner, N.; Salz, U. Recent Developments of New Components for Dental Adhesives and Composites. *Macromol. Mater. Eng. 2007,* **2007**, *292*, 245–271.

Ms, S.; Auj, Y.; S. A. Physicomechanical Evaluation of Low-Shrinkage Dental Nanocomposites Based on Silsesquioxane Cores. *European Journal of Oral Sciences* **2007**, 230–238.

Mu, X.; Sowan, N.; Tumbic, J. a.; Bowman, C. N.; Mather, P. T.; Qi, H. J. Photo-Induced Bending in a Light-Activated Polymer Laminated Composite. *Soft Matter* **2015**, *11* (13), 2673–2682.

Nair, D. P.; Cramer, N. B.; Scott, T. F.; Bowman, C. N.; Shandas, R. NIH Public Access. **2011**, *51* (19), 4383–4389.

Nicolaÿ, R.; Kamada, J.; Van Wassen, A.; Matyjaszewski, K. Responsive Gels Based on a Dynamic Covalent Trithiocarbonate Cross-Linker. *Macromolecules* **2010**, *43* (9), 4355–4361.

Nilsson, B. L.; Soellner, M. B.; Raines, R. T. Ynthesis Of. **2005**, 91–118.

Odell, J. a.; Keller, a.; Rabin, Y. Flow-Induced Scission of Isolated Macromolecules. *J. Chem. Phys.* **1988**, *88* (6), 4022–4028.

Odian, G. *Principles of Polymerization*; John Wiley & Sons, 2004.

Oehlenschlaeger, K. K.; Guimard, N. K.; Brandt, J.; Mueller, J. O.; Lin, C. Y.; Hilf, S.; Lederer, A.; Coote, M. L.; Schmidt, F. G.; Barner-Kowollik, C. Fast and Catalyst-Free Hetero-Diels-Alder Chemistry for on Demand Cyclable Bonding/Debonding Materials. *Polym. Chem.* **2013**, *4* (16), 4348–4355.

Ou, Y.; Yang, F.; Yu, Z.-Z. *A New Conception on the Toughness of Nylon 6/Silica Nanocomposite Prepared via in Situ Polymerization*; 1998; Vol. 36.

Park, H. Y.; Kloxin, C. J.; Abuelyaman, A. S.; Oxman, J. D.; Bowman, C. N. Stress Relaxation via Addition–Fragmentation Chain Transfer in High T g , High Conversion Methacrylate-Based Systems. *Macromolecules 45* (14), 5640-5646.

Park, H. Y.; Kloxin, C. J.; Fordney, M. F.; Bowman, C. N. Stress Reduction and T g Enhancement in Ternary Thiol-Yne-Methacrylate Systems via Addition-Fragmentation Chain Transfer. *Macromolecules* **2012**, *45* (14), 5647–5652.

Park, H. Y.; Kloxin, C. J.; Fordney, M. F.; Christopher, N. *Dent. Mater.* **2013**, *28* (8), 888–893.

Podgórski, M.; Becka, E.; Claudino, M.; Shah, P. K.; Stansbury, J. W.; Bowman, C. N. Ester-Free Thiol – Ene Dental Restoratives — Part A : *Dent. Mater.* **2015**, *31* (11), 1255–1262.

Podgórski, M.; Worrell, B. T.; Sinha, J.; Mcbride, M. K.; Bowman, C. N. Thermal Metamorphosis in (Meth)Acrylate Photopolymers: Stress Relaxation, Reshaping, and Second-Stage Reaction. *Macromolecules* **2019**, *52*, 8114–8123.

Price, J. L.; Hadley, E. B.; Steinkruger, J. D.; Gellman, S. H. NIH Public Access. **2011**, *49* (2), 368–371.

Qi, Y.; Caillard, J.; Long, R. Journal of the Mechanics and Physics of Solids Fracture Toughness of Soft Materials with Rate-Independent Hysteresis. *J. Mech. Phys. Solids* **2018**, *118*, 341–364.

Qiu, M.; Wu, S.; Tang, Z.; Guo, B. Exchangeable Interfacial Crosslinks towards Mechanically Robust Elastomer/Carbon Nanotubes Vitrimers. *Compos. Sci. Technol.* **2018**, *165*, 24–30.

Queiroz, G.; Universidade, M. M.; Universidade, M. M. Evaluation of Linear Polymerization Shrinkage, Flexural Strength and Modulus of Elasticity of Dental Composites. **2010**, *13* (March), 51–55.

Ritchie, R. O. The Conflicts between Strength and Toughness. *Nat. Mater.* **2011**, *10* (11), 817–822.

Rostovtsev, V. V.; Green, L. G.; Fokin, V. V.; Sharpless, K. B. A Stepwise Huisgen Cycloaddition Process: Copper(I)-Catalyzed Regioselective "Ligation" of Azides and Terminal Alkynes. *Angew. Chemie - Int. Ed.* **2002**, *41*, 2596–2599.

Röttger, M.; Domenech, T.; Van Der Weegen, R.; Breuillac, A.; Nicolaÿ, R.; Leibler, L. High-Performance Vitrimers from Commodity Thermoplastics through Dioxaborolane Metathesis. *Science* **2017**, *356* (6333), 62–65.

Ruiz de Luzuriaga, A.; Martin, R.; Markaide, N.; Rekondo, A.; Cabañ ero, G.; Rodrí guez, J.; Odriozola, I. Epoxy Resin with Exchangeable Disulfide Crosslinks to Obtain Reprocessable, Repairable and Recyclable Fiber-Reinforced Thermoset Composites. *Mater. Horizons* **2016**, 241–247.

Ryu, J.; D'Amato, M.; Cui, X.; Long, K. N.; Jerry Qi, H.; Dunn, M. L. Photo-Origami-Bending and Folding Polymers with Light. *Appl. Phys. Lett.* **2012**, *100*, 161908.

Schneider, L. F. J.; Cavalcante, L. M.; Silikas, N. Shrinkage Stresses Generated during Resin-Composite Applications: A Review. *J. Dent. Biomech.* **2010**, *1* (1), 131630–131630.

Scott, T. F.; Schneider, A. D.; Cook, W. D.; Bowman, C. N. Photoinduced Plasticity in Cross-Linked Polymers. *Science* **2005**, *308* (5728), 1615–1617.

Shah, P. K.; Stansbury, J. W. Role of Filler and Functional Group Conversion in the Evolution of Properties in Polymeric Dental Restoratives. *Dent. Mater.* **2014**, *30* (5), 586–593.

Shah, P. K.; Stansbury, J. W.; Bowman, C. N. Application of an Addition-Fragmentation-Chain Transfer Monomer in Di(Meth)Acrylate Network Formation to Reduce Polymerization Shrinkage Stress. *Polym. Chem.* **2017**, *8* (30), 4339–4351.

Sheridan, R. J.; Bowman, C. N. Understanding the Process of Healing of Thermoreversible Covalent Adaptable Networks. *Polym. Chem.* **2013**, *4* (18), 4974–4979.

Solid, L. D.; Hrubesh, L. W.; Chan, H. M.; Grenestedt, J. L.; Harmer, M. P.; Caram, H. S.; Roy, S. K.; Handbook, P. T.; Raton, B.; Ashby, M. F.; et al. Silica-Like Malleable Materials From. *Science* **2011**, *334*, 965–968.

Song, H. B.; Baranek, A.; Bowman, C. N. Kinetics of Bulk Photo-Initiated Copper(I)-Catalyzed Azide-Alkyne Cycloaddition (CuAAC) Polymerizations. *Polym. Chem.* **2016**, *7*, 603–612.

Song, H. B.; Baranek, A.; Worrell, B. T.; Cook, W. D.; Bowman, C. N. Photopolymerized Triazole-Based Glassy Polymer Networks with Superior Tensile Toughness. *Adv. Funct. Mater.* **2018**, *28* (22), 1–9.

Song, H. B.; Sowan, N.; Shah, P. K.; Baranek, A.; Flores, A.; Stansbury, J. W.; Bowman, C. N. Reduced Shrinkage Stress via Photo-Initiated Copper(I)-Catalyzed Cycloaddition Polymerizations of Azide-Alkyne Resins. *Dental Materials*. Elsevier Inc. June 25, 2016.

Song, H. B.; Wang, X.; Patton, J. R.; Stansbury, J. W.; Bowman, C. N. Kinetics and Mechanics of Photo-Polymerized Triazole-Containing Thermosetting Composites via the Copper (I) - Catalyzed Azide-Alkyne Cycloaddition. *Dent. Mater.* **2017**, *33* (6), 621–629.

Sowan, N.; Cox, L. M.; Shah, P. K.; Song, H. B.; Stansbury, J. W.; Bowman, C. N. Dynamic Covalent Chemistry at Interfaces: Development of Tougher, Healable Composites through Stress Relaxation at the Resin-Silica Nanoparticles Interface. *Adv. Mater. Interfaces* **2018**, 1800511.

Sun, S.; Li, C.; Zhang, L.; Du, H. L.; Burnell-Gray, J. S. Effects of Surface Modification of Fumed Silica on Interfacial Structures and Mechanical Properties of Poly(Vinyl Chloride) Composites. *Eur. Polym. J.* **2006**, *42* (7), 1643–1652.

Sun, S.; Wu, P. Mechanistic Insights into Cu (I) -Catalyzed Azide - Alkyne " Click " Cycloaddition Monitored by Real Time Infrared Spectroscopy. **2010**, No. I, 8331–8336.

Tasdelen, M. A.; Yagci, Y. Light-Induced Copper(I)-Catalyzed Click Chemistry. *Tetrahedron Lett.* **2010**, *51* (52), 6945–6947.

Tornøe, C. W.; Christensen, C.; Meldal, M. Peptidotriazoles on Solid Phase: [1,2,3]-Triazoles by Regiospecific Copper(I)-Catalyzed 1,3-Dipolar Cycloadditions of Terminal Alkynes to Azides. *J. Org. Chem.* **2002**, *67* (9), 3057–3064.

Tsai, J. L.; Hsiao, H.; Cheng, Y. L. Investigating Mechanical Behaviors of Silica Nanoparticle Reinforced Composites. *J. Compos. Mater.* **2010**, *44* (4), 505–524.

Üstündag, E.; Dragoi, D.; Clausen, B.; Brown, D.; Bourke, M. A. M.; Balch, D. K.; Dunand, D. C. Internal Stresses in Bulk Metallic Glass Matrix Composites. **2001**, *644* (4), 1–6.

Wan, Q.; Liu, M.; Xu, D.; Huang, H.; Mao, L.; Zeng, G.; Deng, F.; Zhang, X.; Wei, Y. Facile Fabrication of Amphiphilic AIE Active Glucan via Formation of Dynamic Bonds: Self Assembly, Stimuli Responsiveness and Biological Imaging. *J. Mater. Chem. B* **2016**, *4* (22), 4033–4039.

Wang, C.; Mavila, S.; Worrell, B. T.; Xi, W.; Goldman, T. M.; Bowman, C. N. Productive Exchange of Thiols and Thioesters to Form Dynamic Polythioester-Based Polymers. **2018**.

Wkiner, K. A.; Springer-, E.; Erikison, K.; Asoy, J. Colin George Whitesides. **1987**, *240*, 1987–1988.

Worrell, B. T.; Malik, J. A.; Fokin, V. V. Direct Evidence of a Dinuclear Copper Intermediate in Cu(I)-Catalyzed Azide-Alkyne Cycloadditions. *Science* **2013**, *340*, 457–461.

Worrell, B. T.; McBride, M. K.; Lyon, G. B.; Cox, L. M.; Wang, C.; Mavila, S.; Lim, C.-H.; Coley, H. M.; Musgrave, C. B.; Ding, Y.; et al. Bistable and Photoswitchable States of Matter. *Nat. Commun.* **2018**, *9* (1), 2804.

Yang, Y.; Pei, Z.; Zhang, X.; Tao, L.; Wei, Y.; Ji, Y. Carbon Nanotube–Vitrimer Composite for Facile and Efficient Photo-Welding of Epoxy. *Chem. Sci.* **2014**, *5*, 3486–3492.

Yang, Z.; Wang, Q.; Wang, T. Dual-Triggered and Thermally Reconfigurable Shape Memory Graphene-Vitrimer Composites. *ACS Appl. Mater. Interfaces* **2016**, *8* (33), 21691–21699.

Young, R. J.; Maxwell, D. L.; Kinloch, A. J. The Deformation of Hybrid-Particulate Composites. *J. Mater. Sci.* **1986**, *21* (2), 380–388.

Zajdowicz, S.; Byul, H.; Baranek, A.; Bowman, C. N. Evaluation of Biofilm Formation on Novel Copper-Catalyzed Azide-Alkyne Cycloaddition (CuAAC) -Based Resins for Dental Restoratives. *Dent. Mater.* **2018**, *34* (4), 657–666.

Zehnder, A. T. *Fracture Mechanics*; Springer US, 2012.

Zhang, H.; Tang, L. C.; Zhang, Z.; Friedrich, K.; Sprenger, S. Fracture Behaviours of in Situ Silica Nanoparticle-Filled Epoxy at Different Temperatures. *Polymer (Guildf).* **2008**, *49* (17), 3816–3825.

Zhang, T.; Lin, S.; Yuk, H.; Zhao, X. Predicting Fracture Energies and Crack-Tip Fields of Soft Tough Materials. *Extrem. Mech. Lett.* **2015**, *4*, 1–8.

Zhang, X.; Wang, K.; Liu, M.; Zhang, X.; Tao, L.; Chen, Y.; Wei, Y. Polymeric AIE-Based Nanoprobes for Biomedical Applications: Recent Advances and Perspectives. *Nanoscale* **2015**, *7* (27), 11486–11508.

Zheng, Y.; Zheng, Y.; Ning, R. Effects of Nanoparticles SiO2 on the Performance of Nanocomposites. *Mater. Lett.* **2003**, *57* (19), 2940–2944.

Ying, H.; Zhang, Y.; Cheng, J. Dynamic Urea Bond for the Design of Reversible and Self-Healing Polymers. *Nat. Commun.* **2014**, *5*, 1–9.